Supplementary Information to: Evaluation of coal mine methane inventory methods using aircraft-based approaches in the Bowen Basin, Australia

Stephen J. Harris[1,2], Sven Krautwurst[3], Jorg Hacker[4,5], Mark Lunt[6], Jakob Borchardt[3], Mei Bai[4,7], Hartmut Boesch[3], Tarra Brain[2], John Philip Burrows[3], Shakti Chakravarty[4], Robert A. Field[1], Rebecca E. Fisher[8], James L. France[6,8], Konstantin Gerilowski[3], Oke Huhs[3], Wolfgang Junkermann[4,9], Bryce F.J. Kelly[2], Martin Kumm[10], Mathias Lanoisellé[8], Wolfgang Lieff[4], Andrew McGrath[4,5], Adrian Murphy[4], Thomas Röckmann[11], Zoe Salmon[2], Josua Schindewolf[12], Jakob Thoböll[3], Carina van der Veen[11], Heinrich Bovensmann[3]

[1]UNEP's International Methane Emissions Observatory (IMEO), Paris, France
[2]School of Biological, Earth and Environmental Sciences, University of New South Wales, Sydney, NSW, Australia
[3]University of Bremen, Institute of Environmental Physics (IUP), Bremen, Germany
[4]Airborne Research Australia, Parafield, SA, Australia
[5]College of Science and Engineering, Flinders University, Adelaide, SA, Australia
[6]Environmental Defense Fund, Perth, WA, Australia
[7]The University of Melbourne, School of Agriculture, Food and Ecosystem Sciences, Parkville, VIC, Australia
[8]Department of Earth Sciences, Royal Holloway, University of London, Egham, TW20 0EX, UK
[9]Karlsruhe Institute of Technology, Garmisch Partenkirchen, Germany
[10]Jade University of Applied Sciences, Wilhelmshaven, Germany
[11]Institute for Marine and Atmospheric Research, Faculty of Science, Utrecht University, Utrecht, 3584 CC, the Netherlands
[12]Alfred Wegener Institute - Helmholtz Centre for Polar and Marine Research, Bremerhaven, Germany

Correspondence to: Stephen Harris (stephen.harris@un.org; s.j.harris@unsw.edu.au)

SI-1: Coal production and reported CH_4 emissions by mine in the Bowen Basin

Table S1 summarises coal production statistics and reported CH_4 emissions for all operational coal mines during FY24 located within the Bowen Basin (Queensland Government, 2025a). The emissions data in this table are sourced from the Australia's Safeguard Mechanism database (CER, 2025b) and are used in SI-2 to construct the bottom-up UNSW inventory.

Run-of-mine (ROM) coal extraction totalled 254 Mt, with 215Mt (85%) extracted from surface mining and 39Mt (15%) from underground operations. 198 Mt (78%) was extracted from open-cut, 27 Mt (11%) from underground, and 29 Mt (11%) was extracted from mine complexes (Fig. 2; Queensland Government, 2025a). Saleable coal totalled 188 Mt, of which 72% (135 Mt) was metallurgical coal (comprising 54% coking coal [101 Mt] and 18% Pulverized Coal Injection (PCI) coal [34 Mt]), and 28% (52 Mt) was thermal coal. Five mines produced only thermal coal, 17 produced only metallurgical coal, and 25 produced both metallurgical and thermal coal.

Table S1. Production summary and reported CH_4 emissions for all operational coal mines during FY24 located within the Bowen Basin, and identifiers used in this study.

Mine ID[a]	Coal type	Reported under Safeguard?	Reported average annual CH_4 emissions (kg hr^{-1} CH_4)	NGER Method	FY24 Production (t)	Coking coal (t)	PCI coal (t)	Metallurgical coal (t)	Thermal coal (t)	Net output (t)	CH_4 emissions intensity (t CO_2e t^{-1} ROM)
Open-cut											
OC-1	Metallurgical & Thermal	Yes	1,112	1	8,786,474	4,639,097	-	4,639,097	1,712,544	6,351,641	0.031
OC-2	Thermal	No	0	Not reported	1,240,391	-	-	-	1,240,391	1,240,391	N/A
OC-3	Thermal	Yes	1	2	12,385,695	-	-	-	12,385,695	12,385,695	0.000020
OC-4	Metallurgical & Thermal	Yes	200	1	1,575,990	-	1,482,656	1,482,656	49,986	1,532,642	0.031
OC-5	Metallurgical & Thermal	Yes	1,597	1	12,569,179	9,850,576	-	9,850,576	251,464	10,102,040	0.031
OC-6	Metallurgical	No	0	Not reported	345,596	-	323,718	323,718	-	323,718	N/A
OC-7	Metallurgical & Thermal	Yes	1,995	1,2	12,851,376	3,240,705	3,755,138	6,995,843	3,180,105	10,175,948	0.038
OC-8	Metallurgical	Yes	770	1	6,125,257	-	5,348,178	5,348,178	-	5,348,178	0.031
OC-9	Metallurgical	Yes	286	1	2,257,483	-	1,812,207	1,812,207	-	1,812,207	0.031
OC-10	Metallurgical & Thermal	No	0	Not reported	198,180	24,239	-	24,239	13,178	37,417	N/A
OC-11	Metallurgical	Yes	2	2	1,775,236	1,631,429	-	1,631,429	-	1,631,429	0.00029
OC-12	Metallurgical	Yes	428	1	3,376,218	-	2,571,839	2,571,839	-	2,571,839	0.031
OC-13	Metallurgical	Yes	476	1	3,755,354	1,091,316	1,137,719	2,229,035	-	2,229,035	0.031
OC-14	Thermal	Yes	1	2	11,511,608	-	-	-	11,422,493	11,422,493	0.000018
OC-15	Thermal	No	0	Not reported	1,995,018	-	-	-	1,505,264	1,505,264	N/A
OC-16	Metallurgical & Thermal	Yes	265	2	11,236,347	5,519,494	2,484,042	8,003,536	1,061,606	9,065,142	0.0058
OC-17	Metallurgical & Thermal	Yes	113	2	11,243,284	6,336,396	-	6,336,396	239,429	6,575,825	0.0025
OC-18	Metallurgical	No	0	Not reported	1,293,166	1,433,249	-	1,433,249	-	1,433,249	N/A
OC-19	Metallurgical	Yes	63	2	15,755,505	6,800,799	-	6,800,799	-	6,800,799	0.0010
OC-20	Metallurgical & Thermal	Yes	218	1	1,602,295	660,801	-	660,801	385,560	1,046,361	0.033
OC-21	Metallurgical	Yes	17	2	13,001,105	8,134,360	-	8,134,360	-	8,134,360	0.00032
OC-22	Metallurgical	Yes	393	2	6,652,584	1,928,794	2,483,457	4,412,251	-	4,412,251	0.015
OC-23	Metallurgical & Thermal	Yes	142	2	4,746,873	4,058,382	-	4,058,382	504	4,058,886	0.0073
OC-24	Metallurgical	No	0	Not reported	524,882	268,787	153,635	422,422	-	422,422	N/A
OC-25	Metallurgical & Thermal	Yes	464	1	3,663,958	332,380	1,702,255	2,034,635	105,672	2,140,307	0.031
OC-26	Metallurgical & Thermal	Yes	451	1	3,562,296	2,208,168	-	2,208,168	300,497	2,508,665	0.031
OC-27	Metallurgical & Thermal	No	0	Not reported	535,584	2,829	14,385	17,214	472,332	489,546	N/A
OC-28	Metallurgical	Yes	482	1	3,808,373	-	2,723,872	2,723,872	-	2,723,872	0.031
OC-29	Metallurgical & Thermal	No	0	Not reported	1,681,385	638,033	27,341	665,374	401,294	1,066,668	N/A
OC-30	Metallurgical	Yes	1,048	1	8,278,823	-	6,349,849	6,349,849	-	6,349,849	0.031
OC-31	Metallurgical & Thermal	Yes	319	1	1,215,988	434,956	-	434,956	216,472	651,428	0.064
OC-32	Metallurgical & Thermal	Yes	4,334	2	9,592,586	3,895,983	-	3,895,983	3,977,955	7,873,938	0.111
OC-33	Metallurgical & Thermal	Yes	883	1	6,976,767	2,299,845	-	2,299,845	2,175,346	4,475,191	0.031
OC-34	Metallurgical & Thermal	Yes	327	1	2,587,424	505,108	-	505,108	1,391,968	1,897,076	0.031
OC-35	Metallurgical & Thermal	Yes	657	1	5,192,481	369,484	-	369,484	2,735,517	3,105,001	0.031

Mine ID[a]	Coal type	Reported under Safeguard?	Reported average annual CH_4 emissions (kg hr^{-1} CH_4)	NGER Method	FY24 Production (t)	Coking coal (t)	PCI coal (t)	Metallurgical coal (t)	Thermal coal (t)	Net output (t)	CH_4 emissions intensity (t CO_2e t^{-1} ROM)
OC-36	Metallurgical & Thermal	Yes	12	2	4,142,294	690,763	-	690,763	2,045,757	2,736,520	0.0007
Total (Open-cut)			**17,053**		**198,043,055**	**66,995,973**	**32,370,291**	**99,366,264**	**47,271,029**	**146,637,293**	**0.021**
Underground											
UG-1	Metallurgical & Thermal	Yes	382	Not reported	99,009	51,524	-	51,524	18,960	70,484	0.947
UG-2	Metallurgical & Thermal	Yes	3,823	1,4	7,739,428	3,949,469	-	3,949,469	1,175,400	5,124,869	0.121
UG-3	Metallurgical	Yes	2,577	2,4	6,087,553	4,051,360	-	4,051,360	-	4,051,360	0.104
UG-4	Metallurgical	Yes	3,571	1,2,4	6,941,619	4,277,435	-	4,277,435	-	4,277,435	0.126
UG-5	Metallurgical & Thermal	Yes	2,225	1,4	2,054,850	1,119,278	232,235	1,351,513	18,132	1,369,645	0.266
UG-6	Metallurgical	Yes	4,997	1,2,4	3,554,822	3,513,457	-	3,513,457	-	3,513,457	0.345
UG-7	Metallurgical & Thermal	Yes	409	1,4	264,800	131,134	30,579	161,713	4,008	165,721	0.378
UG-8	Metallurgical	Yes	624	4	7,094	7,094	-	7,094	-	7,094	21.562
Total (Underground)			**18,607**		**26,749,175**	**17,100,751**	**262,814**	**17,363,565**	**1,216,500**	**18,580,065**	**0.171**
Mine Complex											
MC-1	Thermal	Yes	867	1,4 (UG); 1(OC)	2,260,084	-	-	-	3,410,057	3,410,057	0.094
MC-2	Metallurgical & Thermal	Yes	3509	1,2,4 (UG); 1 (OC)	9,034,145	4,160,197	1,729,667	5,889,864	339,751	6,229,615	0.095
MC-3	Metallurgical & Thermal	Yes	3086	1,4 (UG); 2 (OC)	18,175,868	12,782,818	-	12,782,818	85,332	12,868,150	0.042
Total (Mine Complex)			**7,462**		**29,470,097**	**16,943,015**	**1,729,667**	**18,672,682**	**3,835,140**	**22,507,822**	**0.062**
Total (All coal mines)			**43,122**		**254,262,327**	**101,039,739**	**34,362,772**	**135,402,511**	**52,322,669**	**187,725,180**	**0.042**

[a]Open-cut coal mines were numbered OC-1 to OC-36, underground coal mines UG-1 to UG-8, and mine complexes MC-1 to MC-3.

SI-2: Location of known CH_4 sources and construction of the UNSW inventory

This section describes the methods used to derive the location of known CH_4 sources in the Bowen Basin and construct the bottom-up UNSW inventory (Table S2).

Coal Mines

The locations of open-cut coal mines and underground mining infrastructure, including ventilation fans and flares, were obtained from Google Earth. The data were cross-referenced with the Queensland Globe database to determine whether specific mining infrastructure was located on particular mining leases (Queensland Government, 2025d). Annual CH_4 emissions from 39 coal mines were derived from the FY24 Safeguard Mechanism database (CER, 2025b). Eight open-cut mines located in the basin did not report under the Safeguard Mechanism for FY24, likely because their emissions did not exceed the reporting threshold. For these facilities, fugitive CH_4 emissions were estimated using Method 1 based on reported ROM production (Queensland Government, 2025a). Although this means the UNSW inventory may differ slightly from official government estimates for the Bowen Basin, the difference is expected to be minor, as these eight mines account for only 3% of total regional coal production.

Grazing cattle

The location and number of grazing cattle in the Bowen Basin carries uncertainty since herd numbers and their location are not reported in any national database within Australia. Although we cannot approximate their exact location, to approximate the number of grazing cattle we use 2022 estimates of head cattle in the Fitzroy Plains (2,523,546 head; Meat and Livestock Australia, 2022), less the number of feedlot cattle capacity (164,142 head), alongside the area of grazing land within the Fitzroy Plains (12,000,000 ha) to determine an average cattle density of 0.20 head ha^{-1}. This density is extrapolated over the study area (6,000,000 ha), to derive an estimate of the total number of grazing cattle in the Bowen Basin, which equates to approximately 1,180,000 head of grazing cattle. The cattle density used in this approximation is broadly consistent with recommended stocking rates of 0.1-0.5 Adult Equivalent (AE) ha^{-1} yr^{-1} within the Brigalow Belt bioregion (Thornton and Elledge, 2021), and estimated sustainable stocking rates of 0.17-0.45 head ha^{-1} on post-mining pasture rehabilitation sites within the Bowen Basin (Grigg et al., 2006). Total emissions from grazing cattle were estimated using the implied emission factor for enteric fermentation from pasture cattle in Australia's NIR (0.04993 t CH_4 $head^{-1}$ a^{-1}; Australian Government, 2025a) multiplied by the approximated 1,180,000 head of grazing cattle.

Feedlot cattle

The location of cattle feedlots within the Bowen Basin was derived from the AgTrends Spatial database (Queensland Government, 2025c). Emissions from the 55 cattle feedlots located in the study area were estimated using the implied emission

factor for enteric fermentation from feedlot cattle in Australia's National Inventory (0.03045 t CH_4 $head^{-1}$ a^{-1}; Australian Government, 2025a), multiplied by the maximum licenced capacity at each feedlot derived from the AgTrends Spatial database (Queensland Government, 2025c). This approach assumes emissions at the upper bound of the potential range, given the reliance on maximum licensed capacities rather than actual stocking rates or operational averages. Since the location and maximum capacity of each feedlot was available, emissions from feedlot cattle could be spatially resolved within the inventory (as shown in Fig. 2 of the manuscript).

Farm dams

The locations and sizes of farm dams located within the Bowen Basin were subset from the AusDams interactive portal (AusDams, 2025; Malerba et al., 2021). In total, we identified 20,708 farm dams within the database, with a combined area of 12,450 ha. CH_4 emissions from individual dams were estimated by multiplying the area of each farm dam by the farm dam CH_4 emission factor for September 2023 reported in the AusDams interactive portal (0.3 t CH_4 ha^{-1} a^{-1}; AusDams, 2025; Malerba et al., 2021). Since the location and size of each farm dam was available, the locations of these estimated emissions could be spatially resolved within the inventory (as shown in Fig. 2 of the manuscript).

Coal mine waste gas power stations

Emissions from six coal mine waste gas (CMWG) power stations located in the Bowen Basin were estimated using reported energy production for FY24 (totalling 3,541,032 GJ; CER, 2025c) multiplied by the emission factor for coal mine waste gas that is captured for combustion (4.6 kg CO_2-e GJ^{-1}; Commonwealth of Australia, 2023). The power stations included the Oaky Creek II WCMG Power Station, Oaky Creek WCMG Power Station, German Creek CMM Power Station, Grosvenor 1 WCMG Power Station, Grosvenor 2 WCMG Power Station, and Moranbah North CMM Power Station. Since the energy production was reported for each facility, the location of these estimated emissions could be spatially resolved within the inventory.

Coal seam gas and conventional natural gas (onshore wells)

The location of operational coal seam gas (CSG) and natural gas onshore wells were obtained from the State of Queensland Geoscientific Information/Boreholes MapServer (Queensland Government; 2025e). Emissions from producing onshore CSG wells was derived by multiplying the gas throughput for FY24 for Bowen Basin CSG production fields (229,991 t gas; Queensland Government, 2025f) by the National Inventory Report (2023) emission factor for well-functioning onshore CSG wells (7.2×10^{-7} t CH_4 t^{-1} gas throughput; Australian Government, 2025b). The producing fields included the Dawson River, Moura, Mungi, Mungi North, Mungi West, Nipan, Winchester, Annandale, Grosvenor, Moranbah East, Moranbah West and Red Hill Central gas fields.

Emissions from producing onshore conventional natural gas wells was derived by multiplying the gas throughput for FY24 for Bowen Basin conventional gas production fields (974,180 t gas; Queensland Government, 2025f) by the National Inventory

Report (2023) emission factor for onshore conventional gas wells (4.7×10^{-5} t CH_4 t^{-1} gas throughput; Australian Government, 2025b). The producing fields included the Rolleston, Arcadia, Arcturus, Moorooloo, Springton, Turkey Creek, Fairview, Yandina, Humboldt, Mahalo, Morella South, Towrie and Warrinilla gas fields. Emissions were spread evenly across the reported producing CSG and natural gas wells since production from individual wells was not available.

Coal seam gas and conventional natural gas (venting and flaring)

Venting and flaring were estimated based on published gas throughput figures for FY24 for infrastructure located within the study area (707 t of gas vented or flared; Queensland Government, 2025f). Since a breakdown between flaring and venting was not publicly available, we assumed that 90 % of disposed gas was flared and 10 % was vented, corresponding to 636 t of gas flared and 71 t of gas vented. This assumption is consistent with Queensland regulatory frameworks, which prioritise flaring over venting where gas cannot be commercially utilised. Emissions from flaring were estimated using the National Inventory Report (2023) emission factors for gas flared during natural gas processing (0.02 t CH_4 t^{-1} gas flared; Australian Government, 2025b). The same emission factor applied by Neininger et al. (2021) for vented gas (1.0 t CH_4 t^{-1} gas flared) was applied. Since flared and vented gas volumes are aggregated by production field, and not individual flare or venting locations, these emissions could not be spatially attributed within the inventory.

Coal seam gas and conventional natural gas (transmission and storage)

Transmission pipelines located within the Bowen Basin include the Queensland Gas Pipeline (627 km total length, estimated ~230 km within the study area; KPMG, 2021), Denison North Pipeline (~150km; Denison Gas, 2026), the Dawson Valley Pipeline (47km; AEMC, 2026a), the North Queensland Gas Pipeline (391km total length, estimated ~160km within the study area; AEMC, 2026b; KPMG, 2026), the Gladstone LNG Pipeline (GLNG; 627 km total length, estimated ~230km within the study area; KPMG, 2021), Australia Pacific LNG (APLNG; 530km total length, estimated ~115km within the study area; KPMG, 2021), the Wallumbilla Gladstone Pipeline (WGP; 543km total length, estimated ~50km within the study area; KPMG, 2021) and the Arrow Bowen Pipeline (580km total length, estimated ~250km within the study area; Queensland Government, 2025g). Emissions were estimated based on the approximate length of gas pipeline in the study area (~ 1,232 km) multiplied by the emission factor for emission from natural gas transmission (0.41 t CH_4 km^{-1} pipeline; Australian Government, 2025b). These emissions could not be resolved spatially since georeferenced data for the location of each pipeline running through the Bowen Basin was not publicly available. To our knowledge, there are no dedicated natural gas or coal seam gas (CSG) storage facilities located within the Bowen Basin itself.

Coal seam gas and conventional natural gas (gathering and boosting pipelines)

Publicly available quantitative data on the length of gathering and boosting pipelines in the Bowen Basin's CSG and natural gas fields are limited. The Moranbah Gas Project reports approximately 500 km of field pipeline infrastructure (QPM Energy, 2025), while the Dawson Valley-Meridian gas field is associated with around 160 km of pipeline connections (MiningLink,

2026). To estimate Arcadia's portion, we took the estimated total length of pipelines associated with the GLNG project, reported as approximately 2,000 km (Santos, 2014), which includes transmission, gathering, and boosting pipelines. Transmission pipelines account for roughly 420 km of this total, leaving ~1,580 km for gathering and boosting pipelines. These pipelines serve three production fields: Arcadia, Fairview, and Roma. In the absence of field-specific data, we apportioned the remaining 1,580 km evenly across the three fields, yielding an estimated length of ~530 km of gathering and boosting pipelines for Arcadia. Denison Gas (2020) report a 200km pipeline network servicing its Denison gas assets. Emission factors for gathering and boosting pipelines from the National Inventory Report (2023) (0.23 t CH_4 t^{-1} km^{-1} pipeline; Australian Government, 2025b) were applied to the total length estimate (1,390 km), yielding emissions equivalent to approximately 0.03% of the inventory (Table S2). These estimates are order-of-magnitude approximations intended for inventory-level approximations and not spatially resolved within the inventory.

Coal seam gas (produced water)

The location of CSG water treatment facilities were located using Google Maps (Google LLC, USA). Emissions were estimated based on the volume of produced water (251 ML; Queensland Government, 2025f) multiplied by the emission factor for produced water from coal seam gas production (0.31 t CH_4 ML^{-1} water produced; Australian Government, 2025b). Emissions from each CSG water treatment facilities are spatially resolved in the inventory at the facility scale, but not at sub-facility resolution.

Coal seam gas and conventional natural gas (processing plants)

Gas flow data reported by AEMO for the Rolleston, Moura, Meridian and Arcadia production fields (AEMO, 2026) were used to estimate gas throughput for the corresponding gas processing plants. Flows from the Moranbah production fields were estimated using the 10 PJ of gas produced during 2023 (QPM Energy, 2023) for the Moranbah Gas Plant. Using this approach, the estimated gas flows from the processing plants were 1,197,152 t, corresponding to 99% of the flows reported in the Queensland Government Petroleum and Gas Production and Reserve Statistics database (1,204,171 t; Queensland Government, 2025f). CH_4 emissions were calculated using emission factors from Mitchell et al. (2015), as applied in the 2023 National Inventory Report (Australian Government, 2025a), based on gas throughput at each facility. This approach assumes that all reported gas flow is processed through the plants. Where there were two or more processing plants across a production field, emissions were spread evenly across the facilities.

Coal seam gas and conventional natural gas (gathering and boosting stations)

CH_4 emissions were calculated using emission factors from Zimmerle et al. (2020), as applied in the 2023 National Inventory Report (Australian Government, 2025a), based on gas throughput at each of the processing plants listed above. This approach assumes that all gas reported from the processing facilities subsequently passes through the gathering and boosting stations.

Since gas flows through each gathering and boosting facilities was unavailable, gas flows from each processing facility were spread evenly across gathering and boosting facilities within each field.

Solid waste disposal

Landfills were manually located using Google Maps (Google LLC, USA). These included the Moranbah Waste Management Facility, Dysart Waste Management Facility, Blackwater Landfill, Lochlees Landfill and Middlemount Waste Management Facility. Emissions were estimated by scaling Queensland's total emissions for these sources within Australia's Paris Agreement inventory (DCCEEW, 2026) according to the Bowen Basin's share of the state population (1.9%). Total CH_4 emissions were divided evenly across each facility located in the study area, since emissions from individual facilities were not publicly available.

Abandoned oil and gas wells

The locations of individual abandoned oil and gas wells were obtained from the State of Queensland Geoscientific Information/Boreholes MapServer (Queensland Government, 2025e). Emissions were calculated using National Inventory Report (2023) emission factors for wells that have been either plugged (2.0×10^{-5} t a^{-1} CH_4), unplugged (8.8×10^{-2} t a^{-1} CH_4) or have an unknown sealing status (1.2×10^{-2} t a^{-1} CH_4; Australian Government, 2025b). These emissions were spatially resolved across the inventory.

Fertiliser plants

Emissions from two ammonium nitrate plant facilities were derived from CH_4 emissions reported under the Safeguard Mechanism for FY24 (CER, 2025b). These included the Dyno Nobel Ammonia Plant and Queensland Nitrates Ammonium Nitrate Plant.

Road transportation, residential sources and domestic wastewater

Emissions from road transportation, residential sources and domestic wastewater were estimated by scaling Queensland's total emissions for these sources within Australia's Paris Agreement inventory (DCCEEW, 2026) according to the Bowen Basin's share of the state population (1.9%). For domestic wastewater, total CH_4 emissions were divided evenly across each facility located in the study area using Google Earth, since emissions from individual facilities were not publicly available. These included the Black Gully Wastewater Treatment Plant, Moura Sewage Treatment Plant and the Sewage Treatment Plant at Moranbah Airport.

Abandoned coal exploration boreholes

The contribution of abandoned coal exploration boreholes to CH_4 emissions in the Bowen Basin is another source of uncertainty in the inventory. Since emissions from these sources are not explicitly reported under Australia's Paris Agreement

inventory (DCCEEW, 2026), assigning an evidenced-based emission factor in line with Australian Government reporting for these potential CH_4 sources is not currently possible. Nonetheless, under the assumption that abandoned coal exploration boreholes are sealed using similar approaches to CSG wells, we assigned the 2023 National Inventory Report emission factors from abandoned oil and gas wells (Australian Government, 2025b) to abandoned coal exploration and water boreholes. It is acknowledged that an individual leaky borehole may have emissions that are much higher, as recently shown by Hoerning and Hayes (2025). However, without the explicit known location of these high-emitting boreholes being available, these cannot be incorporated into the UNSW inventory at present.

Termites

Since there is a paucity of data collected for Australia regarding termite population statistics (Law et al., 2024), we do not attempt to resolve the location and population of termites in the study area. Estimating CH_4 emissions from termite mounds, termite-related soil emissions, and termite-affected deadwood and tree stems is similarly challenging due to a paucity of global and country-scale data. Furthermore, to our knowledge, these emissions are not estimated in Australia's Paris Agreement inventory. Nonetheless, the parameters outlined in Law et al. (2024) were used to derive broad approximations of potential emissions in the study area. We use the midpoint of reported emission factors for termites in mounds (1.56 kg CH_4 ha^{-1} a^{-1}) and fallen deadwood (0.07 kg CH_4 ha^{-1} a^{-1}), extrapolated across 6 million ha, to estimate total annual emissions of 9,780 t CH_4 a^{-1}. Assuming termite mound CH_4 oxidation removes approximately 50% of emissions (Nauer et al., 2018), this estimate was halved to 4,890 t CH_4 a^{-1}, or ~0.14 Mt CO_2-e a^{-1}, or 1.0% of the total bottom-up inventory. Given the variability in emission rates and limited data on termite emissions, this estimate likely carries substantial uncertainty.

Macropods

To approximate the number of macropods, we use reported population estimates from the Queensland Macropod Management Program Annual Report (2023) (State of Queensland, 2024) for Eastern Grey Kangaroos, Red Kangaroos and Common Wallaroos to derive an approximated total of macropods in Queensland (16,267,200 head). Using Queensland's total land area (185.3 Mha), we estimate the population density of each macropod species and subsequently interpolated this density (~0.19 macropods/ha) across the study area (6,000,000 ha). Under these rough assumptions, we derived 1,152,000 macropods. While actual densities likely vary widely with habitat quality, climate, land use, and other ecological factors, these approximations, although uncertain, provide a meaningful basis for comparing the potential magnitude of CH_4 emissions from these dispersed sources with those from coal mines in the Bowen Basin (as discussed in Section 2.3.3 and 3.3 in the main manuscript).

Macropod CH_4 emissions were estimated using a similar approach applied by Vendl et al. (2015), who estimated emissions from macropods in Australia based on empirical CH_4 emissions rates from western grey kangaroos and red kangaroos. Considering a macropod with a mean body mass of 20 kg emits roughly 656 g CH_4 $head^{-1}$ a^{-1}, we estimated that the roughly approximated macropod population contribute 756 t a^{-1} CH_4, equivalent to 0.02 Mt CO_2-e a^{-1}, or 0.2% of the total bottom-up

inventory. As with Vendl et al. (2015), we acknowledge that estimating a realistic average body weight for macropods is challenging due to factors such as sex, regional variation, harvest intensity, and the proportion of juveniles. Nonetheless, given the minor contribution of macropods to total inventory emissions, this body mass assumption is unlikely to have a material impact on the overall emissions total, especially since the macropod emission factor is approximately 76 times lower than that used for grazing cattle in Australia's National Inventory Report (Australian Government, 2025a).

Sheep, swine and poultry

To the authors' knowledge, there are no reported sheep farms, piggeries or poultry farms located in the Bowen Basin (Queensland Government, 2025c).

Table S2. The bottom-up UNSW inventory for the Bowen Basin FY24.

CH_4 Source	Activity unit	Quantity	Emission Factor	Emission factor unit	Emissions (kg CH_4 hr^{-1})	Emissions (t CO_2-e a^{-1})	Percentage contribution
Coal mines (Underground)	ROM coal (t)	26,749,175	Variable	t CO_2-e t^{-1} ROM coal	18,607	4,564,039	35%
Coal mines (Open-cut; reported under Safeguard)	ROM coal (t)	198,043,055	Variable	t CO_2-e t^{-1} ROM coal	17,053	4,182,764	32%
Coal mines (Mine complex)	ROM coal (t)	29,470,097	Variable	t CO_2-e t^{-1} ROM coal	7,462	1,830,247	14%
Grazing cattle	Head (approximate)	1,179,702	0.04993	t CH_4 $head^{-1}$ a^{-1}	6,724	1,649,271	13%
Coal mines (Open-cut; not reported under Safeguard)	ROM coal (t)	6,521,036	0.031	t CO_2-e t^{-1} ROM coal	824	202,152	1.6%
Termites	Population (approximate)	See text	Various; see text for details	See text	558	136,920	1.1%
Feedlot cattle	Head	139,895	0.03045	t CH_4 $head^{-1}$ a^{-1}	486	119,274	0.92%
Farm Dams	Hectare	12,540	0.3	t CH_4 ha^{-1} a^{-1}	429	105,337	0.81%
Gas processing plants	t gas throughput (FY24)	Various	$y = 0.6369x^{-0.48}$	Tonnes of emissions / tonnes of gas throughput	206	50,522	0.39%
Solid waste disposal	Urban population	23,825	Population percentage of Queensland emissions	See text	158	38,730	0.30%
Kangaroos	Population (approximate)	1,152,000	Various; see text for details	See text	86	21,160	0.16%
CMWG Power Stations	Electricity production (GJ)	3,541,032	4.6	kg CO_2-e GJ^{-1}	66	16,289	0.13%
Gas transmission and storage	km of pipeline	1,232	0.41	Tonnes of emissions / pipeline kilometre	58	14,143	0.11%
Gas gathering and boosting pipelines	km of pipeline	1,390	0.23	Tonnes of emissions / pipeline kilometre	36	8,952	0.07%
Gas gathering and boosting stations	t gas throughput (FY24)	Various	$y = 2.386x^{-0.761}$	Tonnes of emissions / tonnes of gas throughput	24	5,978	0.05%
Domestic wastewater	Urban population	23,825	Population percentage of Queensland emissions	See text	21	5,214	0.04%

CH_4 Source	Activity unit	Quantity	Emission Factor	Emission factor unit	Emissions (kg CH_4 hr^{-1})	Emissions (t CO_2-e a^{-1})	Percentage contribution
Produced water from coal sema gas production	Megalitres (ML)	251	0.31	Tonnes of emissions / ML	9	2,179	0.02%
Abandoned coal exploration boreholes	Boreholes		Plugged: 0.00002; unplugged: 0.088; unknown: 0.012	t a^{-1} CH_4	9	2,086	0.02%
Coal Seam Gas and natural gas (venting)	t gas throughput (FY24)	71	1	Tonnes of emission / tonne of gas vented	8	1,988	0.02%
Residential	Urban population	23,825	Population percentage of Queensland emissions	See text	7	1,649	0.01%
Conventional natural gas (onshore wells)	t gas throughput (FY24)	974,180	4.7×10^{-5}	Tonnes of emissions / tonnes of gas throughput	5	1,282	0.01%
Road transportation	Urban population	23,825	Population percentage of Queensland emissions	See text	3	798	0.01%
Fertilizer plants	Not reported	2	Not reported	Not reported	2	535	<0.01%
Coal Seam Gas and natural gas (flaring)	t gas throughput (FY24)	636	0.02	Tonnes of emission / tonne of gas flared	1	356	<0.01%
Abandoned oil and gas wells	Wells		Plugged: 0.00002; unplugged: 0.088; unknown: 0.012	t a^{-1} CH_4	0	31	<0.01%
Coal Seam Gas (onshore wells)	t gas throughput (FY24)	229,991	7.2×10^{-7}	Tonnes of emissions / tonnes of gas throughput	0	5	<0.01%
Dairy cattle	Head	0	0.01398	t CH_4 $head^{-1}$ a^{-1}	0	0	0%
Sheep	Head	0	0.00034	t CH_4 $head^{-1}$ a^{-1}	0	0	0%
Swine	Head	0	0.02325	t CH_4 $head^{-1}$ a^{-1}	0	0	0%
Poultry	Head	0	0.00004	t CH_4 $head^{-1}$ a^{-1}	0	0	0%
Total					**52,845**	**12,961,899**	**100%**

SI-3: Aircraft instrumentation

In-situ aircraft

The in-situ aircraft carried its scientific instrumentation in two underwing pods and two additional underwing pylons (Fig. S1). Combined GPS/IMU positions, altitude, ground-speed, aircraft 3D-accelerations and aircraft attitude and angular rates were captured by a combined GPS/IMU system at 50Hz and combined with data from a high-resolution 3D-turbulence probe (BAT probe, Hacker and Crawford, 1999) yielding 3D wind and turbulence data at 20Hz final data frequency. Atmospheric concentrations of CH_4 were measured using an ABB Los Gatos Research Ultraportable Greenhouse Gas Analyzer (UGGA), housed in the left underwing pod. The UGGA has a manufacturer-specified precision of 1.4 ppb for CH_4 at a 1 Hz sampling rate. An external MZ 2C Vario pump (2.5 m^3 hr^{-1} flow rate) reduced instrument response time to under 2 seconds. Air was drawn through a ~15 cm external inlet and response-time correction was performed using co-located measurements from a Licor LI-7500 open-path CO_2/H_2O analyser, also mounted in the left pod. The aircraft was also fitted with an aerosol particle spectrometer to enable correlation with airmass history, and video cameras to monitor activities in the mines during the flight. The measured data was displayed in real-time in the cockpit of the aircraft so that the crew can draw on their expertise as scientists to optimise the flight pattern to the given situation observed. The aircraft had a maximum flight time of ~5 hours and typically performed measurements at cruising speeds of 40 m s^{-1}.

Fig. S1. The two Diamond Aircraft HK36TTC-ECO Dimonas owned and operated by Airborne Research Australia. The aircraft on the left is the remote sensing aircraft, and the aircraft on the right is the in-situ aircraft.

Post-flight calibration of CH_4 mole fraction measurements from the UGGA was performed using a secondary standard gas certified by the Commonwealth Scientific and Industrial Research Organisation (CSIRO). The reference gas (tank# FB03750) had target dry CH_4 concentrations of 1844.28 ± 0.14 ppb. Calibration was based on a single reference level, with instrument

linearity specified by the manufacturer over the range of 0.01–100 ppm for CH_4. A one-point offset correction was applied to CH_4 measurements from each flight, based on the mean concentration measured for the calibration gas. Offset corrections measured in this manner were stable throughout the campaign to a level of ±1.8 ppb (±1σ).

The aircraft was also equipped with a purpose-built device to acquire airborne grab samples for subsequent laboratory isotope analysis, which was used in the present study for source attribution. This type of sampling is inherently difficult due to the aircraft's limited residence time in local CH_4 plumes, which is often just a few seconds. Conventional sampling methods, such as filling evacuated canisters or Flexfoil bags, require several seconds to complete and typically rely on a manual trigger based on real-time signals, which introduces additional delay (France et al., 2021; Lerner et al., 2017; Lampert et al., 2020).

To overcome this and capture plume peaks more effectively, a continuous flow-through sampler was designed and housed in the right underwing pod of the aircraft. Airborne grab samples were collected during the mass balance sampling of selected flights (see Table S12 in SI-12). During sample acquisition, the continuous flow-through sampler was flushed by dynamic pressure approximately 40 cm below the wing's leading edge, using a forward-facing 25 mm diameter inlet tube that leads into a 2 L PERSPEX acrylic sample cylinder housed inside the underwing instrument pod. A 25 mm outlet tube extends toward the trailing edge, ensuring efficient flow and rapid response. At the cruising speed of the aircraft, this arrangement resulted in a nominal residence time in the sampling volume of < 0.2 s. The inlet and outlet of the sampling volume were closed by two 25 mm inner diameter, servo attenuated, ball valves within < 0.5 s. The air sample, taken before and while the valves were closing, was then transferred into one of 10 pre-evacuated Flexfoil sampling bags through a manifold system using an internal polyethylene bellow bag. During sampling, the bellow bag inside the sampler was evacuated and folded around an internal half-pipe along the PERSPEX wall to avoid obstructing the airflow. Once the sampler was closed, the manifold solenoid opened and the bellow bag was inflated with a small diaphragm pump within ~90 s, filling the sample cylinder to displace the sample through the manifold into the corresponding sample bag. After the sample was transferred, the manifold was disconnected, the bellow bag was re-evacuated, the ball valves opened and the sampler was ready for the next sequence. The maximum sample volume was 1.8 L which was transferred into 3 L Tedlar sampling bags. Evacuation and transfer flows were controlled by mass flow meters and solenoid valves and pumps were automatically switched from a handheld Raspberry Pico driven control unit providing a monitoring and control interface. The Pico microcomputer also read the GPS position, time and air pressure and logged internally all servo, bag numbers and solenoid control signals. Each sampling sequence starting with closing the inlet and outlet of the inlet tube was activated by the crew based on closely observing the real-time measurements of CH_4 (and some other parameters) on the real-time display in the cockpit. A more comprehensive description of this sampling device will be described in an upcoming publication.

Remote sensing aircraft

The remote sensing aircraft was equipped with the passive airborne remote sensing imager MAMAP2DL, which mapped atmospheric CO_2 and CH_4 concentration gradients (or column anomalies in % or molec cm^{-2}). These column anomalies were used to identify CH_4 sources on the ground and to derive their emission rates to the atmosphere. The core of the instrument was an imaging grating spectrometer that records spectra with a spectral resolution of about 1 nm (full width at half maximum, FWHM) and exploited absorption features of CO_2 and CH_4 around 1.61 µm. The solar radiation backscattered from the surface was mapped onto a 2D sensor via 28 optical fibres, which also defined the number of ground scenes collected in cross-flight direction and, therefore, the covered cross-flight distance. For typical flight conditions during this study, the resulting ground scene size was ~ 45 × 45 m^2 (across × along the flight direction) after binning along the flight direction to increase the signal-to-noise ratio and achieving more uniform cross-track and along-track sample spacing. The across flight direction swath width was thus ~ 1.3 km. Figure S2 provides a schematic representation of the flight and observation geometry.

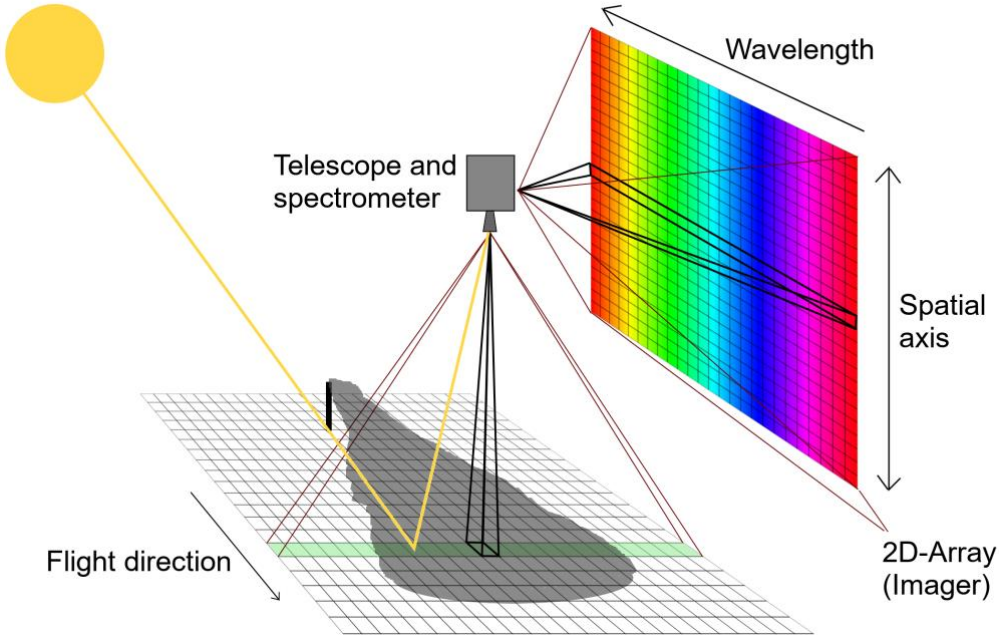

Fig. S2. The schematic diagram shows the measurement principle of MAMAP2DL. The instrument simultaneously acquires 28 ground scenes across the flight track with a swath width of ~ 1.3 km at a flight altitude of ~ 3.3 km AGL. The final ground scene size is ~ 45 x 45 m^2.

The column anomalies of the MAMAP2DL imager were derived along the lines as described in Krautwurst et al. (2021, 2025) and Borchardt et al. (2025) using the Weighting Function Modified - Differential Absorption Spectroscopy (WFMD) approach in combination with the proxy method. Simulated radiances were fitted to the measured spectra by scaling weighting functions. Both radiances and weighting functions were computed by the radiative transfer model (RTM) SCIATRAN (v3.8, Mei et al., 2023; Rozanov et al., 2014) and were adapted to the atmospheric and geometrical conditions of a flight day. The resulting gas

columns were subsequently normalised to the local background to obtain the background normalised column anomaly maps of CH_4, or just CH_4 anomalies. These CH_4 anomalies were orthorectified and, in combination with the prevailing wind field, positive anomalies were interpreted as CH_4 emission plumes originating from mining operations and were used to determine their emission rates (see SI-5). To reduce the errors of the retrieved column anomalies, a specific set of RTM simulations was computed for each flight also using a 1D look-up table for the surface elevation. The precision of the column anomalies for this study was ~ 0.4% (1σ), similar to previous studies (~ 0.4% in Borchardt et al., 2025 and Krautwurst et al., 2025). Accuracy plays only a minor role as any offsets are usually removed by the normalisation process with the local CH_4 background or by the proxy method. The conservative estimate of the potential residual error in accuracy, which cannot be corrected, was ~ 0.2%. In addition, the retrieval had different sensitivities with respect to the altitude at which the CH_4 plume was located, which was corrected during the retrieval process (Krautwurst et al., 2025; Krings et al., 2011, 2013). However, this conversion factor (cf) also had an uncertainty, conservatively being estimated to be ~ 2% of the value of the conversion factor.

The accuracy of the orthorectification process, which determined how well we can assign observed emission plumes and thus estimated emission rates to specific facilities or mines, was estimated to be better than 50 m or a ground scene of MAMAP2DL relative to Google Earth imagery (for details, see Krautwurst et al., 2025). For the correction, we used location and attitude data from a MicroStrain 3DM-GQ7-GNSS/INS system recorded at 10 Hz and mounted near the front telescope, which collected the backscattered electromagnetic radiation from the ground.

SI-4: Airborne survey summary

Table S3 summarises key details from the airborne surveys conducted by both aircraft between 5 September and 5 October 2023. These details include mission dates, flight times, curtain and plume identifiers, wind speeds and directions during the flights, the type of quantification (facility, multi-facility, or sub-facility; see Section 2.4 in the main text), the coal mines quantified, whether CH_4 isotope data were collected during the flight, and whether the data were of sufficient quality to compare against operator estimates.

Table S3. Summary of all research flights performed during the campaign. Note that instrument testing was performed on three flights prior to 5 September 2023, with the first measurements acquired on research flight 4 (RF04).

Date (dd/mm/yy)	Flight ID	Aircraft	Time (UTC)	Identifier[a]	N[b]	Wind speed (m s^{-1})[c]	Wind direction (°)[c]	Quantification type	Quantified coal mine(s)	CH_4 Isotopes[d]	Included in evaluation?[e]
05/09/23	RF04	In-situ	03:14-04.53	230905_C1	13	1.6-3.3	335-16	Multi-facility	OC-13, UG-3, MC-2-UG	No	Yes
		Remote sensing	03:28	P4.1	1	1.9		Facility	OC-13	N/A	No
		Remote sensing	02:43-03:06	P4.2	3	2.0-2.3	353-0	Facility	MC-2-UG	N/A	Yes (1)
		Remote sensing	02:43-02:56	P4.3	2	2.1-2.3	24 (352-353)	N/A	Unidentified source	N/A	No
		Remote sensing	02:43	P4.4	1	2.3	30 (352)	Sub-facility	UG-3	N/A	No
06/09/23	RF05	In-situ	00:58-03:13	230906_C1	5	3.8-6.5	63-76	Multi-facility	OC-16, OC-17	$\delta^{13}C$	Yes
		In-situ	01:17-02:11	230906_C2	2	4.8-5.2	81-83	Multi-facility	OC-18 to OC-32, UG-4 to UG-8, MC-3	$\delta^{13}C$	No
		In-situ	03:20-03:55	230906_C3	3	5.1-5.6	62-75	Facility	OC-16	No	Yes
		Remote sensing	03:31	P5.1	1	5.4	79 (90)	Sub-facility	MC-3-UG	N/A	No
		Remote sensing	03:28	P5.2	1	5.4	81 (89)	Sub-facility	UG-6	N/A	Yes (1)
		Remote sensing	02:14	P5.3	1	4.9	96 (94)	Sub-facility	UG-8	N/A	No
09/09/23	RF06	In-situ	01:58-03:11	230909_C1	9	3.0-4.2	100-139	Multi-facility	UG-3, MC-2	$\delta^{13}C$, $\delta^{2}H$	Yes
		In-situ	03:26-05:14	230909_C2	8	2.1-3.4	106-134	Multi-facility	UG-3, MC-2	$\delta^{13}C$, $\delta^{2}H$	Yes
		Remote sensing	04:09	P6.1	1	4.5	- (142)	Sub-facility	OC-13	N/A	No
		Remote sensing	03:23-04:03	P6.2	4	4.5	113-135 (141)	Facility	MC-2-UG	N/A	Yes (3)
		Remote sensing	02:59-03:25	P6.3	3	4.5	119-128 (142)	Sub-facility	UG-3	N/A	Yes (1)
		Remote sensing	02:32-03:25	P6.4	5	4.5-4.6	112-142 (142)	Sub-facility	UG-3	N/A	Yes (3)
		Remote sensing	02:34	P6.5	1	4.6	103 (142)	Sub-facility	UG-3	N/A	Yes (1)
		Remote sensing	03:38	P6.6	1	4.5	148 (143)	N/A	Unidentified source	N/A	No
11/09/23	RF07	In-situ	01:23-02:19	230911_C1	6	6.6-7.9	104-113	Multi-facility	OC-25 to OC-27, UG-5, UG-6	$\delta^{13}C$	No
		Remote sensing	01:36-01:45	P7.1	2	7.9	99 (115-116)	Sub-facility	MC-3-UG	N/A	No
		Remote sensing	02:09-02:31	P7.2/7.3	3	7.7-7.8	105-121 (117-119)	Sub-facility	UG-6	N/A	Yes (3)
		Remote sensing	01:34	P7.4	1	7.9	112.5 (114)	Sub-facility	UG-6	N/A	Yes (1)
		Remote sensing	02:00	P7.5	1	7.8	107 (117)	Sub-facility	UG-6	N/A	Yes (1)
		Remote sensing	02:13-02:34	P7.6	3	7.7-7.8	97-148 (117-119)	Facility	UG-4	N/A	Yes (2)
		Remote sensing	01:45	P7.7	1	7.9	- (115)	Sub-facility	MC-3-UG	N/A	No
15/09/23	RF08	In-situ	00:42-01:25	230915_C1[f]	3	8.3-8.5	127-128	Facility	OC-32	$\delta^{13}C$, $\delta^{2}H$	Yes
		In-situ	01:27-01:55	230915_C2[f]	3	8.3-8.8	130-139	Facility	OC-32	$\delta^{13}C$, $\delta^{2}H$	Yes
		In-situ	01:57-02:13	230915_C3[f]	2	8.4-8.8	128-138	Facility	OC-32	$\delta^{13}C$, $\delta^{2}H$	Yes
		Remote sensing	01:10-03:53	P8.1[f]	9	7.0-7.3	- (133-136)	Facility	OC-32	N/A	No
16/09/23	RF09	In-situ	04:02-04:26	230916_C1	3	6.5-7.4	99-108	Facility	OC-12	No	Yes
		In-situ	00:37-04:00	230916_C2A	3	6.6-7.3	106-115	Facility	OC-12	$\delta^{13}C$, $\delta^{2}H$	Yes
		In-situ	00:37-04:00	230916_C2B	3	6.6-7.3	106-115	Facility	MC-2-OC, UG-3	$\delta^{13}C$, $\delta^{2}H$	No
		In-situ	00:58-03:02	230916_C3A	3	5.8-7.9	114-126	Facility	MC-2	$\delta^{13}C$, $\delta^{2}H$	Yes
		In-situ	00:58-03:02	230916_C3B	3	5.8-7.9	114-126	Facility	OC-12, OC-13	$\delta^{13}C$, $\delta^{2}H$	Yes
		In-situ	00:58-03:02	230916_C3C	3	5.8-7.9	114-126	Facility	UG-3	$\delta^{13}C$, $\delta^{2}H$	Yes

Date (dd/mm/yy)	Flight ID	Aircraft	Time (UTC)	Identifier[a]	N[b]	Wind speed (m s^{-1})[c]	Wind direction (°)[c]	Quantification type	Quantified coal mine(s)	CH_4 Isotopes[d]	Included in evaluation?[e]
		In-situ	01:18-02:13	230916_C4A	3	5.8-7.8	111-116	Facility	MC-2	$\delta^{13}C$, $\delta^{2}H$	Yes
		In-situ	01:18-02:13	230916_C4B	3	5.8-7.8	111-116	Facility	OC-12, OC-13	$\delta^{13}C$, $\delta^{2}H$	Yes
		In-situ	01:18-02:13	230916_C4C	3	5.8-7.8	111-116	Facility	UG-3	$\delta^{13}C$, $\delta^{2}H$	Yes
		Remote sensing	02:40-02:45	P9.1	2	6.1	- (110-111)	Sub-facility	OC-13	N/A	No
		Remote sensing	02:33-03:25	P9.2	4	6.2-6.3	107-136 (108-110)	Facility	MC-2-UG	N/A	Yes (4)
		Remote sensing	01:59-02:23	P9.3	2	6.1-6.2	105-107 (110-112)	Sub-facility	UG-3	N/A	Yes (2)
		Remote sensing	01:35-01:59	P9.4	3	6.1	103-133 (112)	Sub-facility	UG-3	N/A	Yes (2)
		Remote sensing	01:53-01:58	P9.5	2	6.1	100-120 (111)	Sub-facility	UG-3	N/A	Yes (2)
		Remote sensing	02:36-02:50	P9.6	2	6.1-6.2	85 (110)	N/A	Unidentified source	N/A	No
17/09/23	RF10	In-situ	01:02-02:07	230917_C1	4	6.4-8.1	103-110	Facility	MC-1	No	Yes
		In-situ	00:31-01:42	230917_C2	3	5.9-8.7	98-106	Facility	MC-1	No	Yes
		In-situ	02:27-03:24	230917_C3	4	7.8-8.8	110-115	Facility	UG-2	No	Yes
		Remote sensing	01:56-03:14	P10.1	6	6.6-7.0	98-143 (114)	Sub-facility	UG-2	N/A	Yes (4)
		Remote sensing	01:55-02:45	P10.2	4	6.5-6.9	113 (114)	Sub-facility	UG-2	N/A	Yes (3)
		Remote sensing	01:54-02:17	P10.3	2	6.5-6.6	116-130 (114)	Sub-facility	UG-2	N/A	Yes (2)
		Remote sensing	04:13-04:27	P10.4	2	6.4-6.5	91(112)	Sub-facility	MC-1	N/A	Yes (1)
19/09/23	RF11	Remote sensing	01:35-01:44	P11.1	3	3.0-3.1	- (90)	Facility	OC-13	N/A	No
		Remote sensing	01:44-02:03	P11.2	5	3.0	- (90-91)	Facility	OC-13	N/A	No
21/09/23	RF12	Remote sensing	02:26-03:02	P12.1	4	2.7-3.9	- (164-197)	Sub-facility	UG-2	N/A	No
		Remote sensing	02:31-03:01	P12.2	2	2.9-3.9	- (164-193)	Sub-facility	UG-2	N/A	No
22/09/23	RF13	In-situ	02:17-03:41	230922_C1	14	1.2-3.8	106-154	Multi-facility	OC-22 to OC-24, UG-5	$\delta^{13}C$	No
		Remote sensing	03:25-03:27	P13.1	2	3.3	140 (128-130)	Facility	OC-28, OC-30	N/A	Yes (2)
		Remote sensing	02:46-03:02	P13.2	3	3.0	146 (134-139)	Sub-facility	UG-5	N/A	No
		Remote sensing	02:02-02:18	P13.3	3	2.7-2.8	- (145-151)	Facility	OC-22	N/A	No
23/09/23	RF14	In-situ	01:52-04:20	230923_C1	12	1.9-3.3	84-125	Multi-facility	OC-5, UG-1	$\delta^{13}C$	Yes
25/09/23	RF15	In-situ	01:44-03:00	230925_C1	7	2.5-4.2	79-107	Facility	OC-30	$\delta^{13}C$, $\delta^{2}H$	Yes
26/09/23	RF16	In-situ	01:07-01:39	230926_C1	4	5.2-7.0	71-114	Facility	OC-14	No	Yes
			02:39-04:29	230926_C2	8	2.5-4.2	77-95	Multi-facility	OC-12, UG-3, MC-2	No	Yes
		Remote sensing	04:07-04:16	P16.1	2	3.9	- (96)	Facility	OC-12	N/A	No
		Remote sensing	03:59-04:14	P16.2	4	3.9	84-116 (97)	Facility	OC-12	N/A	No
27/09/23	RF17	In-situ	01:30-04:34	230927_C1	8	5.1-6.5	109-118	Multi-facility	OC-20 to OC-31, UG-4 to UG-8, MC-3	$\delta^{13}C$, $\delta^{2}H$	No
		Remote sensing	03:10-03:26	P17.1	3	6.5	130-153 (117-118)	Sub-facility	MC-3-UG	N/A	No
		Remote sensing	03:23-03:26	P17.2	2	6.5	153 (118)	Sub-facility	MC-3-UG	N/A	No
		Remote sensing	01:44-01:51	P17.3	2	5.8	132 (109-110)	Facility	UG-4	N/A	Yes (1)
		Remote sensing	04:20	P17.4	1	6.1	- (121)	Facility	OC-19	N/A	No
28/09/23	RF18	In-situ	01:43-02:38	230928_C1[f]	9	5.4-9.1	103-133	Facility	OC-32	$\delta^{13}C$, $\delta^{2}H$	Yes
		In-situ	03:00-03:58	230928_C2[f]	10	7.5-12.6	96-120	Facility	OC-32	$\delta^{13}C$, $\delta^{2}H$	Yes
		Remote sensing	02:52-04:06	P18.1[f]	9	10	105	Facility	OC-32	N/A	Yes (6)

Date (dd/mm/yy)	Flight ID	Aircraft	Time (UTC)	Identifier[a]	N[b]	Wind speed (m s^{-1})[c]	Wind direction (°)[c]	Quantification type	Quantified coal mine(s)	CH_4 Isotopes[d]	Included in evaluation?[e]
		Remote sensing	04:47-04:48	P18.2[f]	1	8.1	101 (102)	Sub-facility	UG-5	N/A	No
29/09/23	RF19	In-situ	03:10-03:51	230929_C1[f]	7	8.3-9.1	83-103	Facility	OC-32	No	Yes
		In-situ	01:34-02:47	230929_C2[f]	10	6.9-14.6	80-89	Facility	OC-32	No	Yes
01/10/23	RF20	In-situ	01:16-02:18	231001_C1	4	2.9-6.8	45-102	Multi-facility	OC-5, UG-1	No	No
		Remote sensing	01:23-01:34	P20.1	2	4.0	- (57)	Facility	OC-5	N/A	No
02/10/23	RF21	In-situ	01:42-03:55	231002_C1	7	2.9-5.3	90-120	Multi-facility	OC-22 to OC-30, UG-4 to UG-8, MC-3	$\delta^{13}C$	No
03/10/23	RF22	In-situ	00:06-01:05	231003_C1	8	4.6-5.2	52-70	Facility	OC-12	$\delta^{13}C$	Yes
		In-situ	01:17-02:04	231003_C2	6	3.7-5.9	48-66	Multi-facility	OC-12, MC-2-OC	$\delta^{13}C$	Yes
04/10/23	RF23	In-situ	01:40-03:34	231004_C1	9	0.5-2.1	357-83	Multi-facility	OC-28, OC-30	$\delta^{13}C$	No
05/10/23	RF24	In-situ	01:29-03:24	231005_C1	6	1.1-5.1	200-318	Multi-facility	UG-3, MC-2-UG	No	No
		In-situ		231005_C2	6	1.0-3.9	221-306	Multi-facility	UG-3, MC-2-UG	No	No

[a)]Naming convention for remote sensing aircraft plumes is explained in SI-5. [b)]Refers to number of transects (in-situ aircraft) or legs (remote sensing aircraft). [c)]Wind speed and direction for the in-situ aircraft were determined from the onboard BAT probe (see text for details), whereas wind speeds for the remote sensing aircraft are those from the ECMWF model and wind directions are derived from the observed plume and source location; values in brackets gives data derived from the ECMWF model for comparison. For computation of the remote sensing wind speed and direction of RF18, see Borchardt et al. (2025). [d)]Designates whether a bag sample was acquired for isotopic sampling for $\delta^{13}C$ and/or $\delta^{2}H$ at any occasion during the curtain. [e)]Only quantifications deemed to have been acquired under suitable sampling conditions were included in the evaluation of NGER Methods. In the case of remote sensing plumes, bracketed numbers indicated the number of legs used in the analysis. [f)]Estimates are previously reported in Borchardt et al. (2025) and are used here for comparison with the most recent operator reporting.

SI-5: Airborne sampling and quantification approaches

In-situ aircraft

In-situ aircraft curtains were labelled with an identifier corresponding to the date they were flown (YYMMDD_), followed by the curtain number for that day (C1, C2, etc.). On occasions where CH_4 plumes were detected during ferry flights to and from a targeted facility, no attempt was made to model emission rates from these plumes, as they would carry large uncertainties (typically comprising only one transect within the convective mixed layer) and would not provide practical comparisons to operator estimates for the purpose of evaluating NGER methods for coal mine CH_4. Where there was clear separation between plumes within a curtain originating from different coal mines (that is, background CH_4 concentrations were reached for a substantial portion of the transect prior to sampling another distinct plume) a wind direction filter was applied to isolate emissions and derive a facility-scale for each quantifiable mine. In these cases, each curtain was designated with letters A, B, and C to indicate the separation. If no separation was possible (that is, the plumes were mixed at any point in the sampling of the curtain) the emissions from the curtain were not disaggregated according to individual facilities and considered a multi-facility estimate (as outlined in Section 2.4 of the main manuscript).

In a sustained monitoring program for a single facility or group of facilities, curtains would have been sampled only under the most favourable weather conditions, such as when wind directions were consistent and favourable, wind speeds were sufficiently high, and there was enough time to complete a sufficiently dense number of transects downwind of the target mine(s). In our campaign, however, the limited availability of instrumentation and the unpredictability of weather forecasts did not allow for such selectivity, so several surveys were conducted under less-than-ideal conditions. For this reason, we excluded 10 curtains from our analysis, retaining 29 that were collected under suitable measurement conditions and considered robust enough to compare with operator-reported estimates. The curtains were omitted for one or more of the following reasons:

1. Wind speeds were too low (<2 m s^{-1}) during a significant portion of the measurement. This could lead to the accumulation of emissions within open-cut coal mines, which could introduce a high bias to the emission rate estimate. Two curtains were omitted due to this reason (230922_C1, 231004_C1).
2. Wind directions varied too substantially within the convective mixed layer (> 45°) to confidently and consistently attribute the measured downwind plume to a specific facility or group of facilities. Five curtains were omitted due to this reason (230922_C1, 231001_C1, 231004_C1, 231005_C1, 231005_C2).
3. Transect sampling density was too low (≤2 transects) and did not adequately capture the CH_4 plume below the convective mixing layer height, resulting in large measurement uncertainties that were highly sensitive to assumptions about the mixing layer height and/or the altitude of the lowest flown transect. One curtain was omitted due to this reason (230906_C2).

4. Insufficient background air was sampled on one or both sides of the CH_4 plume(s) at multiple altitudes, introducing a systematic low bias into the flux estimate because the plume was not fully captured within each transect (i.e., the aircraft was not able to measure the full horizontal extent of the plume). Eight curtains were omitted for this reason (230911_C1, 230916_C2B, 230922_C1, 230927_C1, 231001_C1, 231002_C1, 231005_C1, 231005_C2). In some cases, this issue was avoidable because individual transects that did not adequately sample either side of the plume could be removed from the quantifications without compromising its overall sampling density (230923_C1).

The rate of CH_4 emission (E) for the retained 29 curtains was derived from the integral of mass fluxes derived at each sample point in the downwind curtain via:

$$E = \iint \Delta C_i \cdot \frac{\rho_i M}{R T_i} \cdot v_{\perp i}\, dx\, dz \qquad \text{(Eq. S1)}$$

where ΔC_i was the dry concentration enhancement of CH_4 over the background, ρ_i was pressure, M was the molecular weight of CH_4, R was the ideal gas constant, T_i was temperature and $v_{\perp i}$ was perpendicular wind speed. The resulting mass fluxes from Eq. (S1) were integrated across the horizontal length of the CH_4 plume (x) to give the total mass flux within each transect. Transect emission rates were linearly interpolated between transects across the vertical dimension (z) from the ground surface to the convective mixed layer height to yield a total rate of emission for each curtain (Erland et al., 2022; Pühl et al., 2024). Since emissions at the ground surface could not be sampled, a constant extrapolation of emission rates from the lowest transect to the ground surface was applied. Convective mixed layer heights were estimated using onboard vertical meteorological profiles, including dewpoint, virtual potential temperature, and wind direction. When the aircraft did not reach the top of the convective mixed layer, these heights were instead derived from the Hybrid Single Particle Lagrangian Integrated Transport (HYSPLIT) model (Stein et al., 2015, Rolph et al., 2017) at the time flown by the aircraft. In cases where a transect was flown above the top of the CH_4 plume, the maximum plume height was estimated as halfway between the highest transect showing enhancement and the lowest one without. When this was not possible, fluxes from the highest transect were extrapolated to the top of the convective mixed layer and assumed to be half that of the uppermost transect.

In each transect, background CH_4 concentrations were identified by applying a quantile-based threshold incorporating twice the measurement precision of the LGR UGGA instrument (2×1.4 ppb CH_4), followed by smoothing with a 10 s rolling mean and gap-filling via interpolation (see Lunt et al., 2025 and Borchardt et al., 2025 for further details). The smoothed background was then subtracted from the raw CH_4 measurements (Fig. S3a and S3c) to derive ΔC_i (Fig. S3b and S3d). The threshold of twice the measurement precision was applied to minimise the risk of misinterpreting background fluctuations as true ΔC_i enhancements. A key benefit of using the lateral background either side of the plume was that it experiences the same wind history and conditions as the main plume.

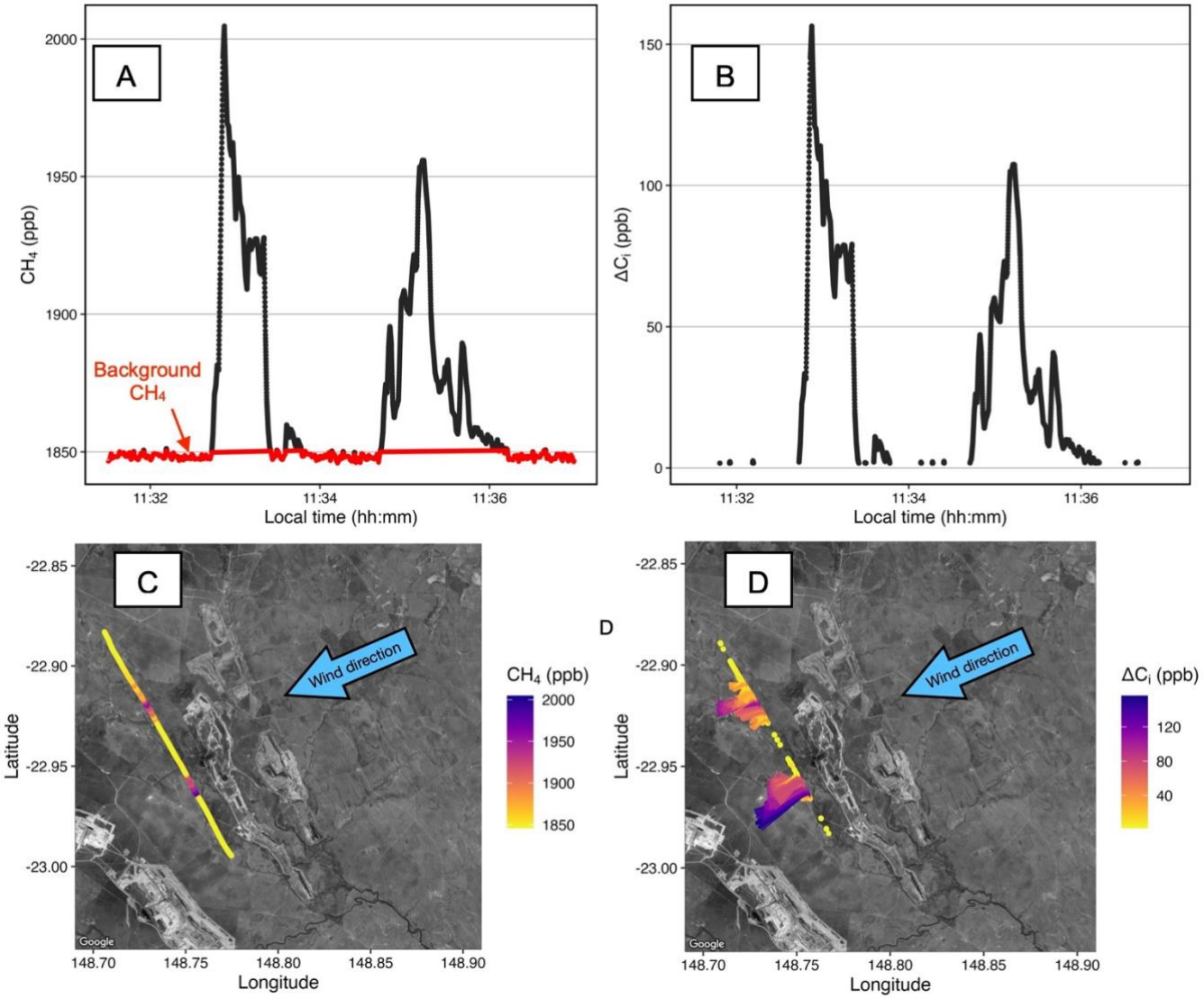

Fig. S3. A) Example raw timeseries CH_4 concentration data (black) measured during a transect flown downwind of an open-cut coal mine. The background CH_4 signal is shown in red. B) ΔC_i concentrations derived after subtraction of the background CH_4 signal in A). C) Location of the raw CH_4 concentration data within a curtain transect, with the mean wind direction in the transect indicated. D) Location of the ΔC_i data within a curtain transect. Each ΔC_i data point is represented by a vector pointing in the wind direction, with its length proportional to the magnitude of ΔC_i. Satellite imagery ©2026 Airbus, CNES/Airbus, Maxar Technologies. Map data ©2026 Google.

The single-screen mass balance approach applied by the in-situ aircraft maximised plume sampling time and allowed more downwind transects to be included in each curtain, thereby reducing the uncertainty of individual estimates and enabling a larger number of coal mines to be sampled. This was also necessary because some coal mines in the study area were up to ~150 km from the airport that served as the study base, reducing the available flight time for sampling. Compared to spiral or

box flight patterns, this approach was more efficient, as it prioritised measuring the downwind plume over background or upwind sampling. However, since CH_4 concentrations were not always measured upwind of the target coal mine, a further assessment of upwind emissions on a curtain-by-curtain basis was undertaken (as addressed in the present study in Sections 3.3 and 4.2 of the main text).

For each curtain the uncertainty in wind speed, pressure, and temperature was estimated by varying each parameter by its respective instrument precision: ±0.3 m/s for wind speed, ±50 Pa for pressure, and ±0.5 K for temperature (based on the BAT probe specifications; Hacker et al., 2016). CH_4 concentration uncertainty was assessed by adjusting the CH_4 enhancements by ±1.4 ppb, reflecting the precision of the UGGA CH_4 analyser. For the background time series, uncertainty was assessed by varying the background concentration by ±1 SD. In the absence of ground-based measurements, the surface flux was equal to the value observed in the lowest flown transect. To estimate the uncertainty associated with this assumption, the surface flux was varied by ±50% of the lowest transect flux. Varying by this percentage typically accounts for an emissions profile that both decreases and increases to the surface (Borchardt et al., 2025). The uncertainty in convective mixed layer height was estimated by varying this height by ±100 m. The uncertainty related to the extrapolation of emissions to the convective mixing layer height was assessed by varying the flux at this height by ±100%. To characterise the uncertainty associated with our sampling design, the flux for each quantification was recalculated multiple times, each time omitting one transect (i.e., using $n-1$ transects). The 1σ uncertainty was then derived from the resulting distribution, providing an assessment of how sensitive the flux estimate was to the inclusion of individual transects. Assuming the uncertainties of individual components were independent, the total uncertainty for each quantification was derived by summing the individual uncertainties in quadrature. The contribution of each source of uncertainty for the retained 29 quantifications is summarised in Table S4.

The individual quantifications had an estimated median 1σ uncertainty of ±21% (mean ±25%). The largest sources of error were uncertainties related to the sampling of the plume (median ±11%), CH_4 concentration (median ±7%), the mixing layer height (median ±7%) and the extrapolation of emissions to this height (median ±4%), wind speed (median ±4%) and the extrapolation of emissions to the ground surface (median ±3%). Since the dominant source of uncertainty was the number of transects included in each curtain, there was a scaling of uncertainty related to the transect density in the curtains. Accordingly, all quantifications comprising 7 or more transects had estimated 1σ uncertainties less than ±20%, with a median of ±13% (mean ±13%).

In clear, dry, and warm conditions, common during Spring in inland Queensland, strong surface heating can produce deep convective mixed layers of around 1500-3000 mAGL, and occasionally up to 3000-4000 mAGL on hot and dry afternoons. Therefore, it was not always possible to reach the convective mixed layer when flying a curtain with sufficient transect density. In such cases, measured fluxes needed to be extrapolated to convective mixing layer heights over greater distances, which increases the uncertainty in the emission estimate. In this study, both the uncertainty in the convective mixing layer height and

the need to extrapolate emissions to this height contributed a moderate level of uncertainty to each curtain (a combined median uncertainty of ±11%; Table S4).

Table S4. Summary of uncertainty contributions for the 29 in-situ aircraft quantifications. All uncertainties are at the 1σ level.

Source of uncertainty	Mean (%)	Median (%)	SD (%)	Max (%)	Min (%)
Wind speed	4.9	4.5	1.5	9.5	3.3
CH_4 background	1.5	1.0	1.6	5.5	0.1
CH_4 concentration	7.8	7.2	3.9	19.3	2.6
Pressure	0.6	0.6	0.2	1.7	0.4
Temperature	0.2	0.2	0.1	0.4	0.0
Mixing layer height	7.6	6.7	5.9	23.1	0.0
Extrapolation of emissions to mixing layer height	4.6	4.0	3.9	12.0	0.0
Ground surface extrapolation	3.7	3.2	2.6	13.0	0.0
Sampling (n-1)	18.3	11.4	18.9	83.6	3.1
Total	25.2	21.1	16.8	85.4	8.4

Remote sensing aircraft

During the campaign, 204 flight legs were collected by the remote sensing aircraft. These legs formed the basis for identifying CH_4 emission sources and estimating their emission rates. A flight leg was defined as a segment of a research flight during which the aircraft maintained level flight in a straight line (i.e., between two turns) and the instrument integration time remained constant.

A consistent naming convention was adopted to organise data from the many flight legs required to interpret observed plume signals, using the format P[*f*].[*s*]_leg-[*n*]. Here, *f* denotes the research flight number (4–20), *s* is a source identifier referring to an individual emission source detected during the flight, and *n* is a leg identifier (a letter incremented from *a*) that distinguishes individual flight legs targeting source *s*. For example, a ventilation shaft identified as the second identifiable CH_4 source during research flight 4 observed during flight leg-c, would be assigned the identifiers $f = 4$, n = *c* and $s = 2$; and would correspondingly be named P4.2_leg-c.

Of the 204 flight legs conducted, 86 contained one or more CH_4 plume signals (122 plume signals in total, identified by visual inspection) or CH_4 enhancements potentially suitable for emission rate estimation. However, several factors precluded certain enhancements or plumes from being used in the quantification process. In total, 66 of the 122 plume signals, spanning 47 of

the 86 legs containing CH_4 plumes, were excluded from emission rate calculations. The reasons for excluding these cases from further emission rate quantification were as follows:

1. No distinct, plume-like structure was observed, as required for the cross-sectional flux method. These cases likely represented accumulated CH_4 clouds formed under calm wind conditions, which could lead to overestimated emission rates.
2. The plume was mixed with emissions from other sources or with plumes originating upwind and could not be separated.
3. The observing geometry caused the plume to appear at the edge of a leg or the leg to be strongly tilted relative to the prevailing wind direction, resulting in either truncation of the plume or the absence of suitable background observations.
4. Cloud contamination caused data gaps within the observed plume and background due to quality filtering. Clouds or their shadows could also introduce artefacts in the retrieval process. Additionally, quality filtering alone could lead to data gaps even in cloud-free scenes.
5. Too few ground scenes within a plume contained an enhancement, typically the case for very small emission sources near the MAMAP2DL detection limit, or the plume could not be reasonably separated from the background, resulting in no discernible plume signal.
6. Enhancements were detected directly over open-cut coal mines, where accurate wind-field modelling was not feasible within the framework of this study. Consequently, the cross-sectional flux method would have yielded unreliable flux estimates.

To compute emission rates from for the 56 plume signals contained in the 39 flight legs of CH_4 column anomaly maps, a cross-sectional flux method is applied as outlined in Borchardt et al. (2025) and Krautwurst et al. (2025) and summarised below. In short, the transported mass of CH_4 molecules $F_{M2D,cs}$ (or the areal integrated CH_4 mass flux or the CH_4 mass flow rate in t hr^{-1}) through a cross-section is calculated by:

$$F_{M2D,cs} = f \cdot \Delta x \cdot u \cdot \cos(\alpha) \cdot \sum \Delta V_i \quad \text{(Eq. S2)}$$

where ΔV_i is the retrieved CH_4 column anomaly (molec cm^{-2}), the term $u \cdot \cos(\alpha)$ (m s^{-1}) is the effective perpendicular wind speed component, Δx is the length element, and f is a conversion factor. Fig. S4 details the procedure, starting with a schematic of a MAMAP2DL flight leg distorted by the movement of the aircraft, to which several artificial cross-sections have been added (a), through which the flux is calculated according to Eq. (S2). The subsequent panels (b) and (c) then show the normalisation process to the local CH_4 background concentrations, based on visually separated background areas from the plume area. Figure S5 then shows a real-world example. The effective wind speed applicable to the plume is computed from ECMWF ERA5 (Hersbach et al., 2020) model data by averaging all model layers from the surface to half of the boundary layer height as given in ERA5 and weighting each layer by the number of molecules. The wind direction is directly estimated visually from the observed CH_4 plumes and their potential origin.

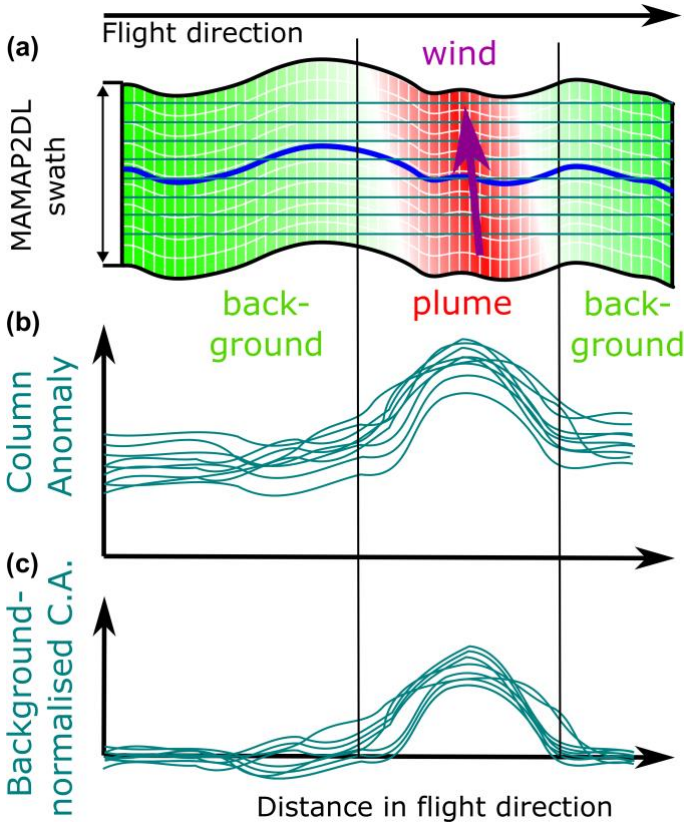

Fig. S4. The schematic details the different steps starting with (a and b) the CH_4 column anomaly maps retrieved from MAMAP2DL to (c) the final background normalised cross-sections needed to quantify the emission rate estimate.

Next, to derive the flux $F_{M2D,leg}$ of a flight leg, the individual cross-sectional fluxes computed by Eq. (S2) are averaged. If there are several legs covering the same source on one flight day, the fluxes of the legs are again averaged to give the mean flux $F_{M2D,ar\text{-}aver}$ of that source on that day.

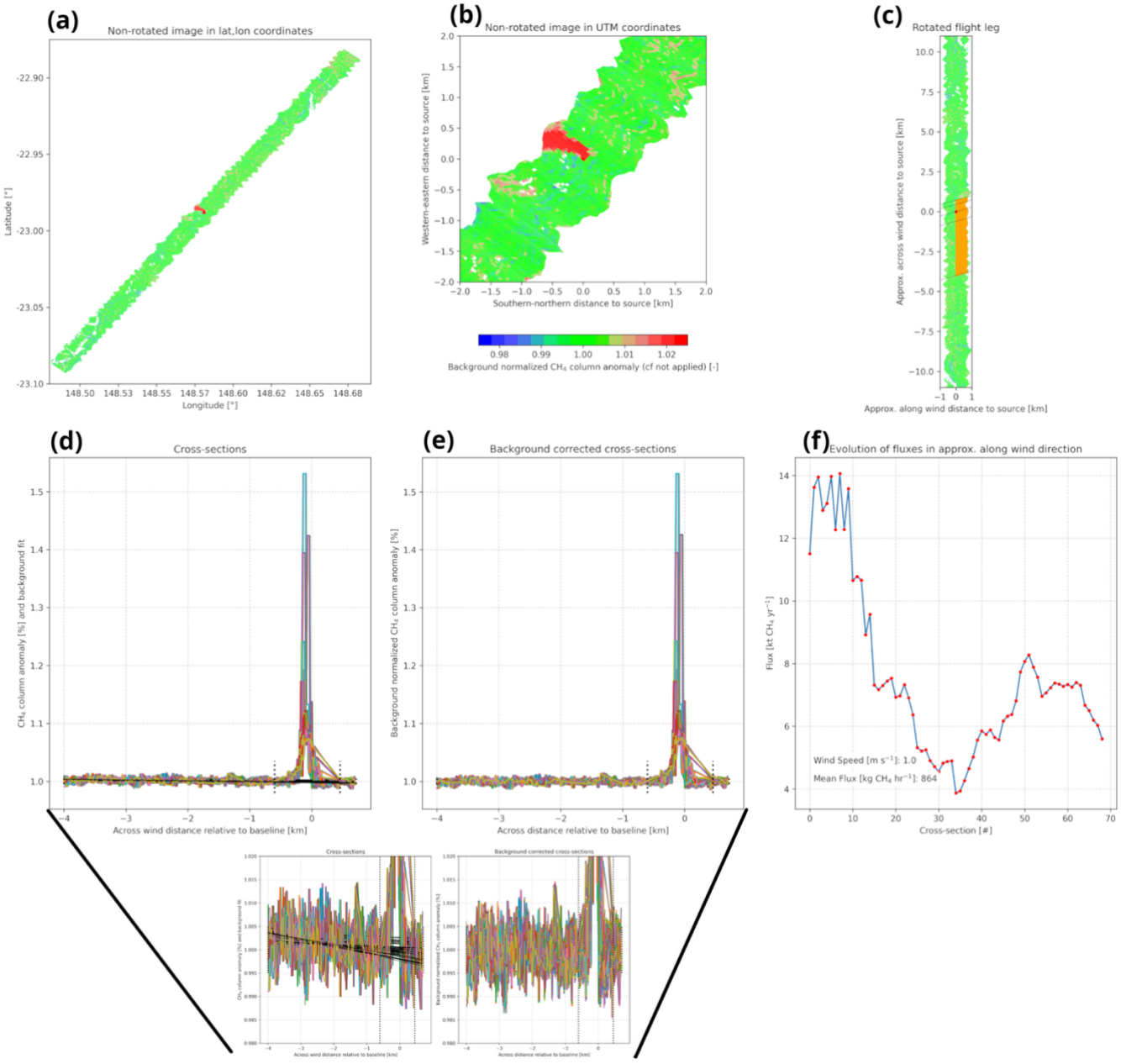

Fig. S5. The subplots show the remote sensing leg of RF06 P6.2-leg-f acquired on 9 September. (a) retrieved CH_4 column anomalies in lat/lon coordinate system (without application of the conversion factor) in lat/lon coordinate system. (b) same as (a) but coordinate system converted to UTM coordinates. (c) same as (b) but rotated so that wind direction and plume points approximately in positive x-direction (for computational reasons, the leg is orientated parallel to the y-axis) including cross-sections through which the flux is computed. (d) CH_4 column anomalies along all cross-sections. (e) same as (d) but CH_4 column anomalies are normalised by the local background (plume signal and background areas are separated by vertical dotted lines). (f) fluxes through the cross-sections as function of the cross-sections spatially resolved from left to right in (c). Fluxes are given for 1 m s^{-1} to allow for easy scaling with prevailing wind speeds and directions during the overflight. The inset at the bottom shows a zoomed-in view of panels (d) and (e), which illustrates a small concentration gradient from left to right for several cross-sections of this leg, as captured by the fitted background lines (solid black). This is subsequently removed before the flux estimate is acquired.

The errors of the different fluxes $F_{M2D,cs}$, $F_{M2D,leg}$, and $F_{M2D,ar\text{-}aver}$ (hereafter: $F_{M2D,plume}$) were estimated by Gaussian error propagation of the individual parameters used in Eq. (S2) where possible and are finally given as errors on the mean. A detailed treatment of the errors can be found in Krautwurst et al. (2025). The main errors in the fluxes or emission rates arise from uncertainties in (a) the effective winds (wind speed (δF_u) and wind direction (δF_α), which are also related to the limited knowledge of the location and vertical distribution of the CH_4 emission plume in the atmosphere), (b) the definition of the background area (δF_{bg}), (c) the column precision ($\delta F_{col\text{-}pr}$) and accuracy ($\delta F_{col\text{-}ac}$) of the CH_4 column anomalies, (d) the conversion factor ($\delta F_{col\text{-}cf}$), and (e) the variability introduced by atmospheric turbulence for the mean flux of a leg ($\delta F_{M2D,\,atm,\,css}$) or an area ($\delta F_{M2D,\,atm,\,legs}$). Table S5 lists typical values for the different components and/or how they have been determined.

Table S5. Summary of relevant error sources applied during error analysis.

Parameter	Assumed uncertainty
δF_u	Variable; SD of vertical wind profile (from ECMWF ERA5) from ground to top of mixing layer
δF_α	10°
δF_{bg}	Variable; up to 50% variation of the background area(s)
$\delta F_{col\text{-}pr}$	~0.4% of the CH_4 background column, but depending on actual cross-section
$\delta F_{col\text{-}ac}$	0.2% of the CH_4 background column
$\delta F_{col\text{-}cf}$	2% of the conversion factor
$\delta F_{M2D,\,atm,\,css}$	Variable; based on SD of cross-sections of one leg
$\delta F_{M2D,\,atm,\,legs}$	Variable; based on SD of legs during one research flight

We derived the wind speed used in the flux estimation from ECMWF ERA5 model data by averaging over half of the convective mixing layer for the remote sensing legs. We believe this is a reasonable assumption on average, as most of the observed plumes are very close to their source. The basic assumption is that the further away the plume is from the source, the better the vertical (but also horizontal) mixing in the atmosphere. However, the plume may also be transported vertically to the top of the boundary layer by convective bubbles close to the source. To account for this uncertainty, we therefore computed the standard deviation (SD) over the whole vertical wind profile in the boundary layer for the wind speed error. If airborne in-situ data were collected at similar times and similar location during a flight, the agreement between the in-situ measured winds within the boundary layer are in reasonable agreement with the estimates based on ERA5 (Table S3).

The approaches for quantification of the emission rates and related errors developed in Krautwurst et al. (2024) and applied in Borchardt et al. (2025) focused on the analysis of emissions from landfills and an open-pit coal mine, respectively, during one overflight (on one day). For the present study, this approach was extended to account for (a) plumes originating from a single facility but observed on multiple days, and (b) multiple plumes originating from the same facility observed on the same day (including at different locations). In case (a), facility-scale quantifications were obtained by averaging flux estimates from

repeated measurements of the same plume, whereas in case (b), they were obtained by summing sub-facility fluxes from all plumes that together represented total facility emissions. Gaussian error propagation was applied in both cases to derive the associated uncertainties. When multiple sets of sub-facility flux estimates (i.e., case b) were available across different days, they were subsequently treated as repeated measurements under case (a), with uncertainties again propagated to the final emission rate estimate.

For case (a):

$$\delta F_{M2D,source} = \frac{\sqrt{\sum \delta F_{M2D,plume,j}^2}}{q} \quad \text{(Eq. S3)}$$

where $\delta F_{M2D,source}$ is the combined error of the emission rate estimates of different days but for the same source, $\delta F_{M2D,plume,j}$ is the error of the emission rate estimate of the plume on day j, and q is the total number of emission rate estimates on the different days.

For case (b):

$$\delta F_{M2D,sources} = \sqrt{\sum \delta F_{M2D,plume,j}^2} \quad \text{(Eq. S4)}$$

where $\delta F_{M2D,source}$ is the combined error of the emission rate estimates of different sources on the same day.

The contribution of the different uncertainty sources responsible for the error of the 46 quantified plumes from which the 24 quantifications are inferred, are listed in Table S5. The two largest estimated error sources were the effect of atmospheric turbulence on the single cross-sections within on leg of one plume signal (median ±23%) and the uncertainty of the background area (median ±19%). The uncertainty of the wind speed contributed significantly with ±15% (median). The uncertainty in wind direction (median ±4%), conversion factor (median ±2%) as well as the column precision and accuracy (median ±0.3%) were only minor uncertainty sources.

Table S5. Summary of uncertainty contributions of the 46 plume signals used to derive the 24 remote sensing quantifications. All uncertainties are at the 1σ level.

Source of uncertainty within plume signals	Mean (%)	Median (%)	SD (%)	Min (%)	Max (%)
Cross-sections (includes the column precision and accuracy)	0.4	0.3	0.3	0.1	1.7
Atmospheric turbulence for cross-section of one leg	26.0	22.5	17.6	2.5	77.3
Wind speed	18.8	14.7	11.1	6.9	44.4
Wind direction	4.9	4.1	2.4	2.2	13.1
Background area	25.9	18.9	26.0	3.5	163.5

Conversion factor	1.8	2.0	0.6	0.2	2.9

Of the 46 quantifiable plume signals, 20 corresponded directly to facility-scale emission rate estimates. The remaining 26 represented sub-facility plumes, which were aggregated into 4 facility-scale estimates, yielding a total of 24 facility quantifications. These 24 individual estimates had a median 1σ uncertainty of ±25% (mean ±28%; derived from quantifications shown later in SI-8).

All plumes quantified by the remote sensing aircraft and used in the bias assessment did not exhibit visually apparent upwind CH_4 enhancements, indicating that the observed emissions arise from the identified sources rather than from inflowing polluted air masses. To support this observation, the upwind portion of a leg containing a quantifiable plume (P6.2_leg-f) was analysed using the standard emission rate quantification procedure, yielding an upwind flux of 0.15 t hr^{-1} CH_4 (Fig. S6, b). This value lies well within the estimated flux error of the plume quantified within the downwind portion of the same leg (Fig. S6, e; 3.7 ± 0.93 [±1σ] t hr^{-1}). Similar low emission rate estimates (0.013 and 0.009 t hr^{-1}) were obtained for two additional upwind legs (P6.2_leg-d and leg-e, Fig. S6, e and f) located up to 3 km upwind of the source and, therefore, did not show any detectable enhancements. On average, the mean upwind emission rate based on the three upwind legs was 0.06 t hr^{-1}, approximately 1.5% of the measured downwind emission rate of P6.2 (based on legs f, g, and h: (3.8 ± 0.82) t hr^{-1}) and well within the quantification error margins. This consistency indicates that the absence of significant upwind contributions is expected to hold for all other plumes measured by the remote sensing aircraft.

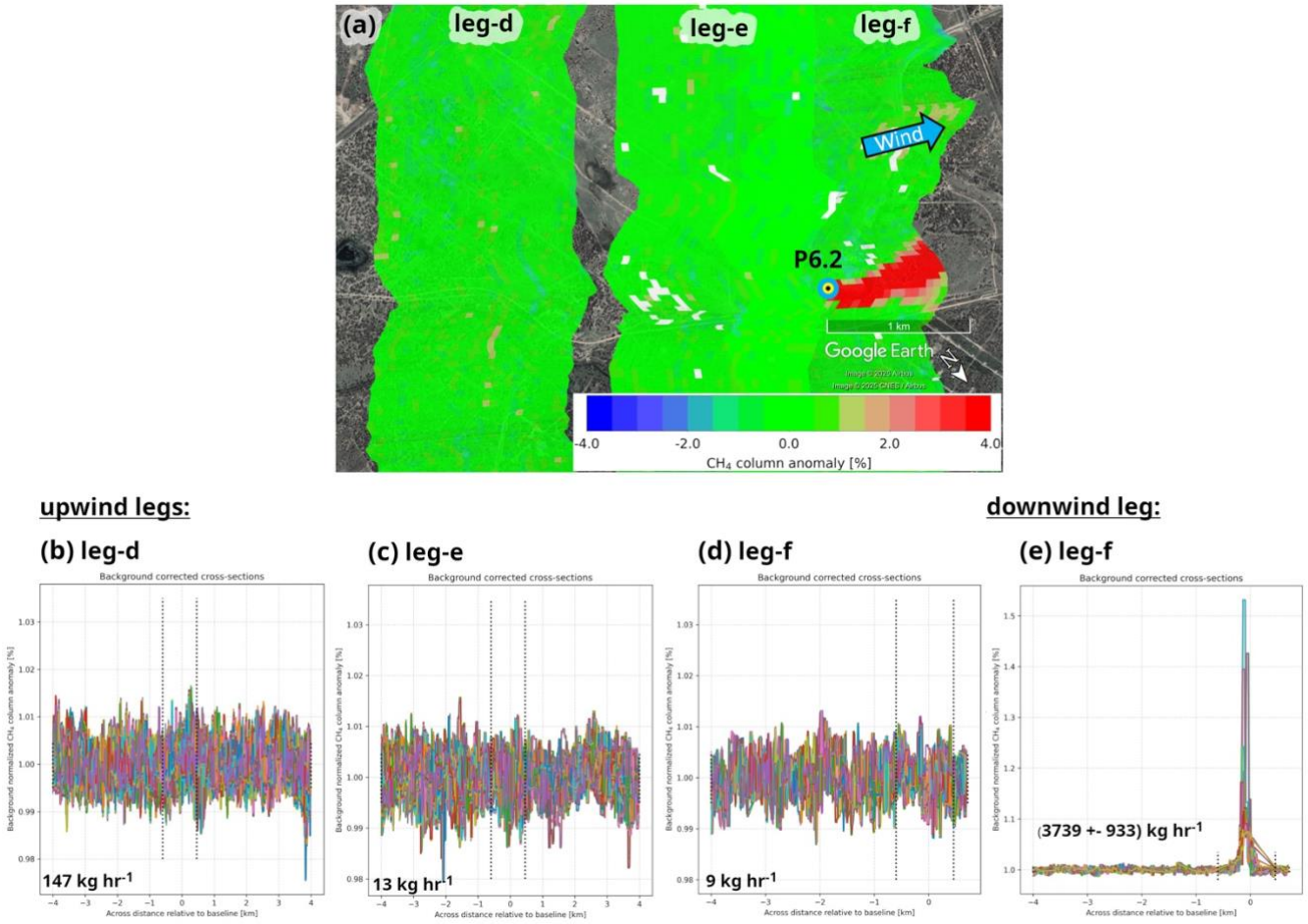

Fig. S6. Upwind legs of P6.2. (a) Google Earth imagery of P6.2_leg-d, -e, -f. (b,c,d,e). Background corrected cross-sections for the upwind legs/part of leg-d, -e, and -f are depicted in (a), (c), and (d). For comparison, also the background corrected cross-sections for the downwind part of leg-f is shown in (e). Satellite imagery ©2025 Airbus, CNES/Airbus, Maxar Technologies. Map data ©2025 Google.

SI-6: Atmospheric concentrations of CH_4 acquired during each in-situ aircraft flight and locations of each curtain

Figs. S7 to S25 plot the atmospheric concentrations of CH_4 measured onboard the in-situ aircraft during each flight. Given the scale of the measurements, readers are referred to the in-situ aircraft dataset in the accompanying data repository to enable higher-resolution plotting and easier data manipulation and visualisation using platforms such as Google Earth.

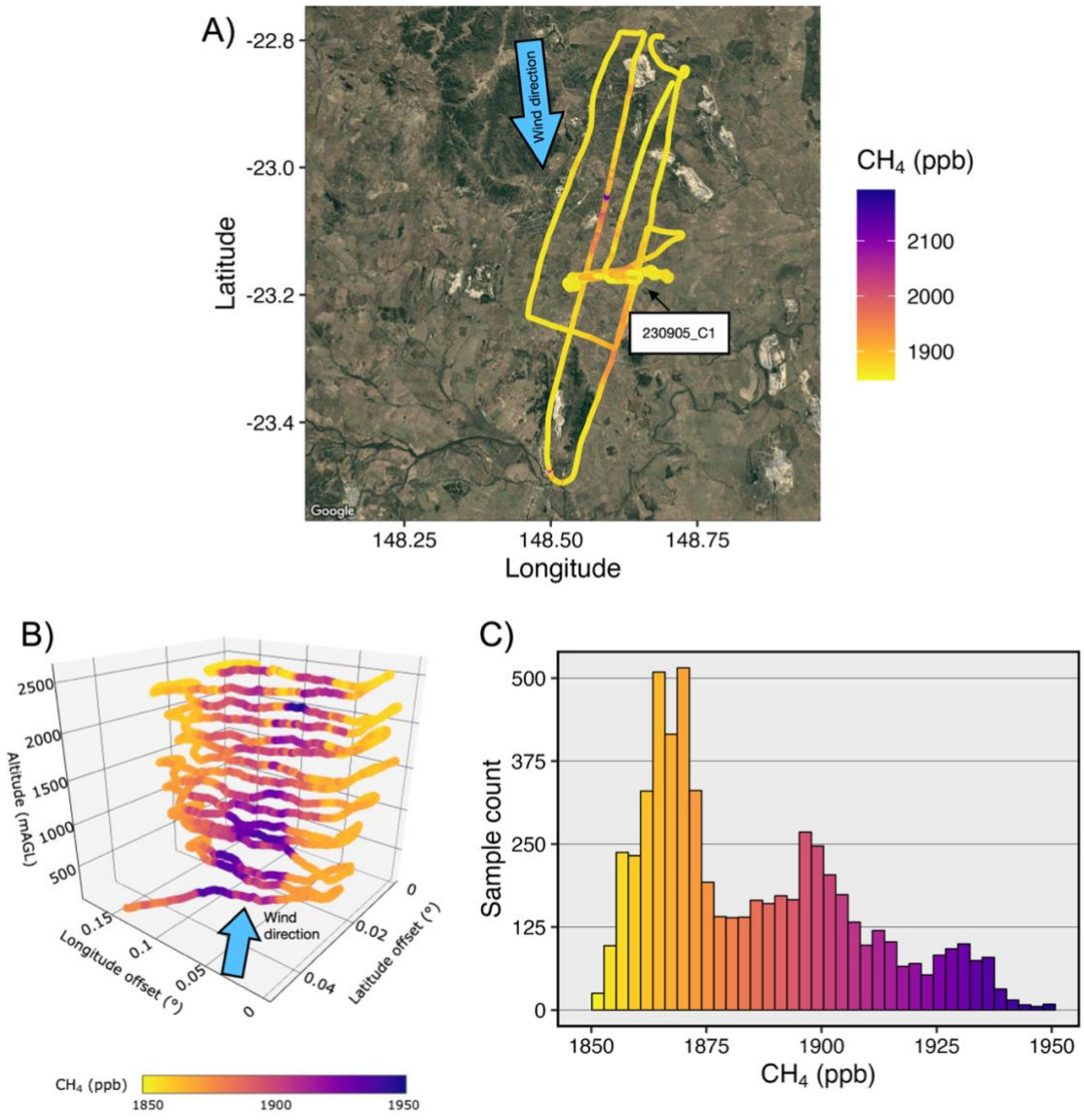

Fig. S7. (A) Atmospheric CH_4 concentrations measured by the in-situ aircraft during the flight on 5 September 2023, with the flown curtain (230905_C1) indicated. (B) Atmospheric CH_4 concentrations within curtain 230905_C1, and (C) histogram of CH_4 concentrations measured within the same curtain. Satellite imagery ©2026 Airbus, CNES/Airbus, Maxar Technologies. Map data ©2026 Google.

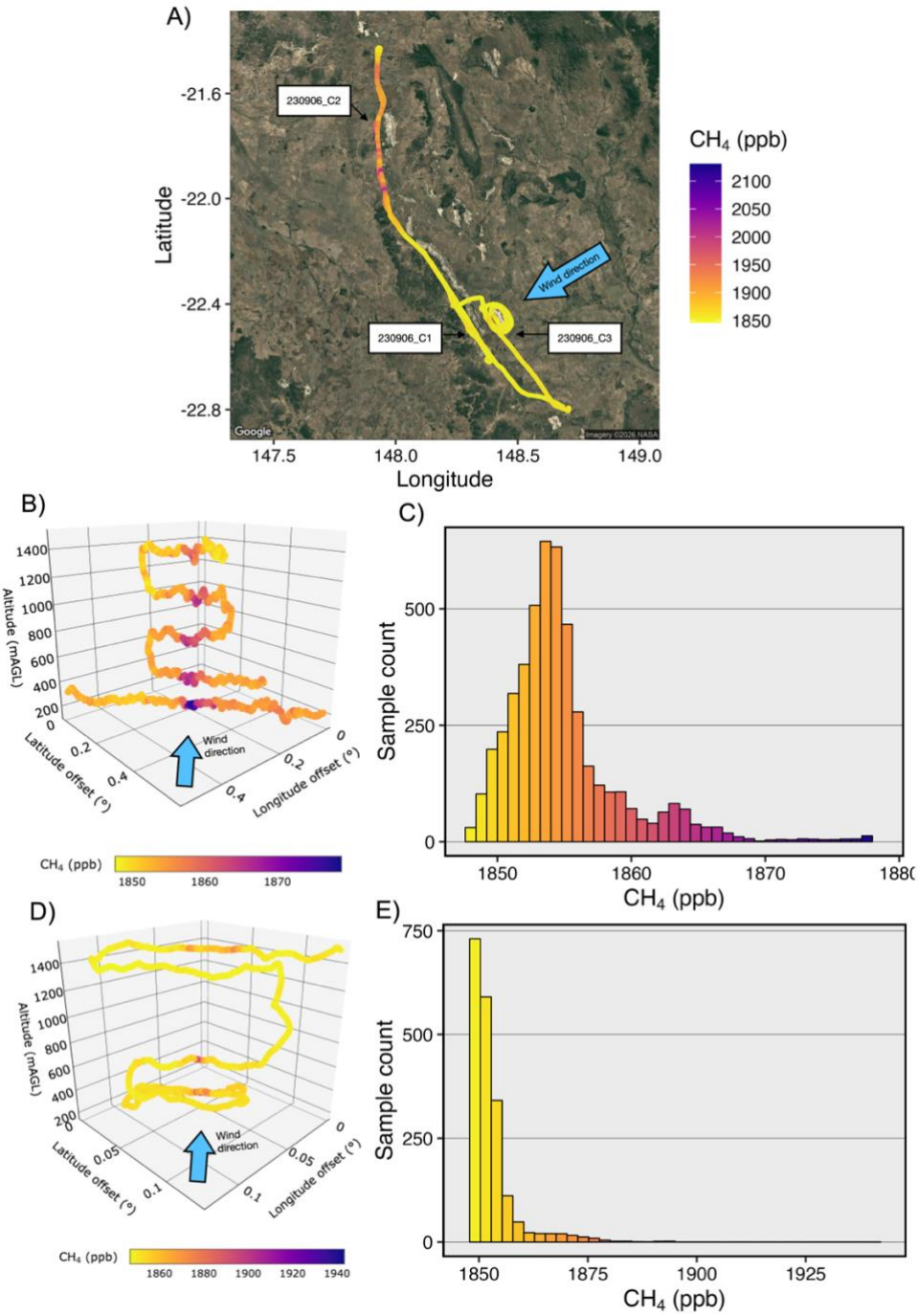

Fig. S8. (A) Atmospheric CH_4 concentrations measured by the in-situ aircraft during the flight on 6 September 2023, with the flown curtains (230906_C1, C2 and C3) indicated. Note curtain 230906_C2 was not used in the analyses (see SI-5), and therefore not shown here. (B, D) Atmospheric CH_4 concentrations within curtains 230906_C1 and 230906_C3, respectively, and (C, E) the corresponding CH_4 concentration histograms. Satellite imagery ©2026 NASA. Map data ©2026 Google.

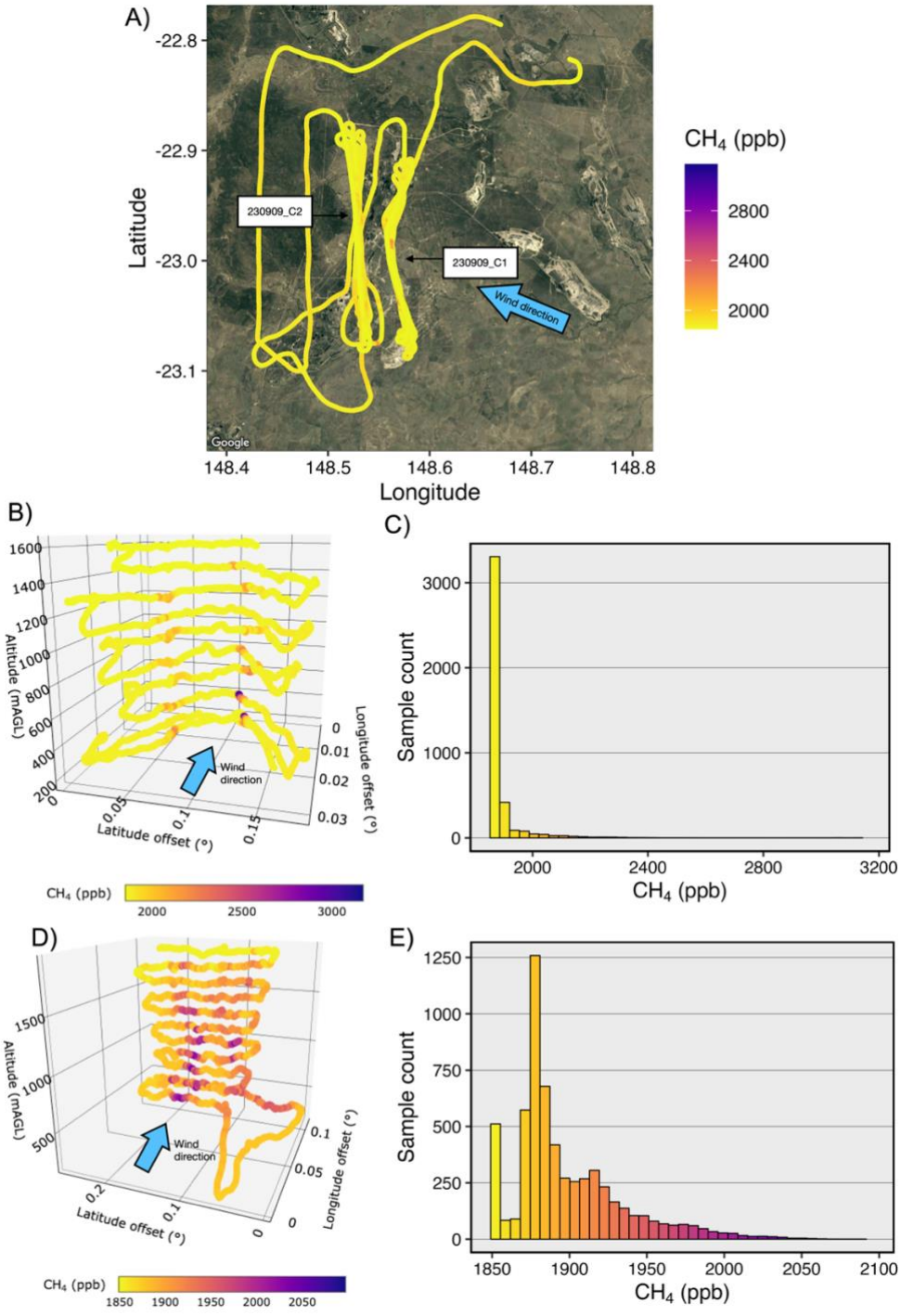

Fig. S9. (A) Atmospheric CH_4 concentrations measured by the in-situ aircraft during the flight on 9 September 2023, with the flown curtains (230909_C1 and C2) indicated. (B, D) Atmospheric CH_4 concentrations within curtains 230909_C1 and 230909_C2, respectively, and (C, E) the corresponding CH_4 concentration histograms. Satellite imagery ©2026 Airbus, CNES/Airbus, Maxar Technologies. Map data ©2026 Google.

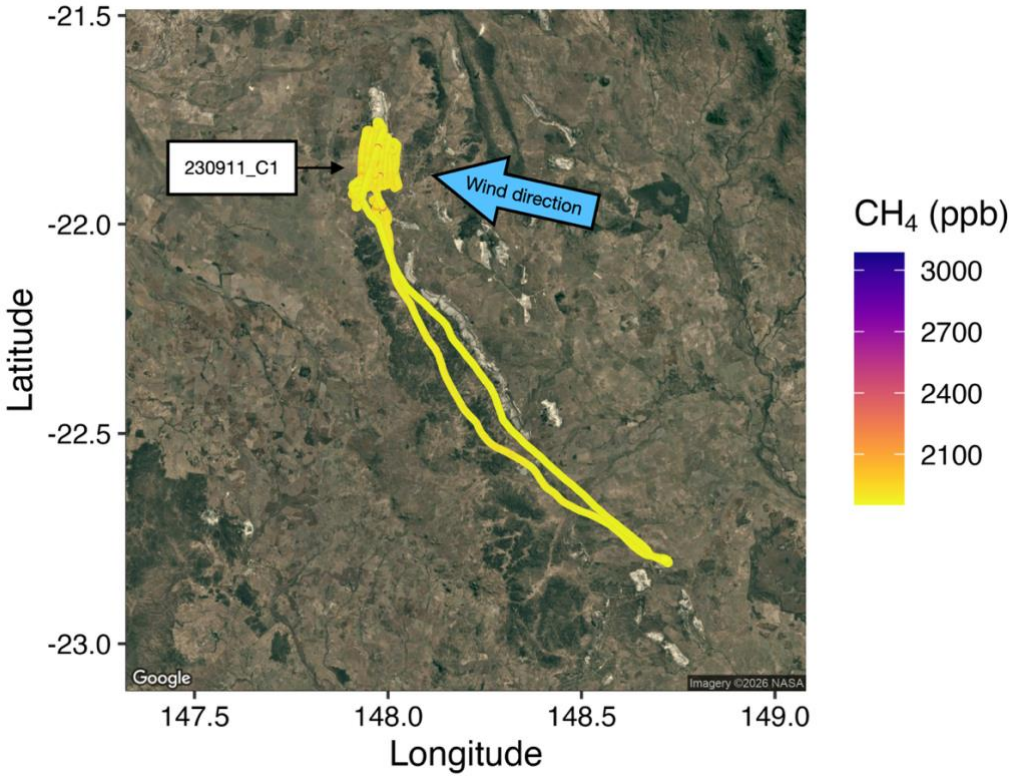

Fig. S10. Atmospheric CH_4 concentrations measured by the in-situ aircraft during the flight conducted on 11 September, 2023, with the flown curtain (230911_C1) indicated. Note curtain 230911_C1 was not used in the analyses (see SI-5), and therefore not shown here. Satellite imagery ©2026 NASA. Map data ©2026 Google.

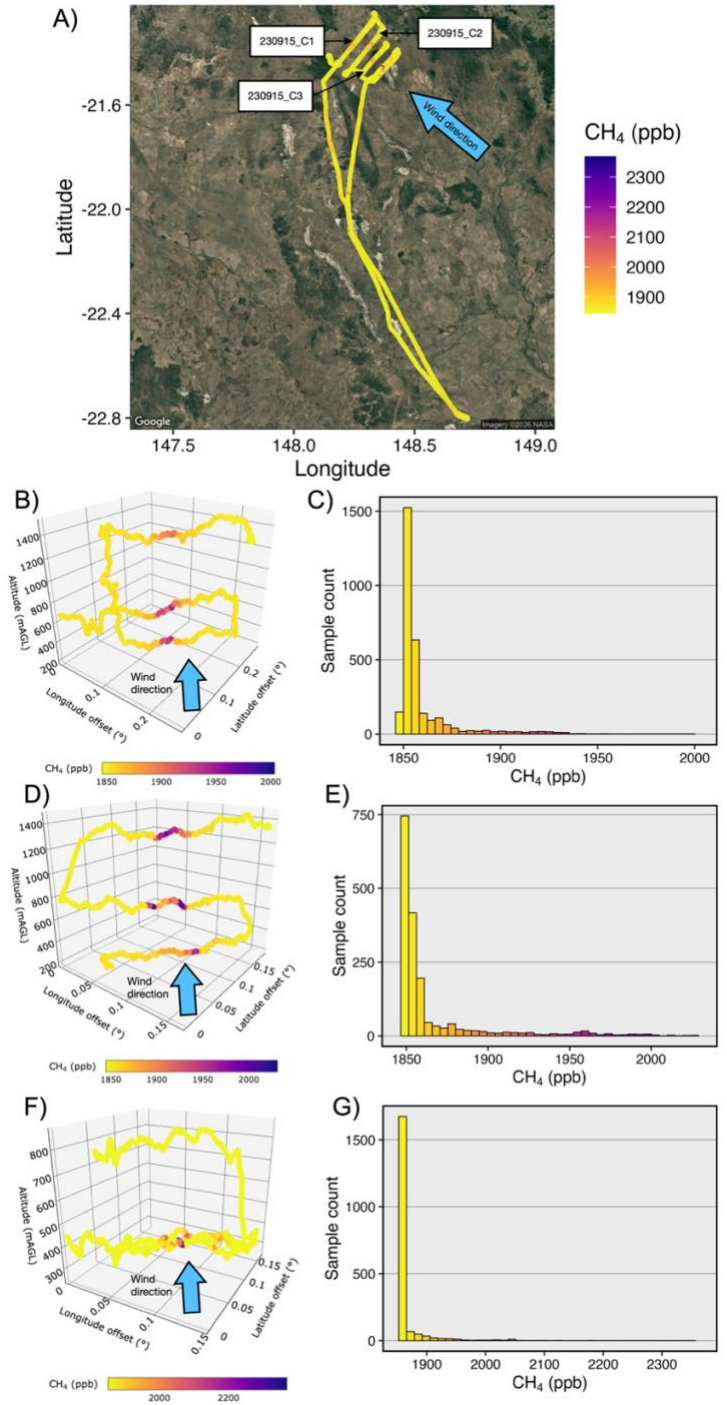

Fig. S11. (A) Atmospheric CH_4 concentrations measured by the in-situ aircraft during the flight on 15 September 2023, with the flown curtains (230915_C1, C2 and C3) indicated. These data were originally reported in Borchardt et al. (2025) and are reproduced here to demonstrate methodological consistency with the present study. (B, D, F) Atmospheric CH_4 concentrations within curtains 230915_C1–C3, respectively, and (C, E, G) the corresponding histograms of CH_4 concentrations. Satellite imagery ©2026 NASA. Map data ©2026 Google.

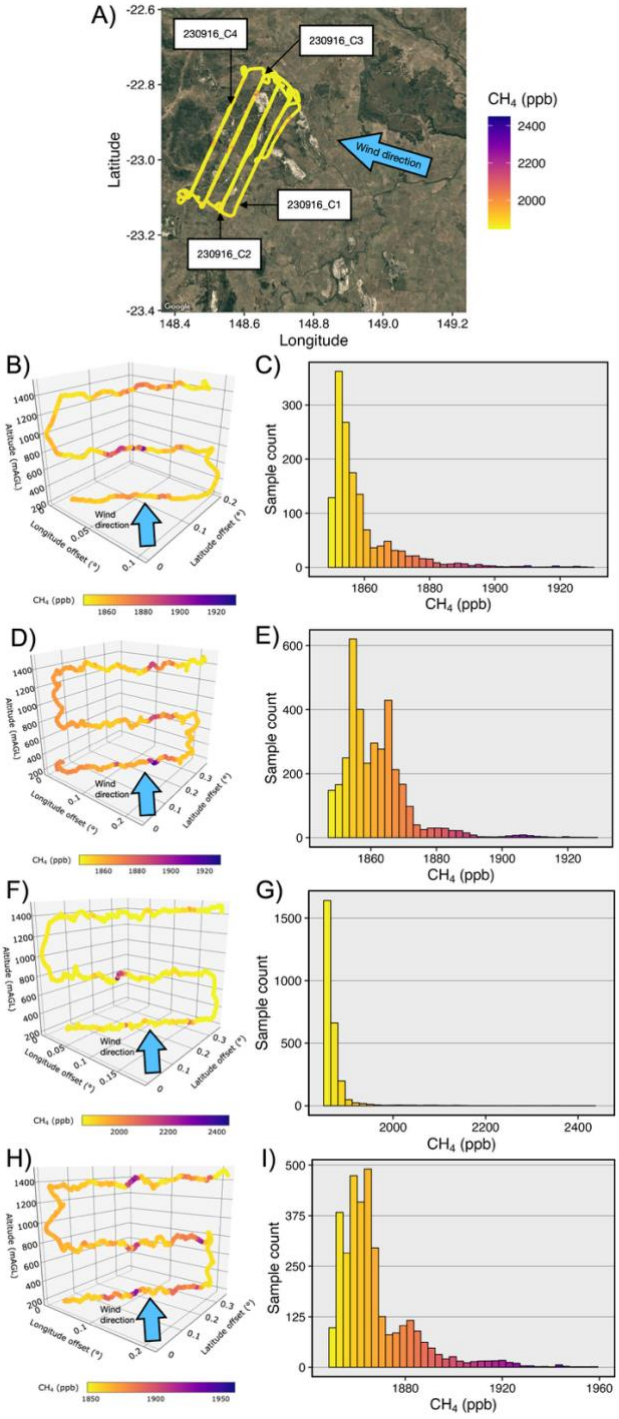

650 **Fig. S12. (A) Atmospheric CH_4 concentrations measured by the in-situ aircraft during the 16 September 2023 flight, with flown curtains (230916_C1–C4) indicated; within-curtain separations (e.g. 230916_C2A and C2B) are omitted for clarity. (B, D, F, H) Atmospheric CH_4 concentrations within curtains 230916_C1–C4, respectively. (C, E, G, I) Corresponding histograms of CH_4 concentrations for each curtain. Satellite imagery ©2026 Airbus, CNES/Airbus, Maxar Technologies. Map data ©2026 Google.**

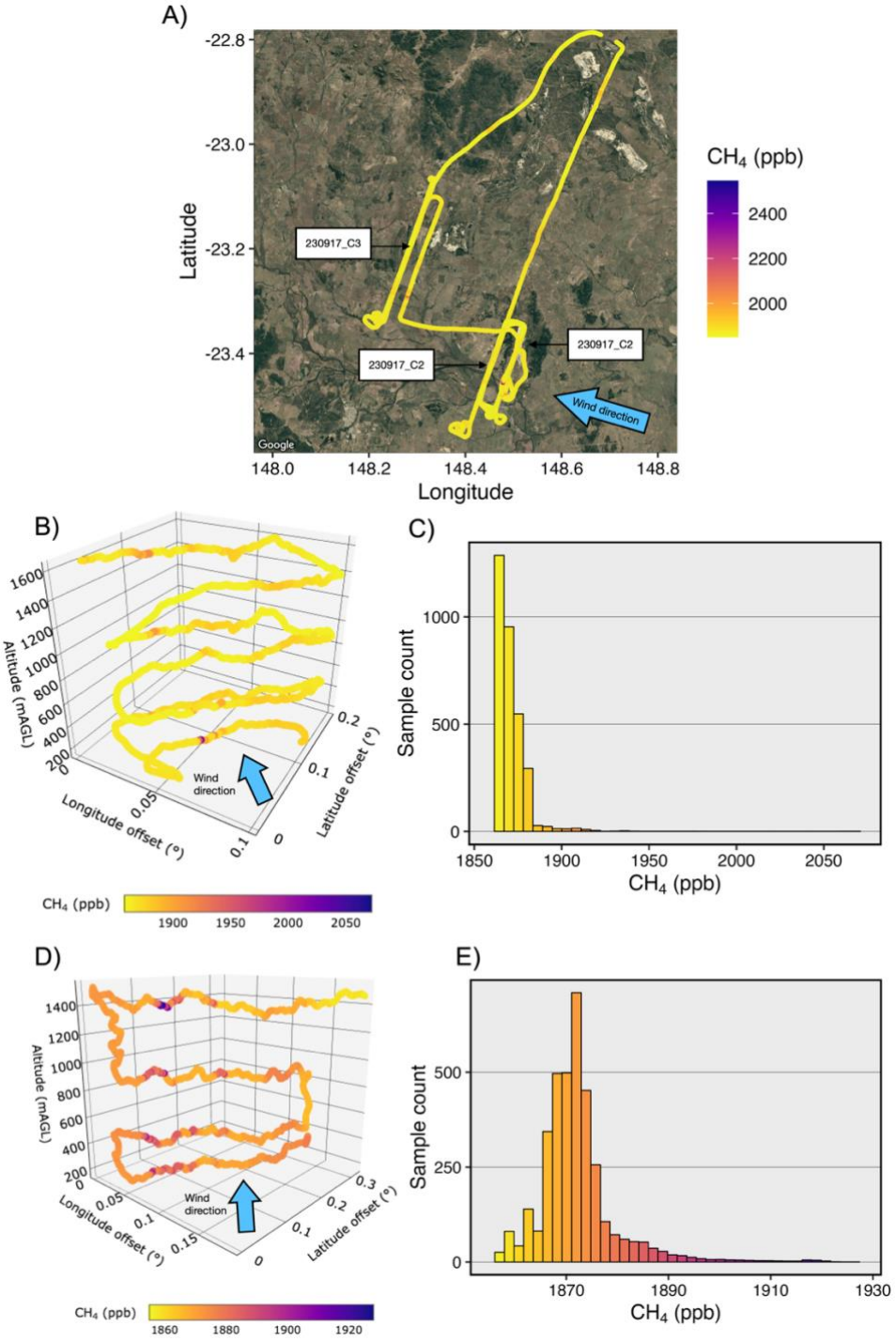

655 **Fig. S13. (A) Atmospheric CH_4 concentrations measured by the in-situ aircraft during the 17 September 2023 flight, with flown curtains (230916_C1–C3) indicated. (B, D) Atmospheric CH_4 concentrations within curtains 230917_C1 and C2 (flown simultaneously) and C4, respectively. (C, E) Corresponding histograms of CH_4 concentrations for each curtain. Satellite imagery ©2026 Airbus, CNES/Airbus, Maxar Technologies. Map data ©2026 Google.**

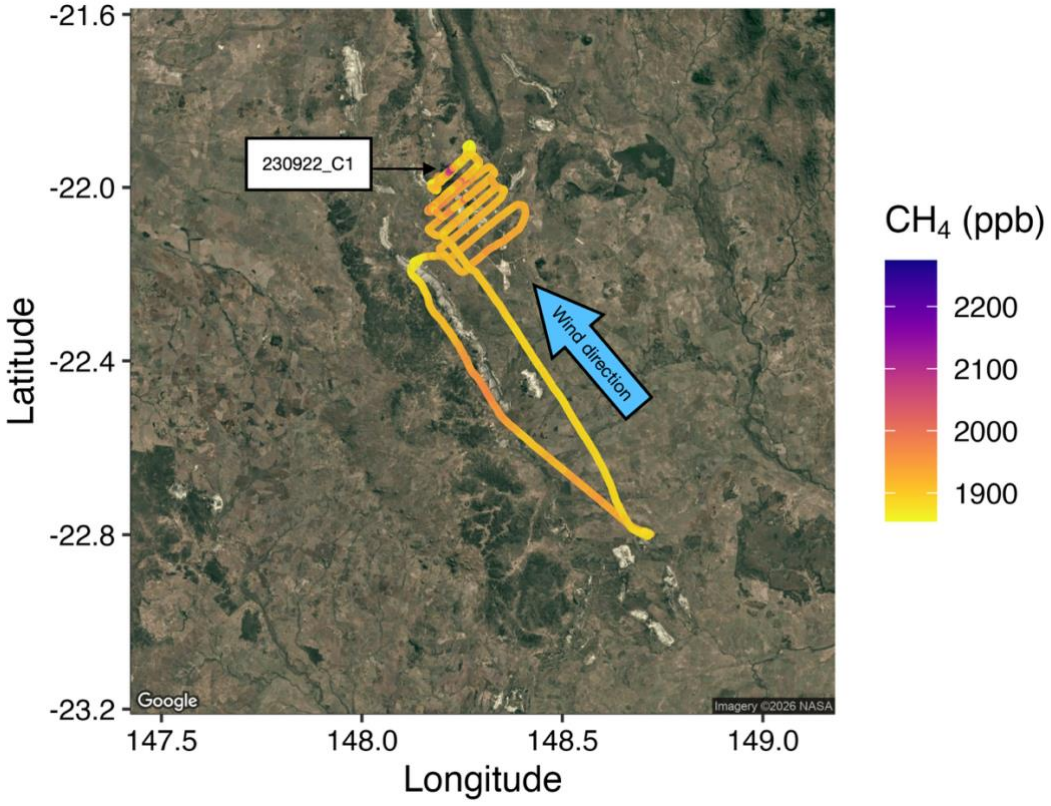

660 **Fig. S14. Atmospheric CH_4 concentrations measured by the in-situ aircraft during the flight conducted on 22 September, 2023, with the flown curtain (230922_C1) indicated. Note curtain 230922_C1 was not used in the analyses (see SI-5), and therefore not shown here. Satellite imagery ©2026 NASA. Map data ©2026 Google.**

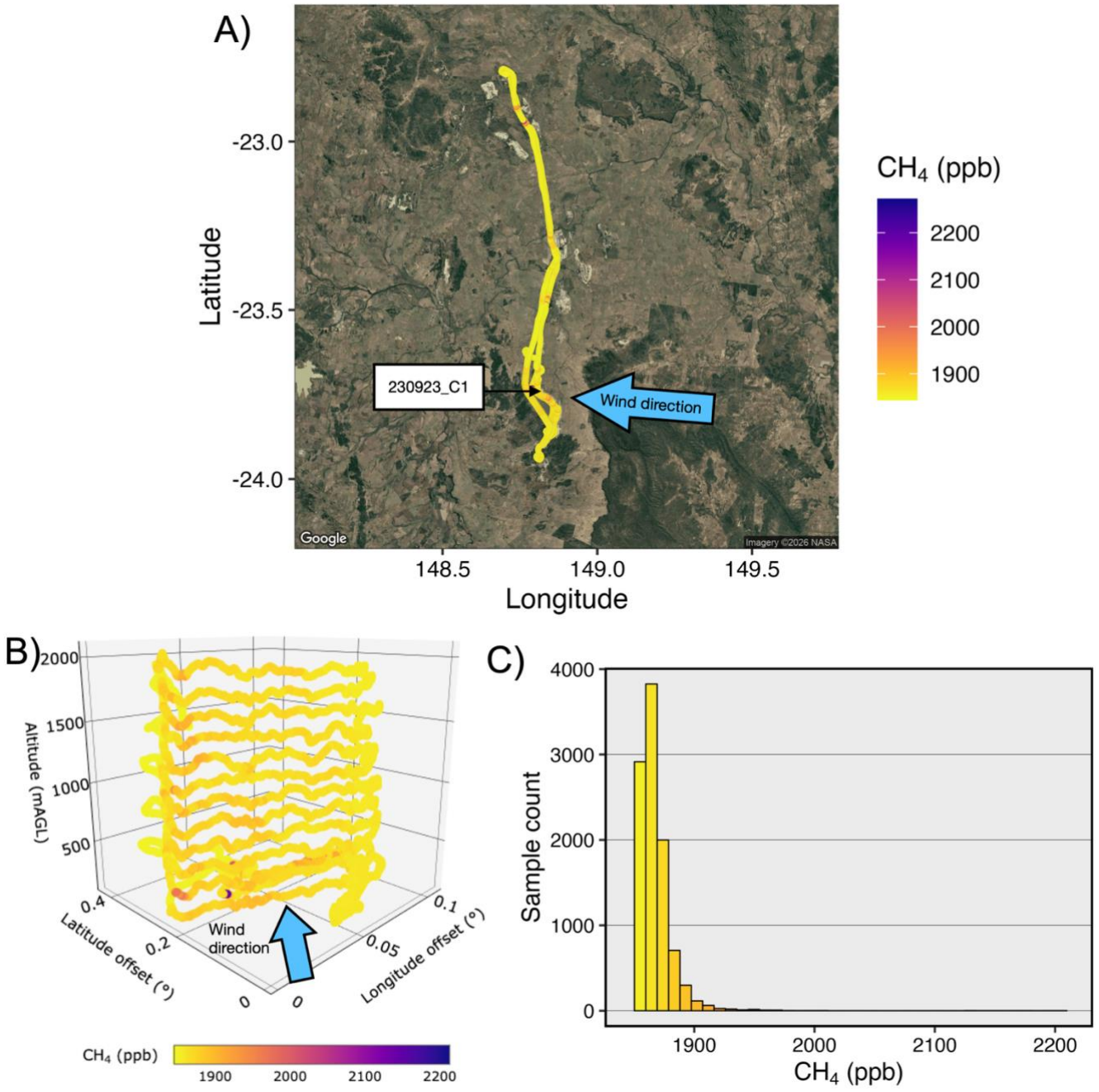

Fig. S15. (A) Atmospheric CH_4 concentrations measured by the in-situ aircraft during the flight on 23 September 2023, with the flown curtain (230923_C1) indicated. (B) Atmospheric CH_4 concentrations within curtain 230923_C1, and (C) histogram of CH_4 concentrations measured within the same curtain. Satellite imagery ©2026 NASA. Map data ©2026 Google.

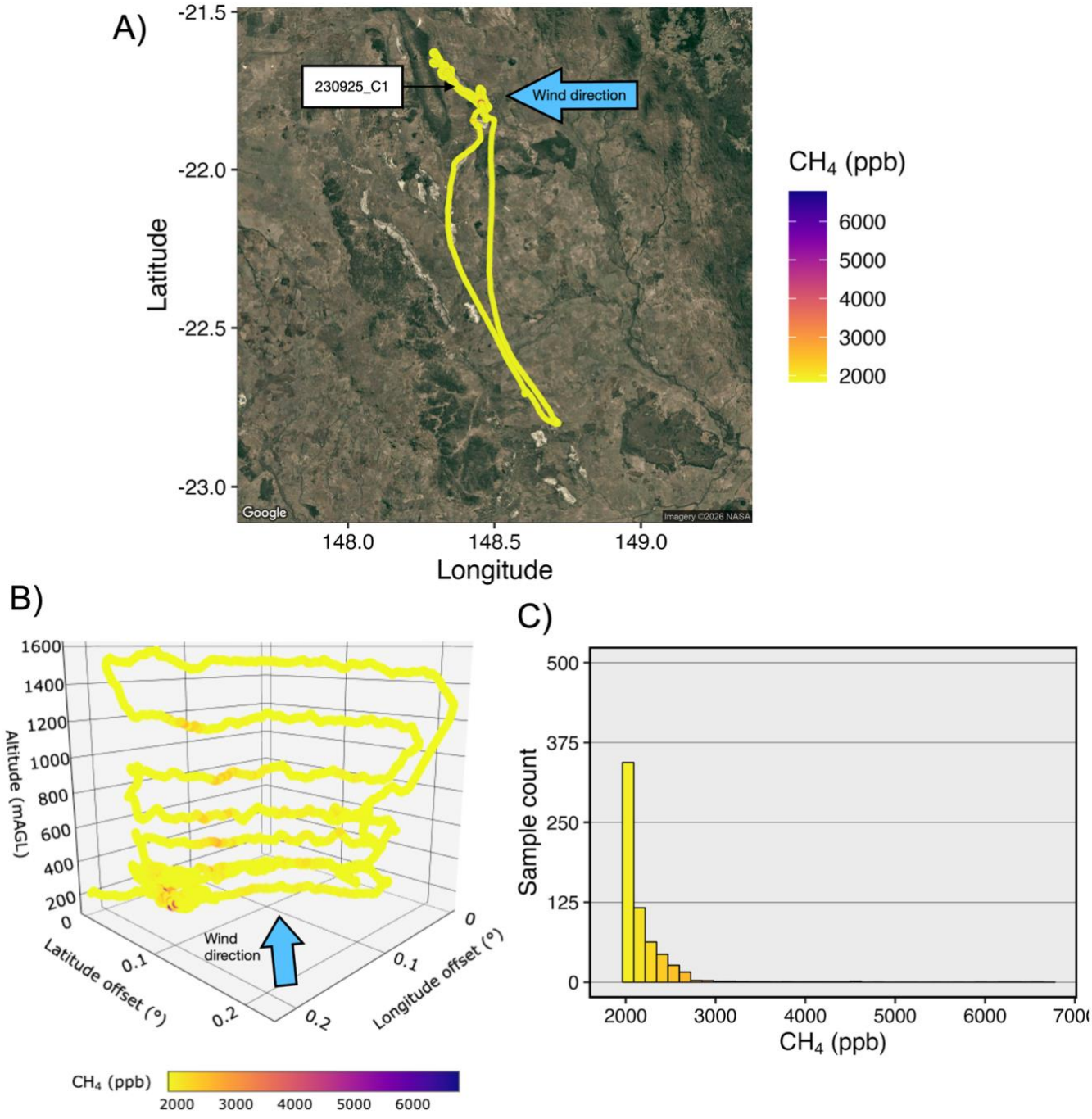

Fig. S16. (A) Atmospheric CH_4 concentrations measured by the in-situ aircraft during the flight on 25 September 2023, with the flown curtain (230925_C1) indicated. (B) Atmospheric CH_4 concentrations within curtain 230925_C1, and (C) histogram of CH_4 concentrations measured within the same curtain. Satellite imagery ©2026 NASA. Map data ©2026 Google.

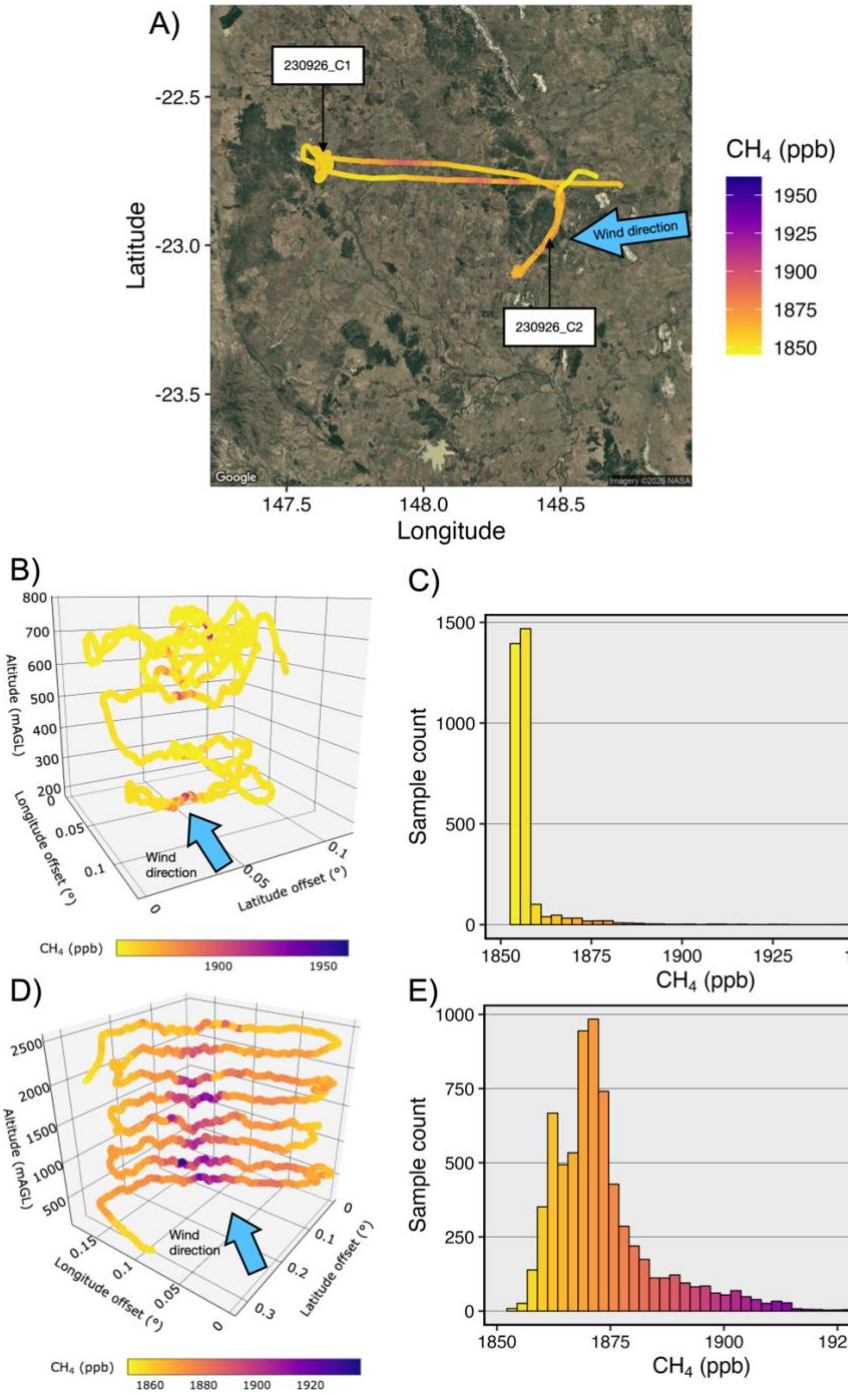

Fig. S17. (A) Atmospheric CH_4 concentrations measured by the in-situ aircraft during the 26 September 2023 flight, with flown curtains (230926_C1–C2) indicated. (B, D) Atmospheric CH_4 concentrations within curtains 230926_C1 and C2 (flown simultaneously) and C4, respectively. (C, E) Corresponding histograms of CH_4 concentrations for each curtain. Note that transects flown upwind of the mine obscure the downwind transects of the curtain in panel (B). Readers are referred to the data repository for clearer, unobstructed views of the downwind curtain. Satellite imagery ©2026 NASA. Map data ©2026 Google.

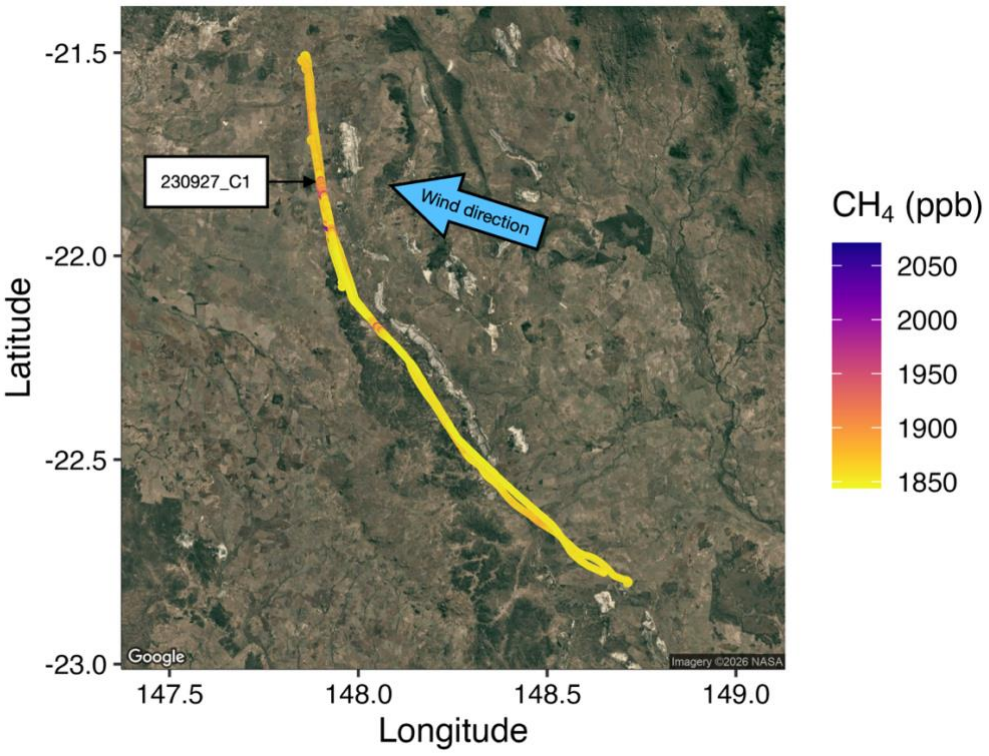

680 **Fig. S18. Atmospheric CH_4 concentrations measured by the in-situ aircraft during the flight conducted on 27 September, 2023, with the flown curtain (230927_C1) indicated. Note curtain 230927_C1 was not used in the analyses (see SI-5), and therefore not shown here. Satellite imagery ©2026 NASA. Map data ©2026 Google.**

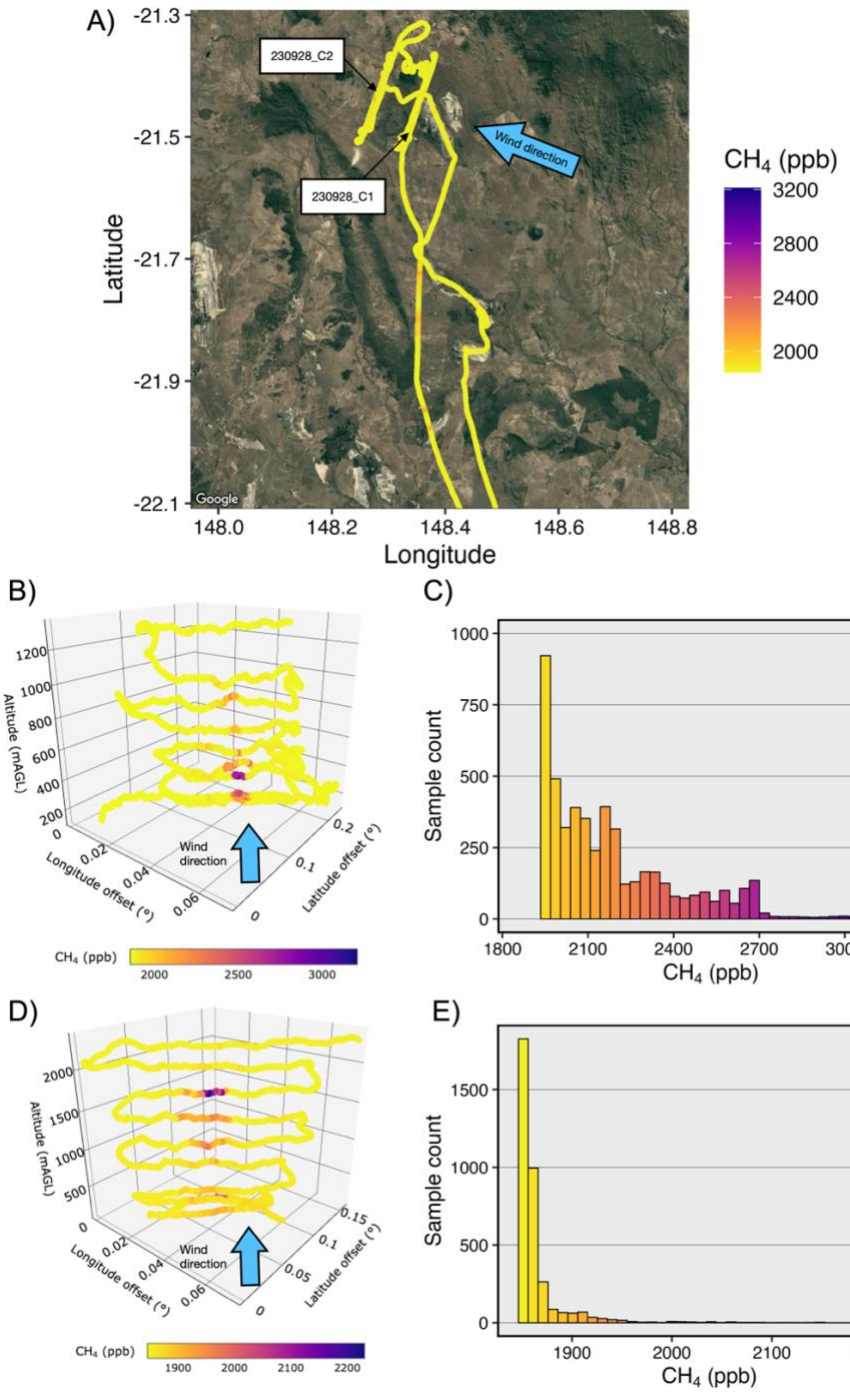

Fig. S19. (A) Atmospheric CH_4 concentrations measured by the in-situ aircraft during the 28 September 2023 flight, with flown curtains (230928_C1–C2) indicated. These data were originally reported in Borchardt et al. (2025) and are reproduced here to demonstrate methodological consistency with the present study. (B, D) Atmospheric CH_4 concentrations within curtains 230928_C1 and C2. (C, E) Corresponding histograms of CH_4 concentrations for each curtain. Satellite imagery ©2026 Airbus, CNES/Airbus, Maxar Technologies. Map data ©2026 Google.

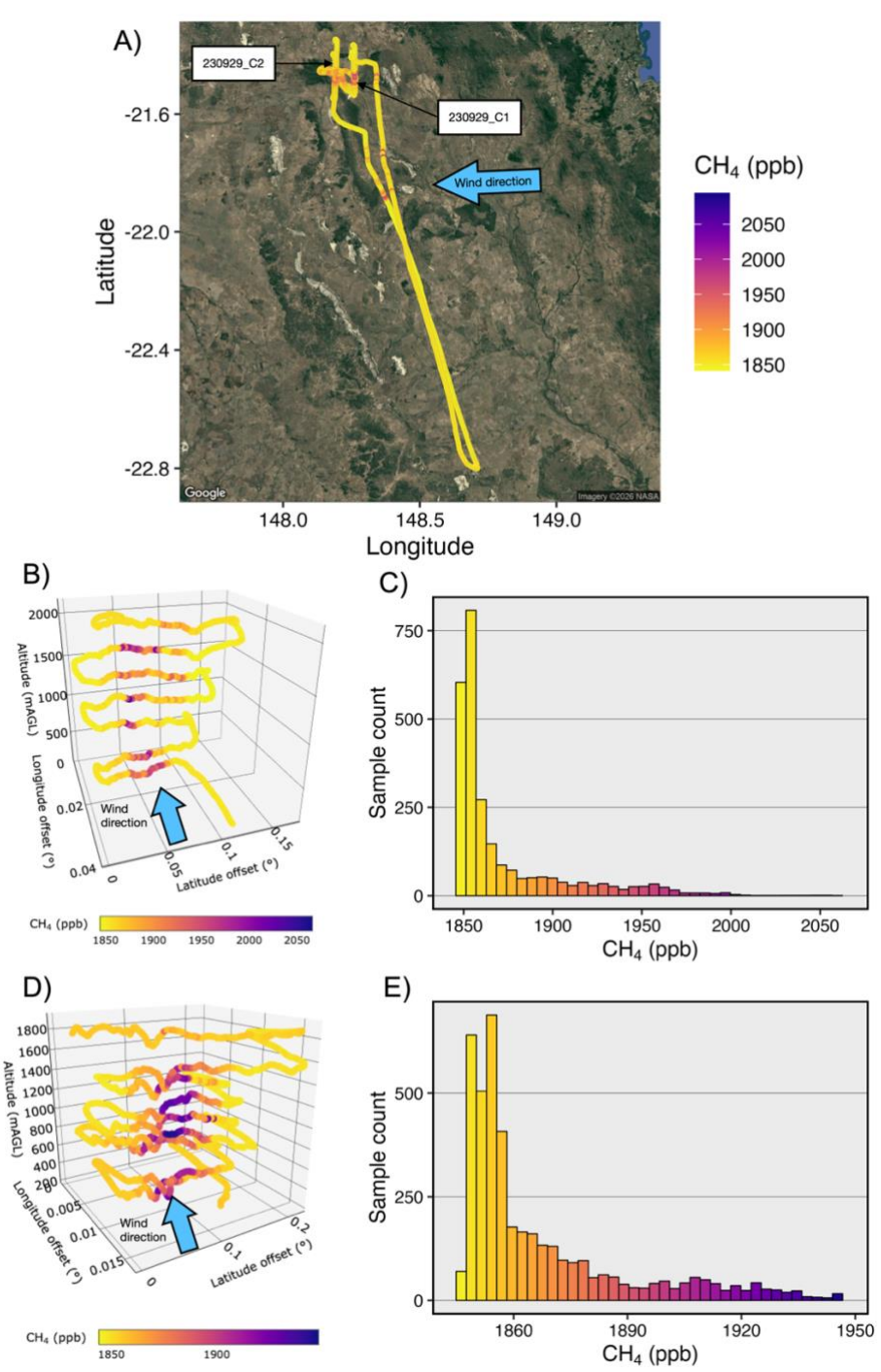

690 **Fig. S20. (A) Atmospheric CH_4 concentrations measured by the in-situ aircraft during the 29 September 2023 flight, with flown curtains (230929_C1–C2) indicated. These data were originally reported in Borchardt et al. (2025) and are reproduced here to demonstrate methodological consistency with the present study. (B, D) Atmospheric CH_4 concentrations within curtains 230929_C1 and C2. (C, E) Corresponding histograms of CH_4 concentrations for each curtain. Satellite imagery ©2026 NASA. Map data ©2026 Google.**

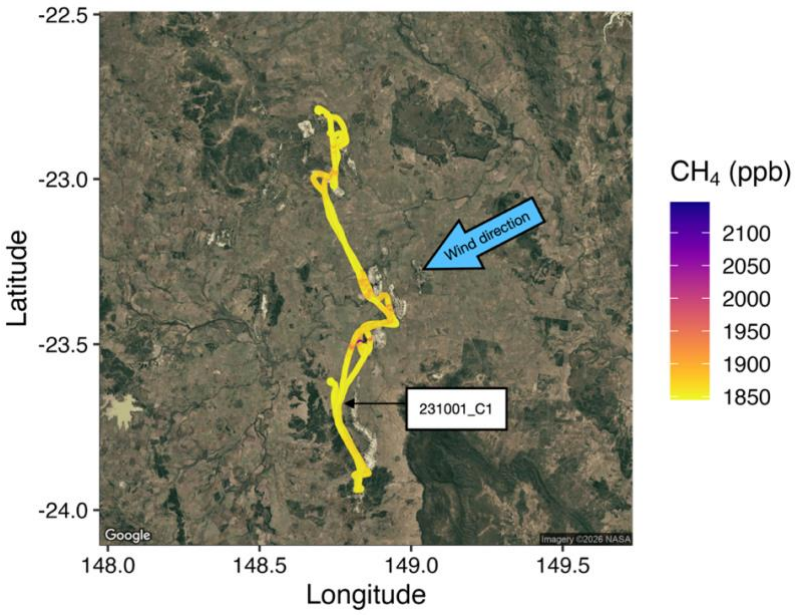

Fig. S21. Atmospheric CH_4 concentrations measured by the in-situ aircraft during the flight conducted on 1 October, 2023, with the flown curtain (231001_C1) indicated. Note curtain 231001_C1 was not used in the analyses (see SI-5), and therefore not shown here. Satellite imagery ©2026 NASA. Map data ©2026 Google.

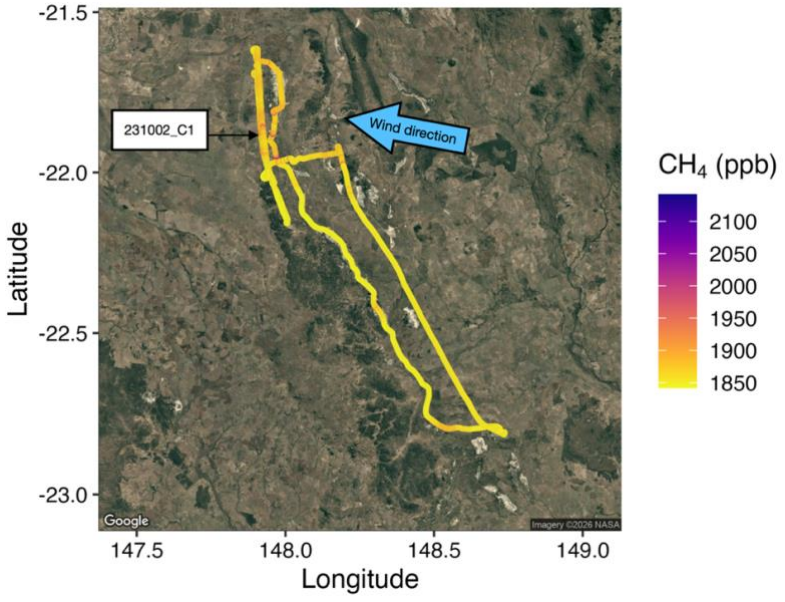

Fig. S22. Atmospheric CH_4 concentrations measured by the in-situ aircraft during the flight conducted on 2 October, 2023, with the flown curtain (231002_C1) indicated. Note curtain 231002_C1 was not used in the analyses (see SI-5), and therefore not shown here. Satellite imagery ©2026 NASA. Map data ©2026 Google.

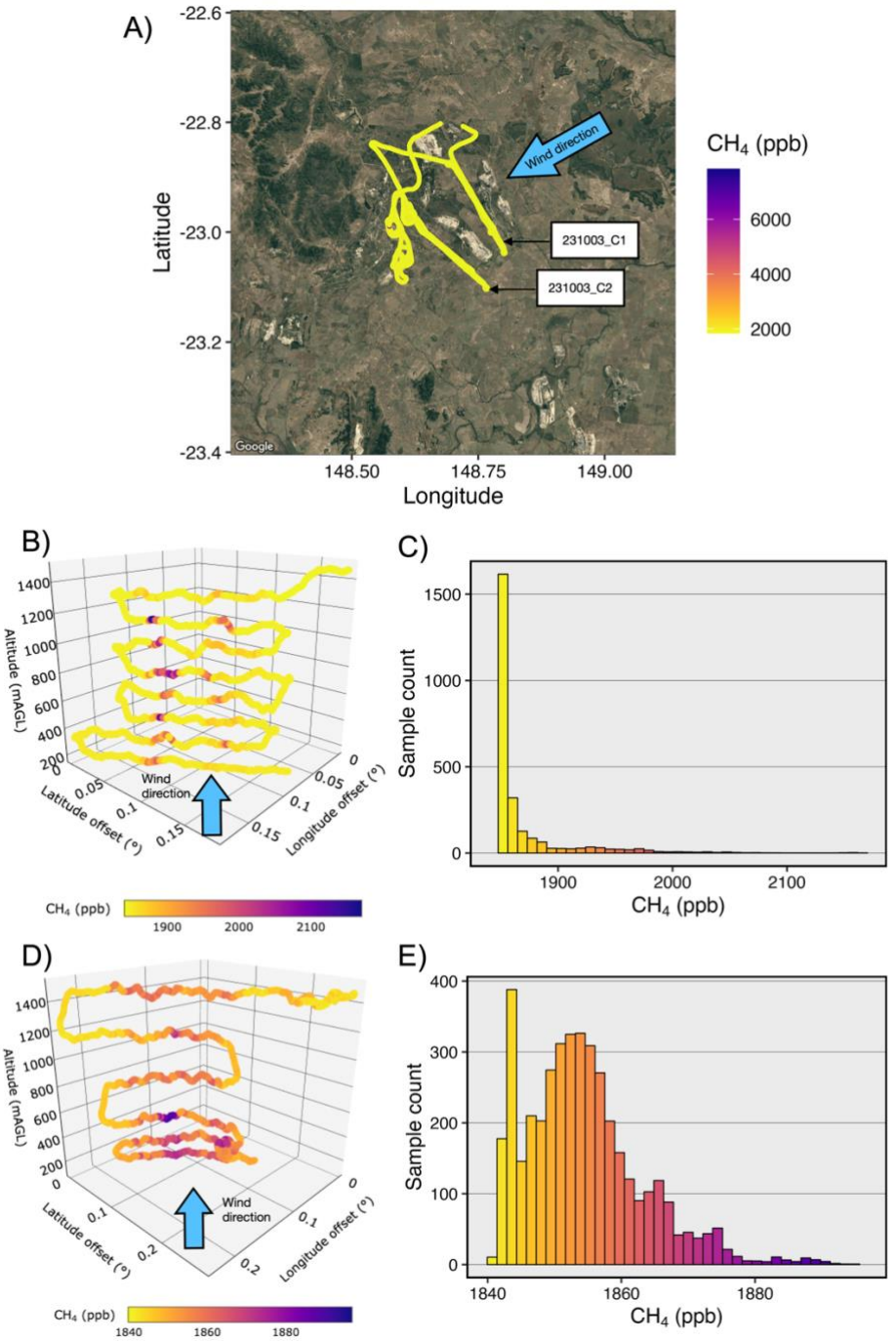

705 **Fig. S23. (A) Atmospheric CH_4 concentrations measured by the in-situ aircraft during the 3 October 2023 flight, with flown curtains (231003_C1–C2) indicated. (B, D) Atmospheric CH_4 concentrations within curtains 231003_C1 and C2. (C, E) Corresponding histograms of CH_4 concentrations for each curtain. Satellite imagery ©2026 Airbus, CNES/Airbus, Maxar Technologies. Map data ©2026 Google.**

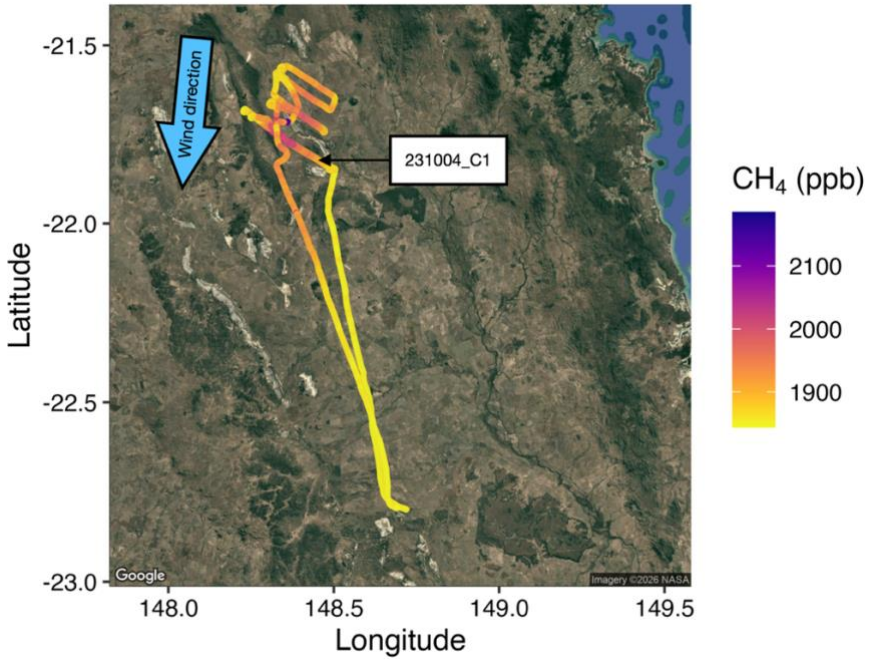

Fig. S24. Atmospheric CH_4 concentrations measured by the in-situ aircraft during the flight conducted on 4 October, 2023, with the flown curtain (231004_C1) indicated. Note curtain 231004_C1 was not used in the analyses (see SI-5), and therefore not shown here. Satellite imagery ©2026 NASA. Map data ©2026 Google.

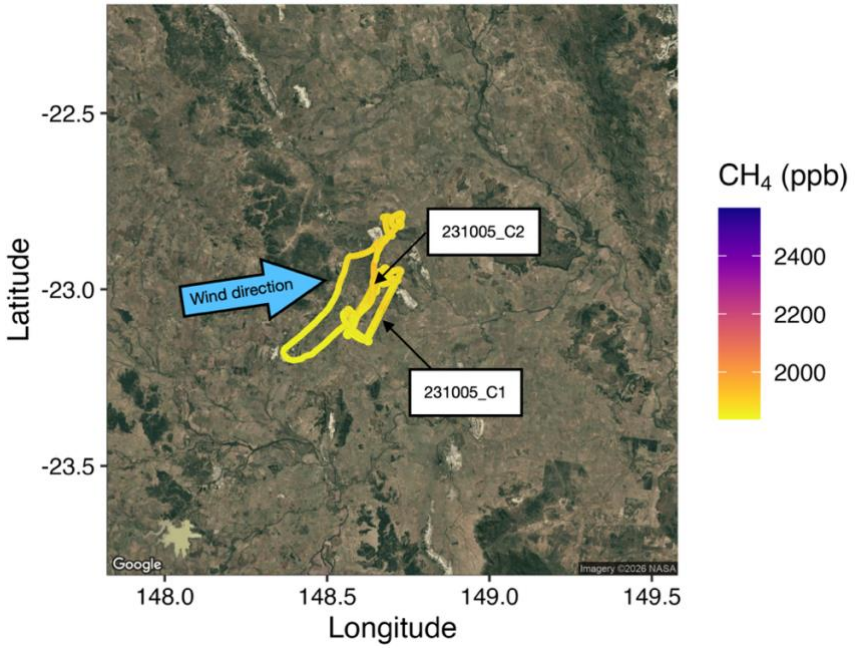

Fig. S25. Atmospheric CH_4 concentrations measured by the in-situ aircraft during the flight conducted on 45October, 2023, with the flown curtains (231005_C1-C2) indicated. Note curtains 231005_C1 and 231005_C2 were not used in the analyses (see SI-5), and therefore not shown here. Satellite imagery ©2026 NASA. Map data ©2026 Google.

SI-7: All flight legs acquired by the remote sensing aircraft

Table S6 lists all flight legs acquired by the remote sensing aircraft, including those containing CH_4 plume signals and the corresponding mines where they were detected. Legs located downwind of a source are identified as downwind observations, whereas those flown directly over a source are designated as overhead observations. Overhead legs typically also include segments upwind of the emission source. For each leg without an emission rate quantification or comparison with operator estimates in Table S6, the reason for omission is listed in the table and corresponds to those described in SI-5 for the remote sensing aircraft.

Table S6. Overview of all legs collected by the remote sensing aircraft.

Flight ID	Date	Time of leg [UTC]	Plume ID	Observa-tion type	Infrastructure type	Attributed coal mine	Plume Latitude (°)	Plume Longitude (°)	Compared with operator estimate?	Reason for omission
RF04_leg-a	05.09.2023	02:23:15 - 02:36:29	No plume observed	N/A	N/A	N/A	N/A	N/A	N/A	N/A
RF04_leg-b	05.09.2023	02:41:22 - 02:44:14	P4.4	Overhead	Ventilation fan	UG-3	-23.052176	148.592645	No	Reason 2
RF04_leg-b	05.09.2023	02:41:22 - 02:44:14	P4.2	Downwind	Downwind of ventilation fan	UG-3	-23.0037207	148.580551	No	Reason 2
RF04_leg-b	05.09.2023	02:41:22 - 02:44:14	P4.3	Downwind	Downwind of unidentified source - possible abandoned coal exploration borehole or groundwater bore	N/A	-23.045681	148.588172	No	Reason 2
RF04_leg-c	05.09.2023	02:48:37 - 02:44:5	No plume observed	N/A	N/A	N/A	N/A	N/A	N/A	N/A
RF04_leg-d	05.09.2023	02:50:30 - 03:00:06	P4.3	Overhead	Unidentified source - possible abandoned coal exploration borehole or groundwater bore	N/A	-23.032649	148.593161	No	Reason 2
RF04_leg-d	05.09.2023	02:50:30 - 03:00:06	P4.2	Downwind	Downwind of ventilation fan	MC-2-UG	-23.029036	148.58571	No	Reason 2
RF04_leg-e	05.09.2023	03:02:30 - 03:09:41	P4.2	Overhead	Ventilation fan	MC-2-UG	-22.990509	148.58068	Yes	N/A
RF04_leg-f	05.09.2023	03:15:04 - 03:23:29	No plume observed	N/A	N/A	N/A	N/A	N/A	N/A	N/A
RF04_leg-g	05.09.2023	03:24:33 - 03:30:16	P4.1	Overhead	Open-cut coal mine	OC-13	-22.848767	148.650406	No	Reason 6

Flight ID	Date	Time of leg [UTC]	Plume ID	Observa-tion type	Infrastructure type	Attributed coal mine	Plume Latitude (°)	Plume Longitude (°)	Compared with operator estimate?	Reason for omission
RF04_leg-h	05.09.2023	03:35:33 - 03:41:33	No plume observed	N/A	N/A	N/A	N/A	N/A	N/A	N/A
RF05_leg-a1	06.09.2023	01:30:05 - 01:36:23	No plume observed	N/A	N/A	N/A	N/A	N/A	N/A	N/A
RF05_leg-a2	06.09.2023	01:36:23 - 01:42:35	No plume observed	N/A	N/A	N/A	N/A	N/A	N/A	N/A
RF05_leg-a3	06.09.2023	01:42:41 - 01:45:26	No plume observed	N/A	N/A	N/A	N/A	N/A	N/A	N/A
RF05_leg-a4	06.09.2023	01:46:47 - 01:58:35	No plume observed	N/A	N/A	N/A	N/A	N/A	N/A	N/A
RF05_leg-b1	06.09.2023	02:04:26 - 02:18:50	P5.3	Overhead	Ventilation fan	UG-8	-21.657933	147.962036	No	Reason 2
RF05_leg-b2	06.09.2023	02:18:53 - 02:34:23	No plume observed	N/A	N/A	N/A	N/A	N/A	N/A	N/A
RF05_leg-b3	06.09.2023	02:34:23 - 02:58:41	No plume observed	N/A	N/A	N/A	N/A	N/A	N/A	N/A
RF05_leg-c1	06.09.2023	03:02:59 - 03:07:14	No plume observed	N/A	N/A	N/A	N/A	N/A	N/A	N/A
RF05_leg-c2	06.09.2023	03:07:29 - 03:12:56	No plume observed	N/A	N/A	N/A	N/A	N/A	N/A	N/A
RF05_leg-c3	06.09.2023	03:12:56 - 03:27:53	No plume observed	N/A	N/A	N/A	N/A	N/A	N/A	N/A
RF05_leg-c4	06.09.2023	03:27:53 - 03:38:44	P5.1	Overhead	Ventilation fan	MC-3-UG	-21.821601	147.981688	No; however flux estimate possible	Not representative of facility-level emissions
RF05_leg-c4	06.09.2023	03:27:53 - 03:38:44	P5.2	Overhead	Ventilation fan	UG-6	-21.878367	148.016135	Yes - averaged with P7.2/7.3 and summed with P7.5 and P7.4	N/A

Flight ID	Date	Time of leg [UTC]	Plume ID	Observa-tion type	Infrastructure type	Attributed coal mine	Plume Latitude (°)	Plume Longitude (°)	Compared with operator estimate?	Reason for omission
RF05_leg-d1	06.09.2023	03:45:30 - 04:07:33	No plume observed	N/A	N/A	N/A	N/A	N/A	N/A	N/A
RF05_leg-d2	06.09.2023	04:07:33 - 04:20:57	No plume observed	N/A	N/A	N/A	N/A	N/A	N/A	N/A
RF05_leg-e	06.09.2023	04:23:45 - 04:30:27	No plume observed	N/A	N/A	N/A	N/A	N/A	N/A	N/A
RF05_leg-f	06.09.2023	04:32:39 - 04:57:21	No plume observed	N/A	N/A	N/A	N/A	N/A	N/A	N/A
RF06_leg-a	09.09.2023	02:12:42 - 02:22:01	No plume observed	N/A	N/A	N/A	N/A	N/A	N/A	N/A
RF06_leg-b	09.09.2023	02:23:51 – 02:36:43	P6.4	Overhead	Ventilation fan	UG-3	-23.045668	148.5914	Yes - summed with P6.3 and P6.5	N/A
RF06_leg-b	09.09.2023	02:23:51 – 02:36:43	P6.5	Overhead	Ventilation fan	UG-3	-23.076595	148.563682	Yes - summed with P6.3 and P6.4	N/A
RF06_leg-c	09.09.2023	02:38:42 - 02:47:54	P6.4	Downwind	Downwind of Ventilation fan	UG-3	-23.041736	148.57905	Yes - summed with P6.3 and P6.5	N/A
RF06_leg-d	09.09.2023	02:50:02 - 03:03:16	P6.3	Overhead	Ventilation fan	UG-3	-23.044412	148.564079	Yes - summed with P6.4 and P6.5	N/A
RF06_leg-d	09.09.2023	02:50:02 - 03:03:16	P6.4	Downwind	Downwind of Ventilation fan	UG-3	-23.036246	148.569209	Yes - summed with P6.3 and P6.5	N/A
RF06_leg-e	09.09.2023	03:04:59 - 03:14:18	P6.3	Downwind	Downwind of Ventilation fan	UG-3	-23.029961	148.552586	No	Reason 2
RF06_leg-e	09.09.2023	03:04:59 - 03:14:18	P6.4	Downwind	Downwind of Ventilation fan	UG-3	-23.029961	148.552586	No	Reason 2
RF06_leg-f	09.09.2023	03:16:06 - 03:29:30	P6.2	Overhead	Ventilation fan	MC-2-UG	-22.985891	148.5778	Yes	N/A
RF06_leg-f	09.09.2023	03:16:06 - 03:29:30	P6.3	Downwind	Downwind of Ventilation fan	UG-3	-23.026250	148.545024	No	Reason 2
RF06_leg-f	09.09.2023	03:16:06 - 03:29:30	P6.4	Downwind	Downwind of Ventilation fan	UG-3	-23.026250	148.545024	No	Reason 2
RF06_leg-g	09.09.2023	03:31:32 - 03:40:30	P6.2	Downwind	Downwind of Ventilation fan	MC-2-UG	-22.978663	148.569256	Yes	N/A

Flight ID	Date	Time of leg [UTC]	Plume ID	Observa-tion type	Infrastructure type	Attributed coal mine	Plume Latitude (°)	Plume Longitude (°)	Compared with operator estimate?	Reason for omission
RF06_leg-g	09.09.2023	03:31:32 - 03:40:30	P6.6	Overhead	Unidentified source - possible abandoned coal exploration borehole or groundwater bore	N/A	-22.935962	148.601947	No; however flux estimate possible	Unidentifie d source
RF06_leg-h	09.09.2023	03:43:43 - 03:56:58	P6.2	Downwind	Downwind of Ventilation fan	MC-2-UG	-22.976913	148.553009	Yes	N/A
RF06_leg-i	09.09.2023	03:58:56 - 04:10:04	P6.1	Overhead	Open-cut coal mine	OC-13	-22.846247	148.650315	No	Reason 6
RF06_leg-i	09.09.2023	03:58:56 - 04:10:04	P6.2	Downwind	Downwind of Ventilation fan	MC-2-UG	-22.968978	148.537475	No	Reason 4
RF06_leg-j1	09.09.2023	04:11:41 - 04:14:05	No plume observed	N/A	N/A	N/A	N/A	N/A	N/A	N/A
RF06_leg-j2	09.09.2023	04:14:56 - 04:16:32	No plume observed	N/A	N/A	N/A	N/A	N/A	N/A	N/A
RF06_leg-j3	09.09.2023	04:17:14 - 04:25:23	No plume observed	N/A	N/A	N/A	N/A	N/A	N/A	N/A
RF06_leg-j4	09.09.2023	04:25:26 - 04:32:41	No plume observed	N/A	N/A	N/A	N/A	N/A	N/A	N/A
RF06_leg-k	09.09.2023	04:34:34 - 04:45:20	No plume observed	N/A	N/A	N/A	N/A	N/A	N/A	N/A
RF06_leg-l	09.09.2023	04:49:13 - 05:02:03	No plume observed	N/A	N/A	N/A	N/A	N/A	N/A	N/A
RF06_leg-m	09.09.2023	05:04:54 - 05:14:15	No plume observed	N/A	N/A	N/A	N/A	N/A	N/A	N/A
RF06_leg-n1	09.09.2023	05:16:53 - 05:23:08	No plume observed	N/A	N/A	N/A	N/A	N/A	N/A	N/A
RF06_leg-n2	09.09.2023	05:23:08 - 05:29:28	No plume observed	N/A	N/A	N/A	N/A	N/A	N/A	N/A
RF07_leg-a	11.09.2023	00:15:05 - 00:24:47	No plume observed	N/A	N/A	N/A	N/A	N/A	N/A	N/A
RF07_leg-b	11.09.2023	02:17:27 - 02:25:45	P7.6	Overhead	Ventilation fan	UG-4	-21.958280	148.008455	No	Reason 4
RF07_leg-c1	11.09.2023	02:26:57 - 02:37:24	P7.2/3	Overhead	Ventilation fan	UG-6	-21.874763	148.018404	Yes - averaged with P5.2 and summed	N/A

Flight ID	Date	Time of leg [UTC]	Plume ID	Observa-tion type	Infrastructure type	Attributed coal mine	Plume Latitude (°)	Plume Longitude (°)	Compared with operator estimate?	Reason for omission
									with P7.4 and P7.5	
RF07_leg-c2	11.09.2023	02:04:51 - 02:15:51	P7.2/3	Overhead	Ventilation fan	UG-6	-21.876288	148.018238	Yes - averaged with P5.2 and summed with P7.4 and P7.5	N/A
RF07_leg-c2	11.09.2023	02:04:51 - 02:15:51	P7.6	Downwind	Downwind of Ventilation fan	UG-4	-21.952241	147.991831	Yes	N/A
RF07_leg-d	11.09.2023	01:55:18 - 02:03:36	P7.2/3	Downwind	Downwind of Ventilation fan	UG-6	-21.866605	147.998069	Yes - averaged with P5.2 and summed with P7.4 and P7.5	N/A
RF07_leg-d	11.09.2023	01:55:18 - 02:03:36	P7.5	Overhead	Ventilation fan	UG-6	-21.887900	147.988911	Yes - summed with P7.4 and average of P7.2/3 and P5.2	N/A
RF07_leg-d	11.09.2023	01:55:18 - 02:03:36	P7.6	Downwind	Downwind of Ventilation fan	UG-4	-21.956328	147.965842	Yes	N/A
RF07_leg-e	11.09.2023	01:29:17 - 01:39:41	P7.1	Overhead	Ventilation fan	MC-3-UG	-21.837944	147.98334	No; however flux estimate possible	Not representative of facility-level emissions
RF07_leg-e	11.09.2023	01:29:17 - 01:39:41	P7.4	Overhead	Ventilation fan	UG-6	-21.884111	147.972607	Yes - summed with P7.5 and average of P7.2/3 and P5.2	N/A
RF07_leg-f	11.09.2023	01:40:32-01:53:18	P7.1	Overhead	Ventilation fan	MC-3-UG	-21.836926	147.984307	No	Reason 4
RF07_leg-f	11.09.2023	01:40:32-01:53:18	P7.7	Overhead	Ventilation fan	MC-3-UG	-21.821103	147.984279	No	Reason 4
RF07_leg-g	11.09.2023	01:08:14 - 01:27:11	No plume observed	N/A	N/A	N/A	N/A	N/A	N/A	N/A
RF07_leg-h	11.09.2023	00:58:08 - 01:07:05	No plume observed	N/A	N/A	N/A	N/A	N/A	N/A	N/A

Flight ID	Date	Time of leg [UTC]	Plume ID	Observation type	Infrastructure type	Attributed coal mine	Plume Latitude (°)	Plume Longitude (°)	Compared with operator estimate?	Reason for omission
RF07_leg-i	11.09.2023	00:45:47 - 00:56:20	No plume observed	N/A	N/A	N/A	N/A	N/A	N/A	N/A
RF07_leg-j	11.09.2023	00:34:56 - 00:43:56	No plume observed	N/A	N/A	N/A	N/A	N/A	N/A	N/A
RF08_leg-a	15.09.2023	02:32:27 - 02:48:06	No plume observed	N/A	N/A	N/A	N/A	N/A	N/A	N/A
RF08_leg-b	15.09.2023	02:14:39 - 02:28:09	P8.1	Overhead	Open-cut coal mine	OC-32	-21.459134	148.379206	No	Reason 4
RF08_leg-c1	15.09.2023	01:37:18 - 01:50:45	P8.1	Downwind	Downwind of open-cut coal mine	OC-32	-21.389812	148.297968	No	Reason 4
RF08_leg-c2	15.09.2023	01:52:39 - 02:09:03	P8.1	Downwind	Downwind of open-cut coal mine	OC-32	-21.387453	148.302634	No	Reason 4
RF08_leg-c3	15.09.2023	03:46:31 - 04:03:10	P8.1	Downwind	Downwind of open-cut coal mine	OC-32	-21.403449	148.287852	No	Reason 4
RF08_leg-d1	15.09.2023	02:56:09 - 03:10:09	P8.1	Downwind	Downwind of open-cut coal mine	OC-32	-21.377863	148.28182	No	Reason 4
RF08_leg-d2	15.09.2023	03:12:03 - 03:28:33	P8.1	Downwind	Downwind of open-cut coal mine	OC-32	-21.380230	148.281026	No	Reason 4
RF08_leg-e1	15.09.2023	01:01:57- 01:15:42	P8.1	Downwind	Downwind of open-cut coal mine	OC-32	-21.361476	148.246907	No	Reason 4
RF08_leg-e2	15.09.2023	01:18:21 - 01:33:51	P8.1	Downwind	Downwind of open-cut coal mine	OC-32	-21.362843	148.247041	No	Reason 4
RF08_leg-e3	15.09.2023	03:30:27- 03:43:13	P8.1	Downwind	Downwind of open-cut coal mine	OC-32	-21.360597	148.249443	No	Reason 4
RF09_leg-a	16.09.2023	01:06:39 - 01:16:15	No plume observed	N/A	N/A	N/A	N/A	N/A	N/A	N/A
RF09_leg-b	16.09.2023	01:17:57 - 01:30:24	No plume observed	N/A	N/A	N/A	N/A	N/A	N/A	N/A
RF09_leg-c	16.09.2023	01:32:15 - 01:41:27	P9.4	Overhead	Ventilation fan	UG-3	-23.044612	148.590302	Yes - summed with P9.3 and P9.5	N/A
RF09_leg-d	16.09.2023	01:42:18 - 01:54:45	P9.4	Downwind	Downwind of Ventilation fan	UG-3	-23.045386	148.586133	Yes - summed with P9.3 and P9.5	N/A
RF09_leg-d	16.09.2023	01:42:18 - 01:54:45	P9.5	Overhead	Ventilation fan	UG-3	-23.076583	148.563954	Yes - summed with P9.3 and P9.4	N/A
RF09_leg-e	16.09.2023	01:56:18 - 02:08:54	P9.3	Overhead	Ventilation fan	UG-3	-23.046111	148.565581	Yes - summed	N/A

Flight ID	Date	Time of leg [UTC]	Plume ID	Observa-tion type	Infrastructure type	Attributed coal mine	Plume Latitude (°)	Plume Longitude (°)	Compared with operator estimate?	Reason for omission
									with P9.4 and P9.5	
RF09_leg-e	16.09.2023	01:56:18 - 02:08:54	P9.4	Downwind	Downwind of Ventilation fan	UG-3	-23.036598	148.578205	No	Reason 5
RF09_leg-e	16.09.2023	01:56:18 - 02:08:54	P9.5	Downwind	Downwind of Ventilation fan	UG-3	-23.073836	148.559999	Yes - summed with P9.3 and P9.4	N/A
RF09_leg-f	16.09.2023	02:10:09 - 02:26:36	P9.3	Overhead	Ventilation fan	UG-3	-23.044887	148.563131	Yes - summed with P9.4 and P9.5	N/A
RF09_leg-g	16.09.2023	02:27:51 - 02:41:30	P9.1	Overhead	Open-cut coal mine	OC-13	-22.844839	148.649818	No	Reason 6
RF09_leg-g	16.09.2023	02:27:51 - 02:41:30	P9.2	Overhead	Ventilation fan	MC-2-UG	-22.986953	148.576961	Yes	N/A
RF09_leg-g	16.09.2023	02:27:51 - 02:41:30	P9.6	Overhead	Unidentified source - possible abandoned coal exploration borehole or groundwater bore	N/A	-22.937697	148.601346	No; however flux estimate possible	Unidentifie d source
RF09_leg-h	16.09.2023	02:42:45 - 02:59:30	P9.1	Overhead	Open-cut coal mine	OC-13	-22.844349	148.649504	No	Reason 6
RF09_leg-h	16.09.2023	02:42:45 - 02:59:30	P9.2	Downwind	Downwind of Ventilation fan	MC-2-UG	-22.982615	148.575347	Yes	N/A
RF09_leg-h	16.09.2023	02:42:45 - 02:59:30	P9.6	Overhead	Unidentified source - possible abandoned coal exploration borehole or groundwater bore	N/A	-22.938507	148.600287	No; however flux estimate possible	Unidentifie d source
RF09_leg-i	16.09.2023	03:01:24 - 03:13:57	P9.2	Downwind	Downwind of Ventilation fan	MC-2-UG	-22.978973	148.563678	Yes	N/A
RF09_leg-j	16.09.2023	03:15:24 - 03:31:27	P9.2	Downwind	Downwind of Ventilation fan	MC-2-UG	-22.981453	148.555011	Yes	N/A
RF09_leg-k	16.09.2023	03:33:21 - 03:41:54	No plume observed	N/A	N/A	N/A	N/A	N/A	N/A	N/A
RF09_leg-l	16.09.2023	03:43:12 - 03:55:04	No plume observed	N/A	N/A	N/A	N/A	N/A	N/A	N/A
RF09_leg-m	16.09.2023	03:56:46 - 04:05:13	No plume observed	N/A	N/A	N/A	N/A	N/A	N/A	N/A
RF09_leg-n	16.09.2023	04:06:19 - 04:17:13	No plume observed	N/A	N/A	N/A	N/A	N/A	N/A	N/A

Flight ID	Date	Time of leg [UTC]	Plume ID	Observa-tion type	Infrastructure type	Attributed coal mine	Plume Latitude (°)	Plume Longitude (°)	Compared with operator estimate?	Reason for omission
RF09_leg-o	16.09.2023	04:19:07 - 04:27:46	No plume observed	N/A	N/A	N/A	N/A	N/A	N/A	N/A
RF10_leg-a	17.09.2023	04:51:41 - 05:06:20	No plume observed	N/A	N/A	N/A	N/A	N/A	N/A	N/A
RF10_leg-b	17.09.2023	04:36:02 - 04:50:11	No plume observed	N/A	N/A	N/A	N/A	N/A	N/A	N/A
RF10_leg-c	17.09.2023	04:20:47 - 04:34:44	P10.4	Overhead	Ventilation fan	MC-1-UG	-23.459825	148.483656	Yes	N/A
RF10_leg-d	17.09.2023	04:19:17 - 04:19:17	P10.4	Overhead	Ventilation fan	MC-1-UG	-23.459825	148.483656	No	Reason 5
RF10_leg-e	17.09.2023	01:06:13 - 01:20:43	No plume observed	N/A	N/A	N/A	N/A	N/A	N/A	N/A
RF10_leg-f	17.09.2023	01:22:40 - 01:35:01	No plume observed	N/A	N/A	N/A	N/A	N/A	N/A	N/A
RF10_leg-g	17.09.2023	01:37:31 - 01:50:40	No plume observed	N/A	N/A	N/A	N/A	N/A	N/A	N/A
RF10_leg-h	17.09.2023	01:52:37 - 02:04:10	P10.1	Overhead	Ventilation fan	UG-2	-23.298537	148.321208	Yes - summed with P10.2 and P10.3	N/A
RF10_leg-h	17.09.2023	01:52:37 - 02:04:10	P10.2	Overhead	Flare	UG-2	-23.322810	148.315776	Yes - summed with P10.1 and P10.3	N/A
RF10_leg-h	17.09.2023	01:52:37 - 02:04:10	P10.3	Overhead	Flare	UG-2	-23.333719	148.309978	Yes - summed with P10.1 and P10.2	N/A
RF10_leg-i	17.09.2023	02:06:31 - 02:19:07	P10.1	Overhead	Ventilation fan	UG-2	-23.298729	148.315425	Yes - summed with P10.2 and P10.3	N/A
RF10_leg-i	17.09.2023	02:06:31 - 02:19:07	P10.2	Downwind	Downwind of flare	UG-2	-23.319647	148.308753	Yes - summed with P10.1 and P10.3	N/A
RF10_leg-i	17.09.2023	02:06:31 - 02:19:07	P10.3	Downwind	Downwind of flare	UG-2	-23.332459	148.304029	Yes - summed with P10.1 and P10.2	N/A
RF10_leg-j	17.09.2023	02:21:10 - 02:33:22	P10.1	Downwind	Downwind of Ventilation fan	UG-2	-23.296099	148.306498	Yes - summed	N/A

Flight ID	Date	Time of leg [UTC]	Plume ID	Observa-tion type	Infrastructure type	Attributed coal mine	Plume Latitude (°)	Plume Longitude (°)	Compared with operator estimate?	Reason for omission
									with P10.2 and P10.3	
RF10_leg-j	17.09.2023	02:21:10 - 02:33:22	P10.2	Downwind	Downwind of flare	UG-2	-23.313697	148.299086	No	Reason 4
RF10_leg-k	17.09.2023	02:35:43 - 02:47:55	P10.1	Downwind	Downwind of Ventilation fan	UG-2	-23.295162	148.297612	Yes - summed with P10.2 and P10.3	N/A
RF10_leg-k	17.09.2023	02:35:43 - 02:47:55	P10.2	Downwind	Downwind of flare	UG-2	-23.312054	148.291276	Yes - summed with P10.1 and P10.3	N/A
RF10_leg-l	17.09.2023	02:49:43 - 03:02:01	P10.1	Downwind	Downwind of Ventilation fan	UG-2	-23.292677	148.286828	No	Reason 2
RF10_leg-m	17.09.2023	03:04:34 - 03:17:31	P10.1	Downwind	Downwind of Ventilation fan	UG-2	-23.286303	148.281942	No	Reason 2
RF10_leg-n	17.09.2023	03:19:31 - 03:32:44	No plume observed	N/A	N/A	N/A	N/A	N/A	N/A	N/A
RF10_leg-o	17.09.2023	03:34:20 - 03:46:38	No plume observed	N/A	N/A	N/A	N/A	N/A	N/A	N/A
RF11_leg-a	19.09.2023	02:24:51 - 02:28:15	No plume observed	N/A	N/A	N/A	N/A	N/A	N/A	N/A
RF11_leg-b	19.09.2023	02:20:48 - 02:23:39	No plume observed	N/A	N/A	N/A	N/A	N/A	N/A	N/A
RF11_leg-c	19.09.2023	02:16:44 - 02:19:47	No plume observed	N/A	N/A	N/A	N/A	N/A	N/A	N/A
RF11_leg-d	19.09.2023	02:12:38 - 02:15:29	No plume observed	N/A	N/A	N/A	N/A	N/A	N/A	N/A
RF11_leg-e	19.09.2023	02:08:26 - 02:11:38	No plume observed	N/A	N/A	N/A	N/A	N/A	N/A	N/A
RF11_leg-f	19.09.2023	02:04:20- 02:07:17	No plume observed	N/A	N/A	N/A	N/A	N/A	N/A	N/A
RF11_leg-g	19.09.2023	02:00:08 - 02:03:08	P11.2	Overhead	Open-cut coal mine	OC-13	-22.845405	148.654648	No	Reason 6
RF11_leg-h	19.09.2023	01:56:11 - 01:58:53	P11.2	Overhead	Open-cut coal mine	OC-13	-22.845863	148.652335	No	Reason 6
RF11_leg-i	19.09.2023	01:51:56 - 01:55:08	P11.2	Overhead	Open-cut coal mine	OC-13	-22.846539	148.650023	No	Reason 6
RF11_leg-j	19.09.2023	01:47:44 - 01:50:35	P11.2	Overhead	Open-cut coal mine	OC-13	-22.848556	148.648964	No	Reason 6

Flight ID	Date	Time of leg [UTC]	Plume ID	Observa-tion type	Infrastructure type	Attributed coal mine	Plume Latitude (°)	Plume Longitude (°)	Compared with operator estimate?	Reason for omission
RF11_leg-k	19.09.2023	01:43:14 - 01:46:35	P11.1	Overhead	Open-cut coal mine	OC-13	-22.834814	148.63847	No	Reason 6
RF11_leg-k	19.09.2023	01:43:14 - 01:46:35	P11.2	Overhead	Open-cut coal mine	OC-13	-22.851028	148.647041	No	Reason 6
RF11_leg-l	19.09.2023	01:38:59 - 01:41:59	P11.1	Overhead	Open-cut coal mine	OC-13	-22.837257	148.6372	No	Reason 6
RF11_leg-m	19.09.2023	01:34:32 - 01:37:35	P11.1	Overhead	Open-cut coal mine	OC-13	-22.835724	148.633888	No	Reason 6
RF11_leg-n	19.09.2023	01:30:11 - 01:33:08	No plume observed	N/A	N/A	N/A	N/A	N/A	N/A	N/A
RF11_leg-o	19.09.2023	01:25:05 - 01:28:44	No plume observed	N/A	N/A	N/A	N/A	N/A	N/A	N/A
RF11_leg-p	19.09.2023	01:20:17 - 01:23:17	No plume observed	N/A	N/A	N/A	N/A	N/A	N/A	N/A
RF11_leg-q	19.09.2023	01:15:14 - 01:18:41	No plume observed	N/A	N/A	N/A	N/A	N/A	N/A	N/A
RF12_leg-a	21.09.2023	02:15:05 - 02:18:38	No plume observed	N/A	N/A	N/A	N/A	N/A	N/A	N/A
RF12_leg-b	21.09.2023	02:20:05 - 02:22:59	No plume observed	N/A	N/A	N/A	N/A	N/A	N/A	N/A
RF12_leg-c	21.09.2023	02:24:23 - 02:27:59	P12.1	Downwind	Downwind of Ventilation fan	UG-2	-23.300746	148.333528	No	Reason 1
RF12_leg-d	21.09.2023	02:29:44 - 02:32:35	P12.1	Overhead/ Downwind	Overhead and/or downwind of Ventilation fan	UG-2	-23.300028	148.326513	No	Reason 1
RF12_leg-d	21.09.2023	02:29:44 - 02:32:35	P12.2	Overhead/ Downwind	Overhead and/or downwind of flares	UG-2	-23.322518	148.31918	No	Reason 1
RF12_leg-e1	21.09.2023	02:33:59 - 02:37:23	P12.1	Overhead	Ventilation fan	UG-2	-23.299151	148.324878	No	Reason 1
RF12_leg-e2	21.09.2023	02:59:57 - 03:03:09	P12.1	Overhead	Ventilation fan	UG-2	-23.297966	148.320969	No	Reason 1
RF12_leg-e2	21.09.2023	02:59:57 - 03:03:09	P12.2	Overhead/ Downwind	Overhead and/or downwind of flares	UG-2	-23.319889	148.3149	No	Reason 1
RF12_leg-f	21.09.2023	02:39:03 - 02:42:09	No plume observed	N/A	N/A	N/A	N/A	N/A	N/A	N/A
RF12_leg-g	21.09.2023	02:43:51 - 02:48:06	No plume observed	N/A	N/A	N/A	N/A	N/A	N/A	N/A
RF12_leg-h	21.09.2023	02:49:57 - 02:53:09	No plume observed	N/A	N/A	N/A	N/A	N/A	N/A	N/A

Flight ID	Date	Time of leg [UTC]	Plume ID	Observa-tion type	Infrastructure type	Attributed coal mine	Plume Latitude (°)	Plume Longitude (°)	Compared with operator estimate?	Reason for omission
RF12_leg-i	21.09.2023	02:54:33 - 02:58:24	No plume observed	N/A	N/A	N/A	N/A	N/A	N/A	N/A
RF12_leg-s1	21.09.2023	01:53:02 - 01:55:44	No plume observed	N/A	N/A	N/A	N/A	N/A	N/A	N/A
RF12_leg-s2	21.09.2023	01:55:47 - 02:10:05	No plume observed	N/A	N/A	N/A	N/A	N/A	N/A	N/A
RF12_leg-s3	21.09.2023	02:10:11 - 02:13:32	No plume observed	N/A	N/A	N/A	N/A	N/A	N/A	N/A
RF12_leg-s4	21.09.2023	03:04:12 - 03:09:09	No plume observed	N/A	N/A	N/A	N/A	N/A	N/A	N/A
RF13_leg-a	22.09.2023	01:17:52 - 01:23:13	No plume observed	N/A	N/A	N/A	N/A	N/A	N/A	N/A
RF13_leg-b	22.09.2023	01:25:25 - 01:32:16	No plume observed	N/A	N/A	N/A	N/A	N/A	N/A	N/A
RF13_leg-c	22.09.2023	01:33:52 - 01:39:25	No plume observed	N/A	N/A	N/A	N/A	N/A	N/A	N/A
RF13_leg-d	22.09.2023	01:41:22 - 01:48:19	No plume observed	N/A	N/A	N/A	N/A	N/A	N/A	N/A
RF13_leg-e	22.09.2023	01:49:37 - 01:55:28	No plume observed	N/A	N/A	N/A	N/A	N/A	N/A	N/A
RF13_leg-f	22.09.2023	01:57:01 - 02:03:49	P13.3	Overhead	Open-cut coal mine	OC-22	-22.080031	148.242096	No	Reason 6
RF13_leg-g	22.09.2023	02:05:40 - 02:11:22	P13.3	Overhead	Open-cut coal mine	OC-22	-22.080136	148.234252	No	Reason 6
RF13_leg-h	22.09.2023	02:12:52 - 02:19:37	P13.3	Overhead	Open-cut coal mine	OC-22	-22.074111	148.229638	No	Reason 6
RF13_leg-i	22.09.2023	02:21:04 - 02:26:40	No plume observed	N/A	N/A	N/A	N/A	N/A	N/A	N/A
RF13_leg-j	22.09.2023	02:28:25- 02:35:31	No plume observed	N/A	N/A	N/A	N/A	N/A	N/A	N/A
RF13_leg-k	22.09.2023	02:37:13 - 02:42:55	No plume observed	N/A	N/A	N/A	N/A	N/A	N/A	N/A
RF13_leg-l	22.09.2023	02:44:22 - 02:51:25	P13.2	Overhead	Ventilation fan	UG-5	-21.993879	148.261222	No	Reason 3

Flight ID	Date	Time of leg [UTC]	Plume ID	Observa-tion type	Infrastructure type	Attributed coal mine	Plume Latitude (°)	Plume Longitude (°)	Compared with operator estimate?	Reason for omission
RF13_leg-m	22.09.2023	02:53:13-02:58:43	P13.2	Downwind	Downwind of Ventilation fan	UG-5	-21.991484	148.255981	No; however flux estimate possible	Not representative of facility-level emissions
RF13_leg-n	22.09.2023	03:00:25-03:07:40	P13.2	Downwind	Downwind of Ventilation fan	UG-5	-21.984927	148.247113	No	Reason 5
RF13_leg-o	22.09.2023	03:11:37 - 03:28:50	P13.1	Downwind	Open-cut coal mines	OC-28, OC-30	-21.779416	148.379154	Yes	N/A
RF13_leg-p	22.09.2023	03:32:53 - 03:55:20	P13.1	Downwind	Open-cut coal mines	OC-28, OC-30	-21.698730	148.332895	Yes	N/A
RF13_leg-q	22.09.2023	04:04:14 - 04:27:05	No plume observed	N/A	N/A	N/A	N/A	N/A	N/A	N/A
RF16_leg-a	26.09.2023	03:04:01 - 03:07:04	No plume observed	N/A	N/A	N/A	N/A	N/A	N/A	N/A
RF16_leg-b	26.09.2023	03:00:01 - 03:03:19	No plume observed	N/A	N/A	N/A	N/A	N/A	N/A	N/A
RF16_leg-c	26.09.2023	02:54:49 - 02:58:58	No plume observed	N/A	N/A	N/A	N/A	N/A	N/A	N/A
RF16_leg-d	26.09.2023	02:49:04 - 02:53:55	No plume observed	N/A	N/A	N/A	N/A	N/A	N/A	N/A
RF16_leg-e	26.09.2023	02:38:28 - 02:46:16	No plume observed	N/A	N/A	N/A	N/A	N/A	N/A	N/A
RF16_leg-f	26.09.2023	02:23:55 - 02:35:07	No plume observed	N/A	N/A	N/A	N/A	N/A	N/A	N/A
RF16_leg-g	26.09.2023	04:16:37 - 04:12:22	P16.1	Overhead	Open-cut coal mine	OC-12	-22.900575	148.768759	No	Reason 3
RF16_leg-g	26.09.2023	04:16:37 - 04:12:22	P16.2	Overhead	Open-cut coal mine	OC-12	-22.949451	148.787442	No	Reason 6
RF16_leg-h	26.09.2023	04:11:16 - 04:06:34	P16.1	Downwind	Downwind of open-cut coal mine	OC-12	-22.901242	148.759864	No	Reason 3
RF16_leg-h	26.09.2023	04:11:16 - 04:06:34	P16.2	Overhead	Open-cut coal mine	OC-12	-22.950933	148.787684	No	Reason 6
RF16_leg-i	26.09.2023	04:05:16 - 04:01:10	P16.2	Downwind	Downwind of open-cut coal mine	OC-12	-22.952057	148.780642	No; however flux estimate possible	Not representative of facility-level emissions

Flight ID	Date	Time of leg [UTC]	Plume ID	Observation type	Infrastructure type	Attributed coal mine	Plume Latitude (°)	Plume Longitude (°)	Compared with operator estimate?	Reason for omission
RF16_leg-j	26.09.2023	04:00:25 - 03:54:04	P16.2	Downwind	Downwind of open-cut coal mine	OC-12	-22.954231	148.778561	No	Reason 4
RF17_leg-a	27.09.2023	02:16:23 - 02:19:32	No plume observed	N/A	N/A	N/A	N/A	N/A	N/A	N/A
RF17_leg-b	27.09.2023	02:12:35 - 02:15:38	No plume observed	N/A	N/A	N/A	N/A	N/A	N/A	N/A
RF17_leg-c	27.09.2023	02:08:23 - 02:11:41	No plume observed	N/A	N/A	N/A	N/A	N/A	N/A	N/A
RF17_leg-d	27.09.2023	02:04:38 - 02:07:26	No plume observed	N/A	N/A	N/A	N/A	N/A	N/A	N/A
RF17_leg-e	27.09.2023	02:00:26 - 02:03:41	No plume observed	N/A	N/A	N/A	N/A	N/A	N/A	N/A
RF17_leg-f	27.09.2023	01:56:28 - 01:59:31	No plume observed	N/A	N/A	N/A	N/A	N/A	N/A	N/A
RF17_leg-g	27.09.2023	01:52:01 - 01:55:25	No plume observed	N/A	N/A	N/A	N/A	N/A	N/A	N/A
RF17_leg-h	27.09.2023	01:47:58 - 01:51:19	P17.3	Overhead	Ventilation fan	UG-4	-21.961701	148.010417	No	Reason 3
RF17_leg-i	27.09.2023	01:43:34 - 01:47:04	P17.3	Overhead	Ventilation fan	UG-4	-21.957774	148.0054	Yes	N/A
RF17_leg-j	27.09.2023	01:38:58- 01:42:37	No plume observed	N/A	N/A	N/A	N/A	N/A	N/A	N/A
RF17_leg-k	27.09.2023	03:41:17 - 03:47:56	No plume observed	N/A	N/A	N/A	N/A	N/A	N/A	N/A
RF17_leg-l	27.09.2023	03:32:41 - 03:40:29	No plume observed	N/A	N/A	N/A	N/A	N/A	N/A	N/A
RF17_leg-m	27.09.2023	03:25:05 - 03:31:56	P17.1	Overhead	Ventilation fan	MC-3-UG	-21.820937	147.983829	No	Reason 3
RF17_leg-m	27.09.2023	03:25:05 - 03:31:56	P17.2	Overhead	Ventilation fan	MC-3-UG	-21.837475	147.984829	No	Reason 3
RF17_leg-n	27.09.2023	03:16:05 - 03:23:50	P17.1	Overhead	Ventilation fan	MC-3-UG	-21.819964	147.982907	No	Reason 5
RF17_leg-n	27.09.2023	03:16:05 - 03:23:50	P17.2	Overhead	Ventilation fan	MC-3-UG	-21.835762	147.984228	No	Not representative of facility-level emissions

Flight ID	Date	Time of leg [UTC]	Plume ID	Observation type	Infrastructure type	Attributed coal mine	Plume Latitude (°)	Plume Longitude (°)	Compared with operator estimate?	Reason for omission
RF17_leg-o	27.09.2023	03:08:38 - 03:15:11	P17.1	Downwind	Downwind of Ventilation fan	MC-3-UG	-21.813972	147.975114	No	Reason 4
RF17_leg-p	27.09.2023	03:00:17 - 03:07:53	No plume observed	N/A	N/A	N/A	N/A	N/A	N/A	N/A
RF17_leg-q	27.09.2023	02:52:44 - 02:59:23	No plume observed	N/A	N/A	N/A	N/A	N/A	N/A	N/A
RF17_leg-r	27.09.2023	02:44:11 - 02:51:44	No plume observed	N/A	N/A	N/A	N/A	N/A	N/A	N/A
RF17_leg-s1	27.09.2023	02:24:59 - 02:40:56	No plume observed	N/A	N/A	N/A	N/A	N/A	N/A	N/A
RF17_leg-s2	27.09.2023	03:53:35 - 04:11:35	No plume observed	N/A	N/A	N/A	N/A	N/A	N/A	N/A
RF17_leg-t1	27.09.2023	01:13:22 - 01:36:16	No plume observed	N/A	N/A	N/A	N/A	N/A	N/A	N/A
RF17_leg-t2	27.09.2023	04:11:44 - 04:24:29	P17.4	Downwind	Downwind of open-cut coal mine	OC-19	-22.223916	148.113302	No	Reason 3
RF18_leg-a	28.09.2023	02:13:50 - 02:18:56	No plume observed	N/A	N/A	N/A	N/A	N/A	N/A	N/A
RF18_leg-b	28.09.2023	02:20:14 - 02:26:14	No plume observed	N/A	N/A	N/A	N/A	N/A	N/A	N/A
RF18_leg-c	28.09.2023	02:27:14 - 02:32:50	No plume observed	N/A	N/A	N/A	N/A	N/A	N/A	N/A
RF18_leg-d	28.09.2023	02:33:41 - 02:41:08	No plume observed	N/A	N/A	N/A	N/A	N/A	N/A	N/A
RF18_leg-e	28.09.2023	02:42:05 - 02:47:50	No plume observed	N/A	N/A	N/A	N/A	N/A	N/A	N/A
RF18_leg-f	28.09.2023	02:48:50 - 02:56:29	P18.1	Overhead	Open-cut coal mine	OC-32	-21.476199	148.390583	No	Reason 6
RF18_leg-g	28.09.2023	02:57:32 - 03:03:32	P18.1	Overhead	Open-cut coal mine	OC-32	-21.472089	148.384935	No	Reason 6
RF18_leg-h	28.09.2023	03:04:41 - 03:13:20	P18.1	Overhead	Open-cut coal mine	OC-32	-21.468643	148.378294	No	Reason 6
RF18_leg-i	28.09.2023	03:14:17 - 03:20:23	P18.1	Downwind	Downwind of open-cut coal mine	OC-32	-21.461728	148.36613	Yes	N/A
RF18_leg-j	28.09.2023	03:21:30 - 03:29:48	P18.1	Downwind	Downwind of open-cut coal mine	OC-32	-21.461396	148.358197	Yes	N/A

Flight ID	Date	Time of leg [UTC]	Plume ID	Observation type	Infrastructure type	Attributed coal mine	Plume Latitude (°)	Plume Longitude (°)	Compared with operator estimate?	Reason for omission
RF18_leg-k	28.09.2023	03:30:42 - 03:37:42	P18.1	Downwind	Downwind of open-cut coal mine	OC-32	-21.467318	148.342926	Yes	N/A
RF18_leg-l	28.09.2023	03:39:03 - 03:45:51	P18.1	Downwind	Downwind of open-cut coal mine	OC-32	-21.478146	148.331898	Yes	N/A
RF18_leg-m	28.09.2023	03:50:21 - 03:57:42	P18.1	Downwind	Downwind of open-cut coal mine	OC-32	-21.447268	148.277552	Yes	N/A
RF18_leg-n	28.09.2023	04:00:24 - 04:11:39	P18.1	Downwind	Downwind of open-cut coal mine	OC-32	-21.428102	148.224153	Yes	N/A
RF18_leg-o	28.09.2023	02:01:35 - 02:10:14	No plume observed	N/A	N/A	N/A	N/A	N/A	N/A	N/A
RF18_leg-p	28.09.2023	04:22:03 - 04:31:12	No plume observed	N/A	N/A	N/A	N/A	N/A	N/A	N/A
RF18_leg-q	28.09.2023	04:33:15 - 04:44:57	No plume observed	N/A	N/A	N/A	N/A	N/A	N/A	N/A
RF18_leg-r	28.09.2023	04:45:45 - 04:48:24	P18.2	Overhead	Ventilation fan	UG-5	-21.993055	148.2553	No	Reason 3
RF20_leg-a	01.10.2023	01:07:19 - 01:13:34	No plume observed	N/A	N/A	N/A	N/A	N/A	N/A	N/A
RF20_leg-b	01.10.2023	01:14:37 - 01:21:07	No plume observed	N/A	N/A	N/A	N/A	N/A	N/A	N/A
RF20_leg-c	01.10.2023	01:21:58 - 01:27:52	P20.1	Overhead	Open-cut coal mine	OC-5	-23.766997	148.862318	No	Reason 6
RF20_leg-d	01.10.2023	01:28:58 - 01:36:58	P20.1	Overhead	Open-cut coal mine	OC-5	-23.767588	148.862102	No	Reason 6
RF20_leg-e	01.10.2023	01:37:40 - 01:44:47	No plume observed	N/A	N/A	N/A	N/A	N/A	N/A	N/A
RF20_leg-f	01.10.2023	01:45:47 - 01:57:14	No plume observed	N/A	N/A	N/A	N/A	N/A	N/A	N/A
RF20_leg-g	01.10.2023	01:58:02 - 02:08:02	No plume observed	N/A	N/A	N/A	N/A	N/A	N/A	N/A
RF20_leg-h	01.10.2023	02:08:56 - 02:19:44	No plume observed	N/A	N/A	N/A	N/A	N/A	N/A	N/A
RF20_leg-i	01.10.2023	02:20:38 - 02:30:53	No plume observed	N/A	N/A	N/A	N/A	N/A	N/A	N/A
RF20_leg-j1	01.10.2023	02:31:53 - 02:43:14	No plume observed	N/A	N/A	N/A	N/A	N/A	N/A	N/A

Flight ID	Date	Time of leg [UTC]	Plume ID	Observa-tion type	Infrastructure type	Attributed coal mine	Plume Latitude (°)	Plume Longitude (°)	Compared with operator estimate?	Reason for omission
RF20_leg-j2	01.10.2023	03:36:41 - 03:47:35	No plume observed	N/A	N/A	N/A	N/A	N/A	N/A	N/A
RF20_leg-k	01.10.2023	02:44:11 - 02:53:44	No plume observed	N/A	N/A	N/A	N/A	N/A	N/A	N/A
RF20_leg-l	01.10.2023	02:54:29 - 03:05:05	No plume observed	N/A	N/A	N/A	N/A	N/A	N/A	N/A
RF20_leg-m	01.10.2023	03:09:08 - 03:21:17	No plume observed	N/A	N/A	N/A	N/A	N/A	N/A	N/A

SI-8: All plumes quantified by the remote sensing aircraft and which were used in the comparison with operator estimates

Figures S26 to S32 show all the legs for which a CH_4 emission rate was estimated using the remote sensing aircraft and used in the analysis. The figures are grouped according to the type(s) of coal mine quantified as outlined in Table S8. Readers are referred to Borchardt et al. (2025) for measurements taken during flight RF18.

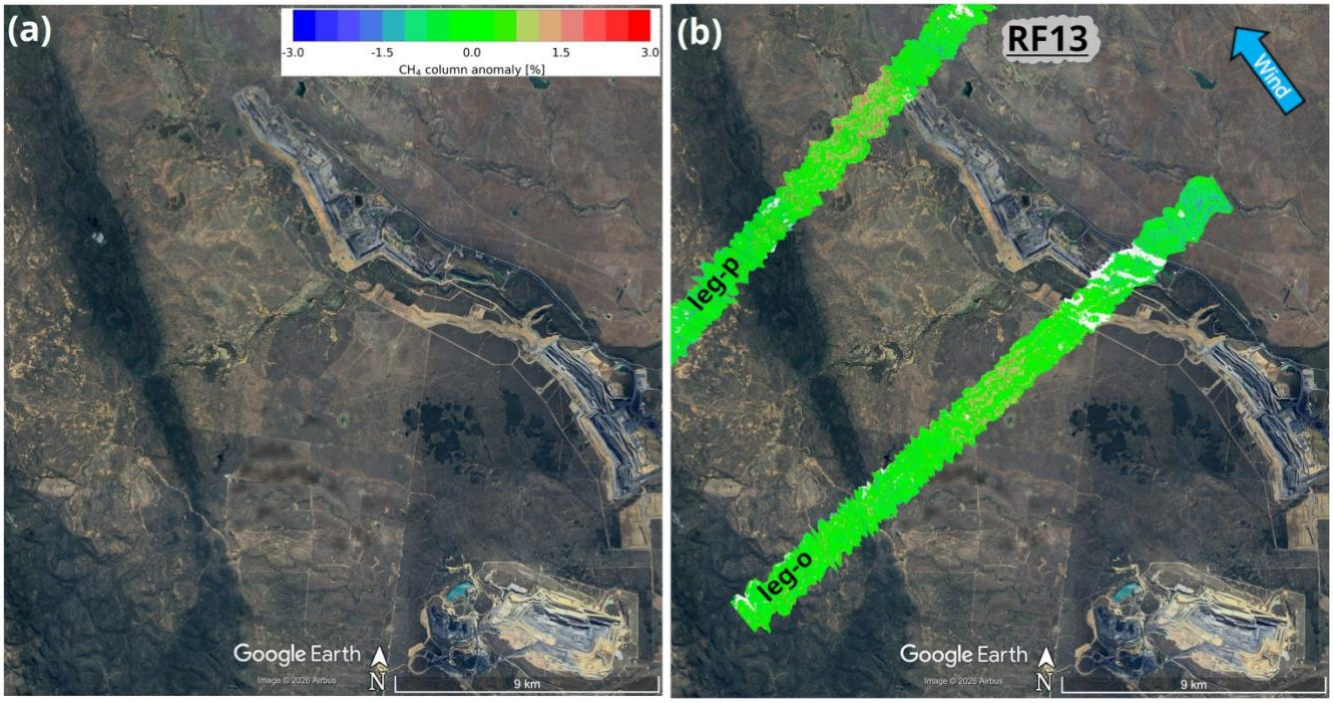

Fig. S26. (a) Google Earth imagery over OC-28 and OC-30. (b) CH_4 column anomalies retrieved from MAMAP2DL data during RF13 on 22 September 2023. P13.1 is a multi-facility estimate based on downwind legs (leg-o and leg-p), representing a mixture of multiple plumes, and therefore no pin is placed on the map. Base map from ©Google; imagery © 2026 Airbus.

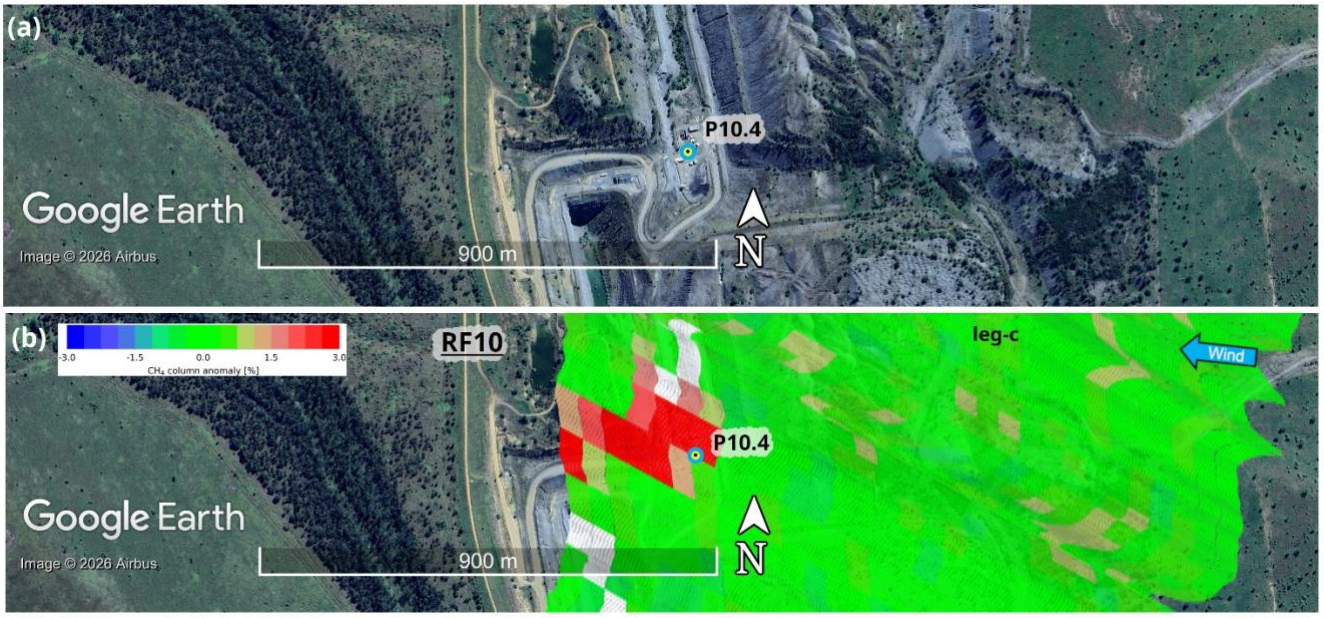

740 **Fig. S27. (a) Google Earth imagery over MC-1-UG. The cyan-yellow circle indicates the approximate source location. (b) CH_4 column anomalies retrieved from MAMAP2DL data during RF10 on 17 September 2023. Plume P10.4 is observed in leg-c. Base map from © Google; imagery © 2026 Airbus.**

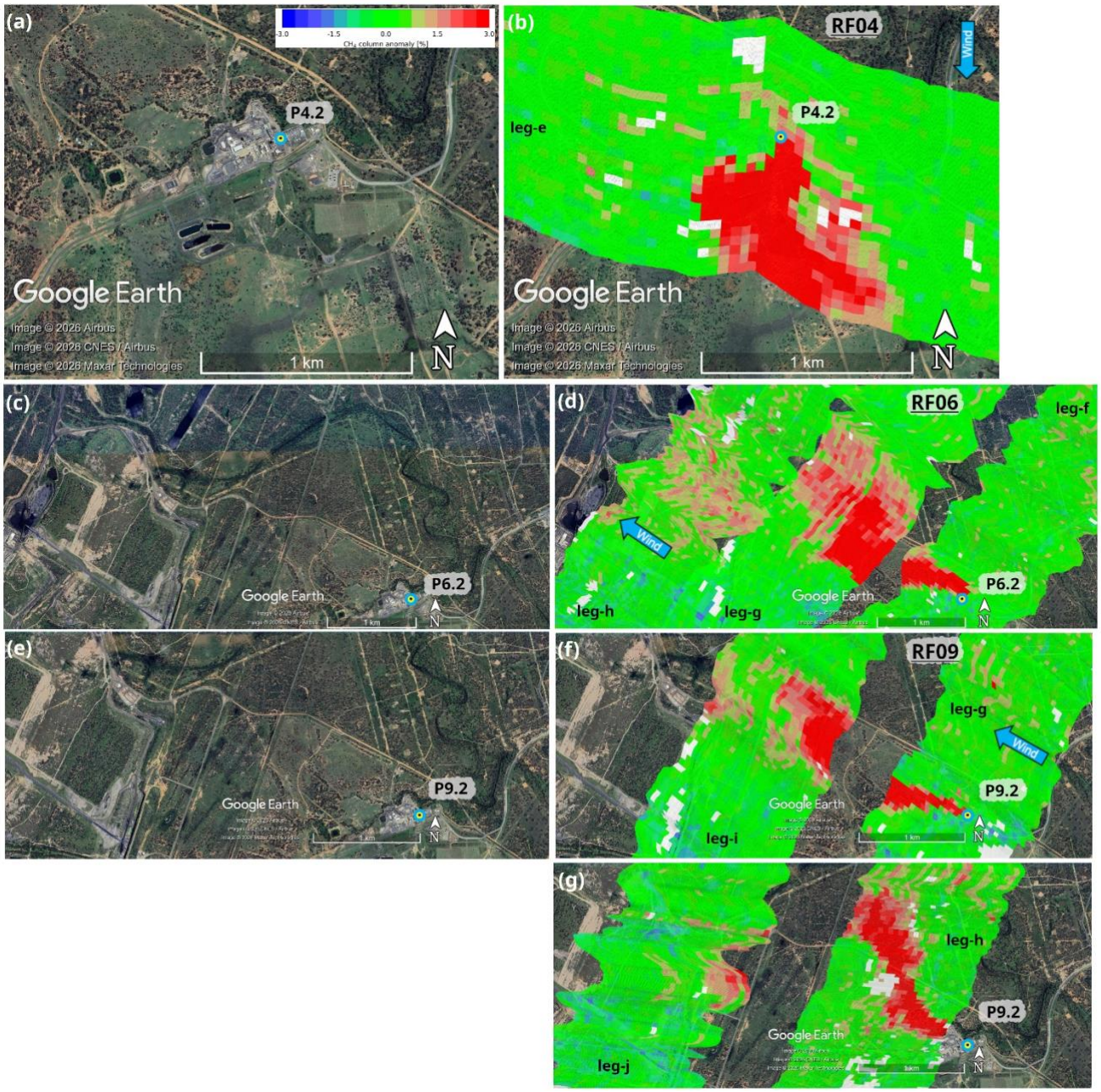

Fig. S28. (a,c,e) Google Earth imagery over MC-2-UG. The cyan-yellow circle indicates the approximate source location. (b,d,f,g) CH_4 column anomalies retrieved from MAMAP2DL data during RF04, RF06, and RF09 on 05, 09, and 16 September 2023, respectively. Plume P4.2 is observed in leg-e (b). Plume P6.2 is observed in leg-h, -g, -f (d). Plume P9.2 is observed in leg-i, -g (f) and in leg-j-, -h (g). Base map from © Google; imagery © 2026 Airbus, CNES / Airbus, and Maxar Technologies.

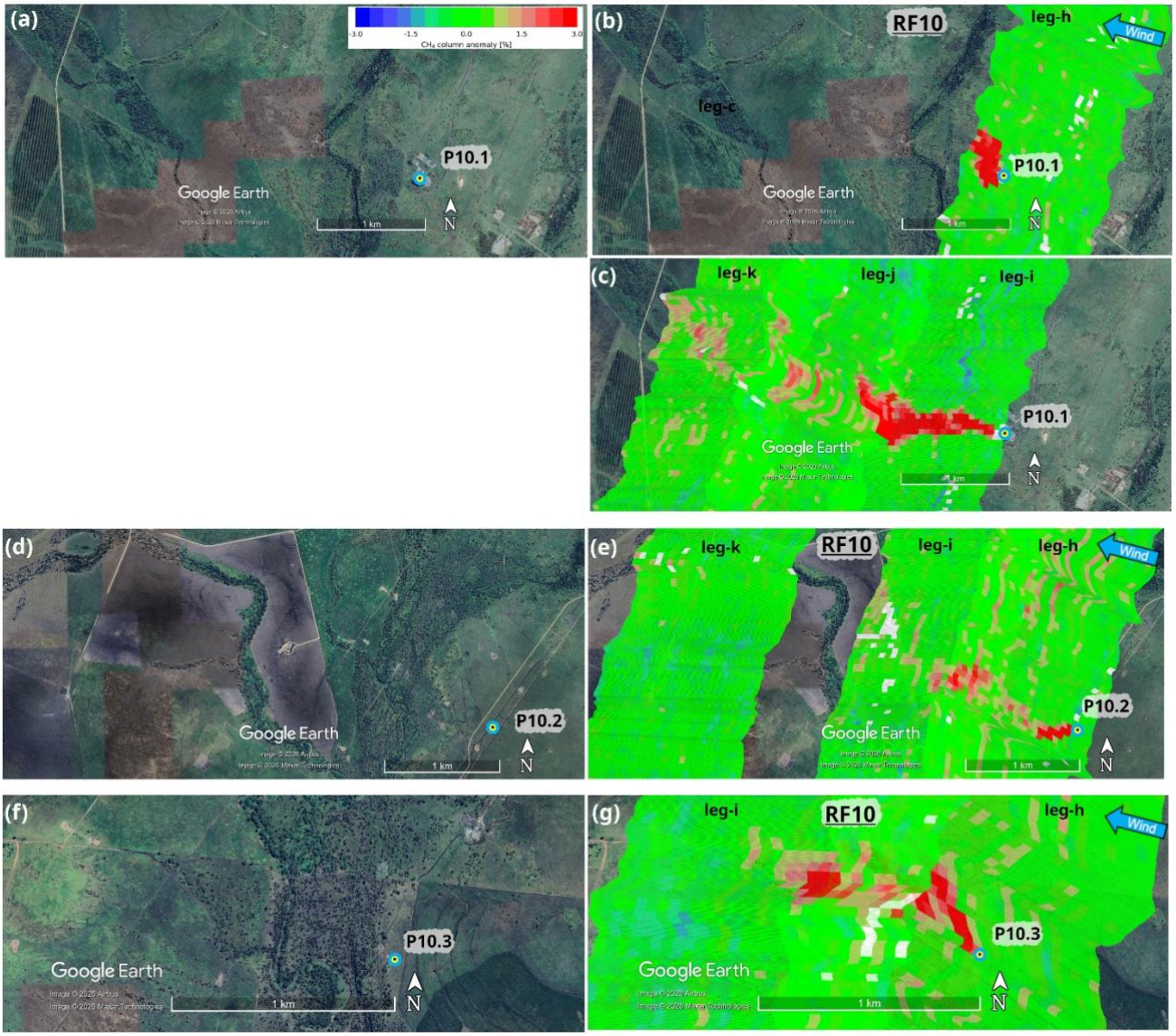

Fig. S29. (a,d,f) Google Earth imagery over UG-2. The cyan-yellow circle indicates the approximate source location. (b,c,e,g) CH_4 column anomalies retrieved from MAMAP2DL data during RF10 on 17 September 2023. Plume P10.1 is observed in leg-h (b) and leg-k, -j, -i (c). Plume P10.2 is observed in leg-k, -i, -h (e). Plume P10.3 is observed in leg-i, -h (g). Base map from © Google; imagery © 2026 Airbus and Maxar Technologies.

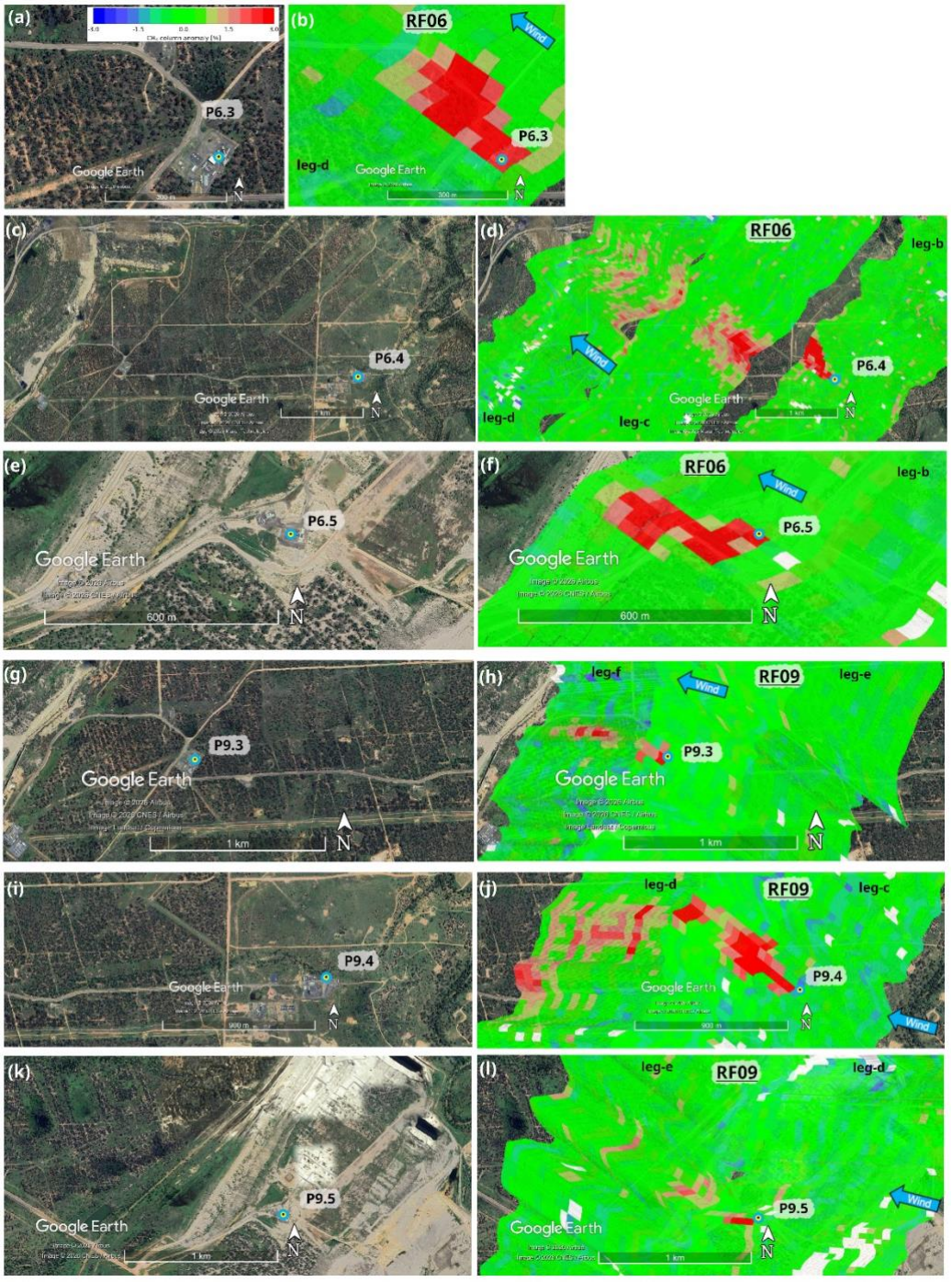

Fig. S30. (a,c,e,g,i,k) Google Earth imagery over UG-3. The cyan-yellow circle indicates the approximate source location. (b,d,f,h,j,l) CH_4 column anomalies retrieved from MAMAP2DL data during RF06 and RF09 on 09 and 16 September 2023, respectively. Plume P6.3 is observed in leg-d (b). Plume P6.4 is observed in leg-b, -c, -d (d). Plume P6.5 is observed in leg-b (f). Plume P9.3 is observed in leg-e, -f (h). Plume P9.4 is observed in leg-c, -d (j). Plume P9.5 is observed in leg-d, -e (l). Base map from © Google; imagery © 2026 Airbus, CNES / Airbus, Maxar Technologies, and Landsat / Copernicus.

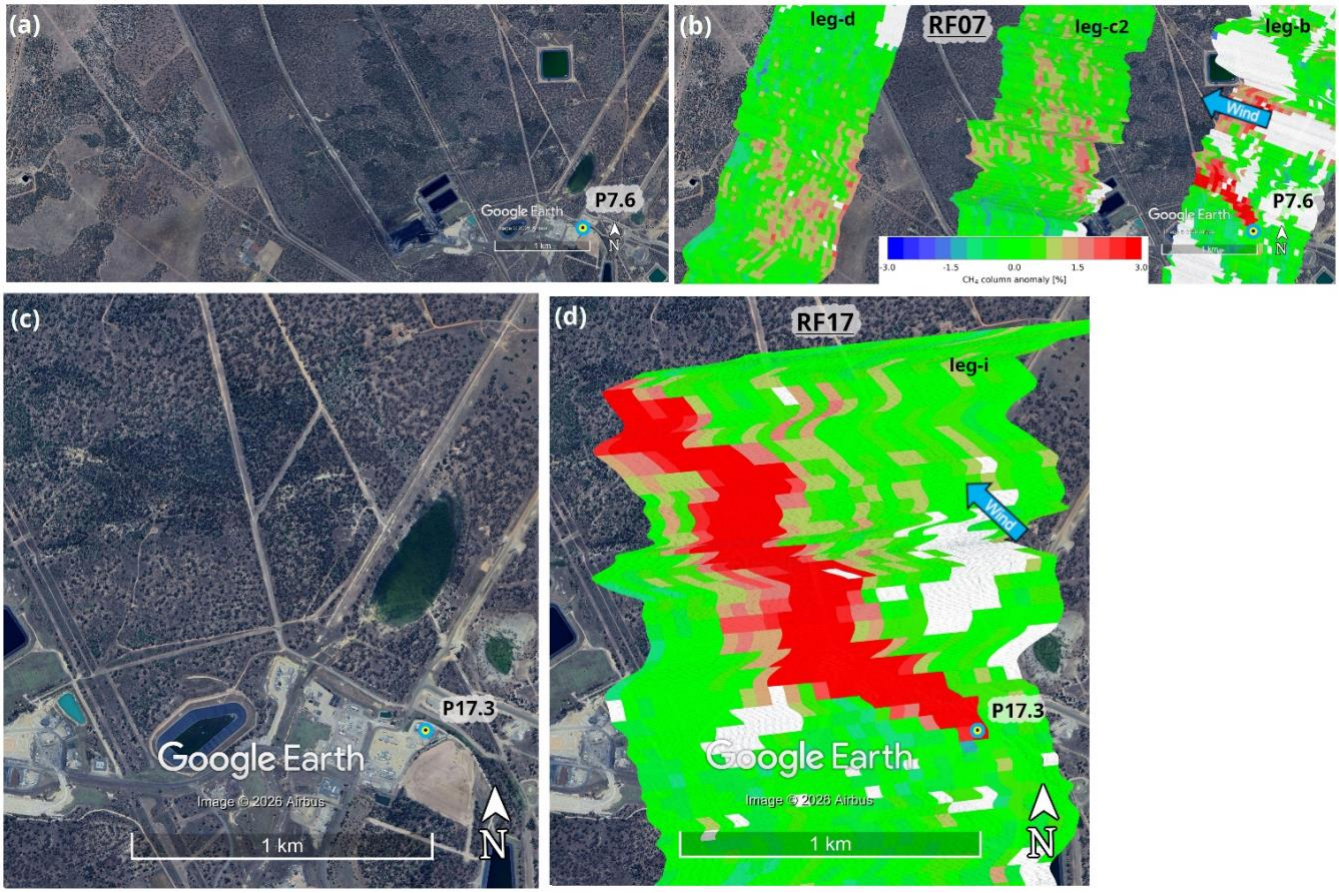

Fig. S31. (a,c) Google Earth imagery over UG-4. The cyan-yellow circle indicates the approximate source location. (b,d) CH_4 column anomalies retrieved from MAMAP2DL data during RF07 and RF17 on 11 and 27 September 2023, respectively. Plume P7.6 is observed in leg-c2, -d (b); additionally, leg-b (most eastern one) is presented which shows that the plume is originating from P7.6, however, this leg was not used for a flux estimate due to cloud contamination. Plume P17.3 is observed in leg-i (d). Base map from © Google; imagery © 2026 Airbus.

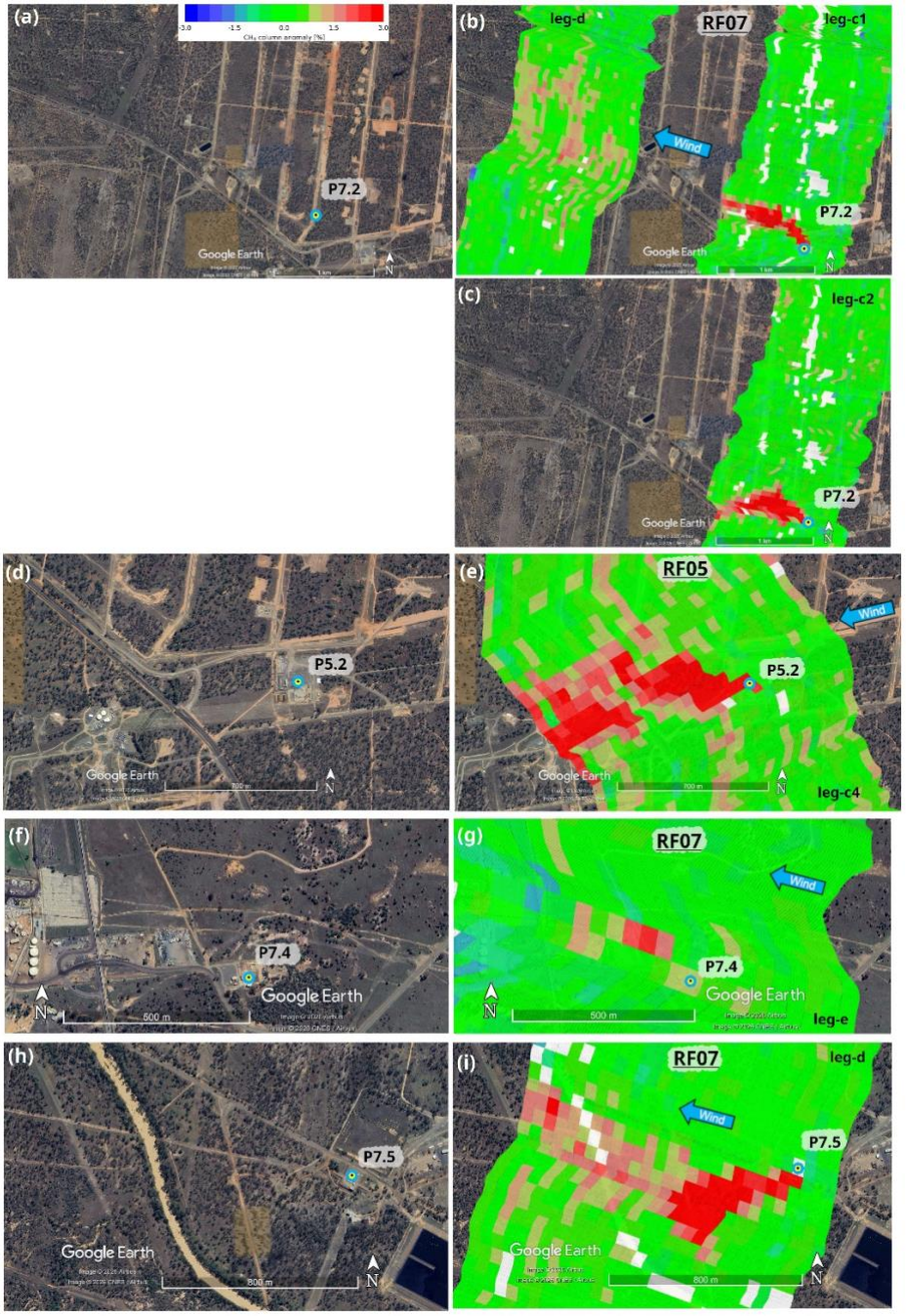

Fig. S32. (a,d,f,h) Google Earth imagery over UG-6. The cyan-yellow circle indicates the approximate source location. (b,c,e,g,i) CH_4 column anomalies retrieved from MAMAP2DL during RF05 and RF07 on 06 and 11 September 2023, respectively. Plume P7.2 is observed in leg-c1, -d (b) and leg-c2 (c). Plume P5.2 is observed in leg-c4 (e). Plume P7.4 is observed in leg-e (g). Plume P7.5 is observed in leg-d (i). Base map from © Google; imagery © 2026 Airbus, and CNES / Airbus.

SI-9: Plumes with unidentifiable source

Table S7 summarises the five plume signals detected by the remote sensing aircraft that had no identifiable source based on Google Earth imagery. Two of the plume signals corresponding to the same source location (P4.3) had detectable emissions but could not be quantified because the plumes were mixed with emissions from other sources or with plumes originating upwind and could not be separated. Three of the plume signals corresponding to the same source location (P6.6 and P9.6) had quantifiable emission rates.

Table S7. Overview of plume signal which could not be assigned to source location(s).

Flight/Leg ID	Date and time [UTC]	Plume ID	Plume latitude	Plume longitude	CH_4 emission rate (kg hr^{-1})	Possible Source
RF04_leg-b	05.09.2023, 02:43:22	P4.3	-23.031972	148.592645	Not quantified but detectable	Possible abandoned coal exploration borehole or groundwater bore
RF04_leg-d	05.09.2023, 02:56:34	P4.3	-23.032649	148.593161	Not quantified but detectable	Possible abandoned coal exploration borehole or groundwater bore
RF06_leg-g	09.09.2023, 03:37:48	P6.6	-22.935850	148.602551	56±27	Possible abandoned coal exploration borehole or groundwater bore
RF09_leg-g	16.09.2023, 02:35:46	P9.6	-22.937663	148.601490	53±30	Possible abandoned coal exploration borehole or groundwater bore
RF09_leg-h	16.09.2023, 02:50:22	P9.6	-22.938116	148.598086	10±29	Possible abandoned coal exploration borehole or groundwater bore

SI-10: Individual in-situ and remote sensing aircraft quantifications and comparison with operator reported emissions

Table S8 shows the CH_4 emission rates derived for each quantified curtain from the in-situ aircraft and each plume quantified by the remote sensing aircraft. Table S9 lists sub-facility quantifications derived from the remote sensing aircraft that could not be compared with operator estimates because they could not be combined with other quantifications to represent total facility emissions.

Table S8. All quantifications acquired by the in-situ and remote sensing aircraft and comparison with operator reported emissions determined using different NGER methodologies. Estimates are grouped according to the type(s) of coal mine quantified.

Quantification type (aircraft)	Mine(s)	Quantification ID	CH_4 emission rate (kg hr^{-1} $CH_4 \pm 1\sigma$)[a]	Mean annual reported CH_4 emissions (kg hr^{-1} CH_4)	NGER Method
Facility (in-situ)	OC-12	230916_C1	3,994±1,297	428	1
Facility (in-situ)	OC-12	230916_C2A	4,634±674	428	1
Facility (in-situ)	OC-12	231003_C1	4,607±647	428	1
Facility (in-situ)	OC-12	*$\bar{x}$ and s.e. (n=3)*	4,412±504	428	1
Facility (in-situ)	OC-16	230906_C3	995±374	265	2
Facility (in-situ)	OC-30	230925_C1	8,248±1,150	1,048	1
Facility (in-situ)	OC-32[b]	230915_C1	7,372±1,912	4,334	2
Facility (in-situ)	OC-32[b]	230915_C2	11,078±2,416	4,334	2
Facility (in-situ)	OC-32[b]	230915_C3	9,587±8,186	4,334	2
Facility (in-situ)	OC-32[b]	230928_C1	9,699±1,116	4,334	2
Facility (in-situ)	OC-32[b]	230928_C2	8,125±1,215	4,334	2
Facility (in-situ)	OC-32[b]	230929_C1	12,053±1,425	4,334	2
Facility (in-situ)	OC-32[b]	230929_C2	9,389±1,032	4,334	2
Facility (in-situ)	OC-32[b]	*$\bar{x}$ and s.e. (n=7)*	9,615±934	4,334	2
Facility (in-situ)	OC-14	230926_C1	222±50	1	2
Facility (remote sensing)	OC-32[b]	P18.1 - Leg i	8,294±2,186	4,334	2
Facility (remote sensing)	OC-32[b]	P18.1 - Leg j	10,118±2,377	4,334	2
Facility (remote sensing)	OC-32[b]	P18.1 - Leg k	18,847±3,606	4,334	2
Facility (remote sensing)	OC-32[b]	P18.1 - Leg l	8,143±2,347	4,334	2
Facility (remote sensing)	OC-32[b]	P18.1 - Leg m	11,860±2,553	4,334	2
Facility (remote sensing)	OC-32[b]	P18.1 - Leg n	10,173±2,471	4,334	2
Facility (remote sensing)	OC-32[b]	*P18.1 $\bar{x}$ and s.e. (n=6)*	11,239±2,632	4,334	2
Multi-facility (in-situ)	OC-12, MC-2-OC	231003_C2	3,928±905	932	1,1
Multi-facility (in-situ)	OC-12, OC-13	230916_C3B	4,670±1,211	903	1,1
Multi-facility (in-situ)	OC-12, OC-13	230916_C4B	5,339±954	903	1,1
Multi-facility (in-situ)	OC-12, OC-13	*$\bar{x}$ and s.e. (n=2)*	5,005±765	903	1,1
Multi-facility (in-situ)	OC-16, OC-17	230906_C1	1,199±390	379	2,2
Multi-facility (remote sensing)	OC-28, OC-30	P13.1 - Leg o	6,799±965	1,530	1,1
Multi-facility (remote sensing)	OC-28, OC-30	P13.1 - Leg p	6,436±1022	1,530	1,1
Multi-facility (remote sensing)	OC-28, OC-30	*P13.1 $\bar{x}$ and s.e. (n=2)*	6,618±828	1,530	1,1
Facility (remote sensing)	MC-1-UG	P10.4 - Leg c	1,342±433	771	1,4
Facility (remote sensing)	MC-1-UG	*P10.4$\bar{x}$ and s.e (n=1)*	1,342±520	771	1,4
Facility (remote sensing)	MC-2-UG	P4.2 - Leg e	2,474±462	3,004	1, 2, 4

Quantification type (aircraft)	Mine(s)	Quantification ID	CH_4 emission rate (kg hr^{-1} $CH_4 \pm 1\sigma$)[a]	Mean annual reported CH_4 emissions (kg hr^{-1} CH_4)	NGER Method
Facility (remote sensing)	MC-2-UG	*P4.2$\bar{x}$ and s (n=1)*	2,474±703	3,004	1, 2, 4
Facility (remote sensing)	MC-2-UG	P6.2 - Leg f	3,739±933	3,004	1, 2, 4
Facility (remote sensing)	MC-2-UG	P6.2 - Leg g	5,016±982	3,004	1, 2, 4
Facility (remote sensing)	MC-2-UG	P6.2 - Leg h	2,770±663	3,004	1, 2, 4
Facility (remote sensing)	MC-2-UG	*P6.2 $\bar{x}$ and s (n=3)*	3,842±817	3,004	1, 2, 4
Facility (remote sensing)	MC-2-UG	P9.2 - Leg g	1,972±1,070	3,004	1, 2, 4
Facility (remote sensing)	MC-2-UG	P9.2 - Leg h	2,695±1,167	3,004	1, 2, 4
Facility (remote sensing)	MC-2-UG	P9.2 - Leg i	3,542±1,205	3,004	1, 2, 4
Facility (remote sensing)	MC-2-UG	P9.2 - Leg j	3,126±1,010	3,004	1, 2, 4
Facility (remote sensing)	MC-2-UG	*P9.2 $\bar{x}$ and s (n=4)*	2,834±855	3,004	1, 2, 4
Facility (remote sensing)	MC-2-UG	*$\bar{x}$ and s.e. P4.2, P6.2, P9.2 (n=3)*	3,050±459	3,004	1, 2, 4
Sub-Facility (remote sensing)	UG-2	P10.1 - Leg h	6,603±3,859	N/A	N/A
Sub-Facility (remote sensing)	UG-2	P10.1 - Leg i	2,795±1,133	N/A	N/A
Sub-Facility (remote sensing)	UG-2	P10.1 - Leg j	2,467±1,161	N/A	N/A
Sub-Facility (remote sensing)	UG-2	P10.1 - Leg k	3,470±1,327	N/A	N/A
Sub-Facility (remote sensing)	UG-2	*P10.1 $\bar{x}$ and s.e (n=4)*	3,834±1,794	N/A	N/A
Sub-Facility (remote sensing)	UG-2	P10.2 - Leg h	737±507	N/A	N/A
Sub-Facility (remote sensing)	UG-2	P10.2 - Leg i	1,001±578	N/A	N/A
Sub-Facility (remote sensing)	UG-2	P10.2 - Leg k	822±483	N/A	N/A
Sub-Facility (remote sensing)	UG-2	P10.2 *$\bar{x}$ and s.e (n=3)*	854±399	N/A	N/A
Sub-Facility (remote sensing)	UG-2	P10.3 - Leg h	1,227±677	N/A	N/A
Sub-Facility (remote sensing)	UG-2	P10.3 - Leg i	682±648	N/A	N/A
Sub-Facility (remote sensing)	UG-2	*P10.3 $\bar{x}$ and s.e (n=2)*	954±580	N/A	N/A
Facility (remote sensing)	UG-2	*$\sum$P10.1,P10.2,P10.3 (n=3)*	5,642±1,927	3,823	1, 4
Facility (in-situ)	UG-2	230917_C3	3,765±991	3,823	1, 4
Sub-Facility (remote sensing)	UG-3	P6.3 - Leg d	352±231	N/A	N/A
Sub-Facility (remote sensing)	UG-3	*P6.3 $\bar{x}$ and s.e (n=1)*	352±243	N/A	N/A
Sub-Facility (remote sensing)	UG-3	P6.4 - Leg b	1,791±532	N/A	N/A
Sub-Facility (remote sensing)	UG-3	P6.4 - Leg c	942±508	N/A	N/A
Sub-Facility (remote sensing)	UG-3	P6.4 - Leg d	1,655±538	N/A	N/A
Sub-Facility (remote sensing)	UG-3	*P6.4 $\bar{x}$ and s.e (n=3)*	1,462±389	N/A	N/A
Sub-Facility (remote sensing)	UG-3	P6.5 - Leg b	521±301	N/A	N/A
Sub-Facility (remote sensing)	UG-3	*P6.5 $\bar{x}$ and s.e (n=1)*	521±321	N/A	N/A
Sub-Facility (remote sensing)	UG-3	*$\sum$ P6.3+P6.4+P6.5*	2,335±560	N/A	N/A
Sub-Facility (remote sensing)	UG-3	P9.3 - Leg e	433±365	N/A	N/A
Sub-Facility (remote sensing)	UG-3	P9.3 - Leg f	441±199	N/A	N/A
Sub-Facility (remote sensing)	UG-3	*P9.3 $\bar{x}$ and s.e (n=2)*	437±217	N/A	N/A
Sub-Facility (remote sensing)	UG-3	P9.4 - Leg c	1,402±486	N/A	N/A
Sub-Facility (remote sensing)	UG-3	P9.4 - Leg d	1066±650	N/A	N/A
Sub-Facility (remote sensing)	UG-3	*P9.4 $\bar{x}$ and s.e (n=2)*	1,234±457	N/A	N/A
Sub-Facility (remote sensing)	UG-3	P9.5 - Leg d	556±505	N/A	N/A
Sub-Facility (remote sensing)	UG-3	P9.5 - Leg e	310±539	N/A	N/A
Sub-Facility (remote sensing)	UG-3	*P9.5 $\bar{x}$ and s.e (n=2)*	433±384	N/A	N/A
Sub-Facility (remote sensing)	UG-3	*$\sum$P9.3+P9.4+P9.5*	2,104±635	N/A	N/A
Facility (remote sensing)	UG-3	$\sum$P6.3+P6.4+P6.5, $\sum$P9.3+P9.4+P9.5 *$\bar{x}$ and s.e (n=2)*	2,220±423	2,577	2, 4
Facility (in-situ)	UG-3	230916_C3C	3,595±735	2,577	2, 4

Quantification type (aircraft)	Mine(s)	Quantification ID	CH_4 emission rate (kg hr^{-1} $CH_4 \pm 1\sigma$)[a]	Mean annual reported CH_4 emissions (kg hr^{-1} CH_4)	NGER Method
Facility (in-situ)	UG-3	230916_C4C	2,293±641	2,577	2, 4
Facility (in-situ)	UG-3	*$\bar{x}$ and s.e (n=2)*	2,944±486	2,577	2, 4
Facility (remote sensing)	UG-4	P7.6 - Leg c2	4,447±1,070	3,571	1, 2, 4
Facility (remote sensing)	UG-4	P7.6 - Leg d	2,914±1,221	3,571	1, 2, 4
Facility (remote sensing)	UG-4	*P7.6 $\bar{x}$ and s.e (n=2)*	3,681±1,002	3,571	1, 2, 4
Facility (remote sensing)	UG-4	P17.3 - Leg i	3,317±1,361	3,571	1, 2, 4
Facility (remote sensing)	UG-4	*P17.3 $\bar{x}$ and s.e (n=1)*	3,317±1,535	3,571	1, 2, 4
Facility (remote sensing)	UG-4	*P7.6, P17.3 $\bar{x}$ and s.e (n=2)*	3,499±917	3,571	1, 2, 4
Sub-Facility (remote sensing)	UG-6	P7.2/P7.3 - Leg c1	2,187±703	N/A	N/A
Sub-Facility (remote sensing)	UG-6	P7.2/P7.3 - Leg c2	2,066±769	N/A	N/A
Sub-Facility (remote sensing)	UG-6	P7.2/P7.3 - Leg d	3,998±1,028	N/A	N/A
Sub-Facility (remote sensing)	UG-6	*P7.2/P7.3 $\bar{x}$ and s.e (n=3)*	2,750±730	N/A	N/A
Sub-Facility (remote sensing)	UG-6	P5.2 - Leg c4	2041±840	N/A	N/A
Sub-Facility (remote sensing)	UG-6	*P5.2 $\bar{x}$ and s.e (n=1)*	2041±947	N/A	N/A
Sub-Facility (remote sensing)	UG-6	*P7.2/P7.3, P5.2 $\bar{x}$ and s.e (n=2)*	2,396±598	N/A	N/A
Sub-Facility (remote sensing)	UG-6	P7.4 - Leg e	223±228	N/A	N/A
Sub-Facility (remote sensing)	UG-6	*P7.4 $\bar{x}$ and s.e (n=1)*	223±233	N/A	N/A
Sub-Facility (remote sensing)	UG-6	P7.5 - Leg d	2,335±825	N/A	N/A
Sub-Facility (remote sensing)	UG-6	*P7.5 $\bar{x}$ and s.e (n=1)*	2,335±965	N/A	N/A
Facility (remote sensing)	UG-6	*$\sum$ Mean (P7.2/P7.3, P5.2) + P7.4 + P7.5*	4,953±1,159	4,997	1, 2, 4
Facility (in-situ)	MC-1	230917_C1	821±346	867	UG:1,4 OC: 1
Facility (in-situ)	MC-1	230917_C2	1,012±359	867	UG:1,4 OC: 1
Facility (in-situ)	MC-1	*$\bar{x}$ and s.e (n=2)*	917±249	867	UG:1,4 OC: 1
Facility (in-situ)	MC-2	230916_C3B	5,011±3,192	3,509	UG: 1,2,4 OC: 1
Facility (in-situ)	MC-2	230916_C4B	3,508±1,239	3,509	UG: 1,2,4 OC: 1
Facility (in-situ)	MC-2	*$\bar{x}$ and s.e (n=2)*	4,260±1,567	3,509	UG: 1,2,4 OC: 1
Multi-facility (in-situ)	OC-5, UG-1	230923_C1	4,582±608	1,979	OC:1 & n.d.
Multi-facility (in-situ)	UG-3, MC-2	230909_C1	6,773±565	6,086	UG: 2, 4 & UG:1,2, 4 OC: 1
Multi-facility (in-situ)	UG-3, MC-2	230909_C3	5,928±759	6,086	UG: 2, 4 & UG:1,2, 4 OC: 1
Multi-facility (in-situ)	UG-3, MC-2	*$\bar{x}$ and s (n=2)*	6,351±468	6,086	UG: 2, 4 & UG:1,2, 4 OC: 1

Quantification type (aircraft)	Mine(s)	Quantification ID	CH_4 emission rate (kg hr^{-1} $CH_4 \pm 1\sigma$)[a]	Mean annual reported CH_4 emissions (kg hr^{-1} CH_4)	NGER Method
Multi-facility (in-situ)	OC-12, UG-3, MC-2	230926_C2	5,801±903	6,513	OC: 1, UG: 2, 4 & UG: 1,2,4 OC: 1
Multi-facility (in-situ)	OC-13, UG-3, MC-2-UG	230905_C1	4,159±694	6,121	OC: 1, UG: 2, 4 & UG: 1,2,4

[a)]Reported uncertainties for emission estimates with one quantification (n=1) represent one standard deviation error. Uncertainty for estimates with two or more quantifications (n>2), error bars represent one standard error of the mean based on multiple quantifications. [b)]Estimates are previously reported in Borchardt et al. (2025) and are used here for comparison with the most recent operator reporting.

Table S9. Sub-facility quantifications not compared with operator estimates

Quantification type (aircraft)	Mine(s)	Quantification ID	CH_4 emission rate (kg hr^{-1} $CH_4 \pm 1\sigma$)
Sub-Facility (remote sensing)	MC-3-UG	P5.1 - Leg c4	539±645
Sub-Facility (remote sensing)	MC-3-UG	*P5.1 $\bar{x}$ and s (n=1)*	539±655
Sub-Facility (remote sensing)	MC-3-UG	P7.1 - Leg e	791±556
Sub-Facility (remote sensing)	MC-3-UG	*P7.1 $\bar{x}$ and s (n=1)*	791±581
Sub-Facility (remote sensing)	MC-3-UG	P17.2 - Leg n	322±259
Sub-Facility (remote sensing)	MC-3-UG	*P17.2 $\bar{x}$ and s (n=1)*	322±268
Sub-Facility (remote sensing)	MC-3-UG	*$\bar{x}$ and s P7.1, P17.2 (n=2)*	556±320
Sub-Facility (remote sensing)	UG-5	P13.2 - Leg m	406±201
Sub-Facility (remote sensing)	UG-5	*P13.2 $\bar{x}$ and s (n=1)*	406±219
Sub-Facility (remote sensing)	OC-12	P16.2 - Leg g	2,370±499
Sub-Facility (remote sensing)	OC-12	P16.2 - Leg h	1,814±455
Sub-Facility (remote sensing)	OC-12	P16.2 - Leg i	3,113±578
Sub-Facility (remote sensing)	OC-12	*P16.2 $\bar{x}$ and s (n=3)*	2,432±480

SI-11: Estimated contribution of potential upwind CH_4 sources to each in-situ curtain

Table S10 breaks down the estimated contribution of potential upwind CH_4 sources to each in-situ aircraft curtain from which a quantification was subsequently derived. Table S11 summarises the results across all curtains included in Table S10.

Table S10. Estimated contribution of potential upwind CH_4 sources to each In-situ aircraft curtain from which a quantification was subsequently derived.

Curtain	In-situ curtain emission rate (kg hr^{-1} CH_4)	Upwind non-coal source	Source count	Upwind area (ha)	Upwind CH_4 emission rate (kg hr^{-1} CH_4)	% relative to curtain	Curtain emission rate uncertainty (%)
230905_C1	4,159	Grazing cattle	6,268	31,340	36	1%	17%
230905_C1	4,159	Feedlot cattle	-	N/A	-	0%	17%
230905_C1	4,159	Farm dams	224	171	6	0%	17%
230905_C1	4,159	Termites	N/A	31,340	6	0%	17%
230905_C1	4,159	CMWG Power Stations	3	N/A	22	1%	17%
230905_C1	4,159	Ammonium nitrate plant	0	N/A	-	0%	17%
230905_C1	4,159	Road transportation	0	N/A	-	0%	17%
230905_C1	4,159	Residential	0	N/A	-	0%	17%
230905_C1	4,159	Solid waste disposal	0	N/A	-	0%	17%
230905_C1	4,159	Domestic wastewater	0	N/A	-	0%	17%
230905_C1	4,159	Gas Development Wells	0	N/A	-	0%	17%
230905_C1	4,159	Macropods	6,017	31,340	0.5	0%	17%
230905_C1	4,159	Abandoned wells and boreholes	134	N/A	0.2	0%	17%
230905_C1	4,159	Gas Facilities	-	N/A	-	0%	17%
230905_C1	**4,159**	**Total**			**69**	**1.7%**	**17%**
230906_C1	1,199	Grazing cattle	10,303	51,517	59	4.9%	33%
230906_C1	1,199	Feedlot cattle	1	N/A	2	0.1%	33%
230906_C1	1,199	Farm dams	150	129	4	0.4%	33%
230906_C1	1,199	Termites	N/A	51,517	9	0.8%	33%
230906_C1	1,199	CMWG Power Stations	0	N/A	-	0.0%	33%
230906_C1	1,199	Ammonium nitrate plant	0	N/A	-	0.0%	33%
230906_C1	1,199	Road transportation	0	N/A	-	0.0%	33%
230906_C1	1,199	Residential	0	N/A	-	0.0%	33%
230906_C1	1,199	Solid waste disposal	0	N/A	-	0.0%	33%
230906_C1	1,199	Domestic wastewater	0	N/A	-	0.0%	33%
230906_C1	1,199	Gas Development Wells	0	N/A	-	0.0%	33%
230906_C1	1,199	Macropods	9,891	51,517	1	0.1%	33%
230906_C1	1,199	Abandoned wells and boreholes	476	N/A	1	0.0%	33%
230906_C1	1,199	Gas Facilities	-	N/A	-	0.0%	33%
230906_C1	**1,199**	**Total**			**75**	**6.2%**	**33%**
230906_C3	995	Grazing cattle	6,670	33,348	38	3.8%	38%

Curtain	In-situ curtain emission rate (kg hr^{-1} CH_4)	Upwind non-coal source	Source count	Upwind area (ha)	Upwind CH_4 emission rate (kg hr^{-1} CH_4)	% relative to curtain	Curtain emission rate uncertainty (%)
230906_C3	995	Feedlot cattle	-	N/A	-	0.0%	38%
230906_C3	995	Farm dams	43	31	1	0.1%	38%
230906_C3	995	Termites	N/A	33,348	6	0.6%	38%
230906_C3	995	CMWG Power Stations	0	N/A	-	0.0%	38%
230906_C3	995	Ammonium nitrate plant	0	N/A	-	0.0%	38%
230906_C3	995	Road transportation	0	N/A	-	0.0%	38%
230906_C3	995	Residential	0	N/A	-	0.0%	38%
230906_C3	995	Solid waste disposal	0	N/A	-	0.0%	38%
230906_C3	995	Domestic wastewater	0	N/A	-	0.0%	38%
230906_C3	995	Gas Development Wells	0	N/A	-	0.0%	38%
230906_C3	995	Macropods	6,403	33,348	0	0.0%	38%
230906_C3	995	Abandoned wells and boreholes	409	N/A	1	0.1%	38%
230906_C3	995	Gas Facilities	-	N/A	-	0.0%	38%
230906_C3	**995**	**Total**			**46**	**4.6%**	**38%**
230909_C1	6,773	Grazing cattle	9,237	46,187	53	0.8%	8%
230909_C1	6,773	Feedlot cattle	-	N/A	-	0.0%	8%
230909_C1	6,773	Farm dams	146	95	3	0.0%	8%
230909_C1	6,773	Termites	N/A	46,187	8	0.1%	8%
230909_C1	6,773	CMWG Power Stations	0	N/A	-	0.0%	8%
230909_C1	6,773	Ammonium nitrate plant	0	N/A	-	0.0%	8%
230909_C1	6,773	Road transportation	0	N/A	-	0.0%	8%
230909_C1	6,773	Residential	0	N/A	-	0.0%	8%
230909_C1	6,773	Solid waste disposal	0	N/A	-	0.0%	8%
230909_C1	6,773	Domestic wastewater	0	N/A	-	0.0%	8%
230909_C1	6,773	Gas Development Wells	0	N/A	-	0.0%	8%
230909_C1	6,773	Macropods	8,868	46,187	1	0.0%	8%
230909_C1	6,773	Abandoned wells and boreholes	192	N/A	0	0.0%	8%
230909_C1	6,773	Gas Facilities	-	N/A	-	0.0%	8%
230909_C1	**6,773**	**Total**			**65**	**1.0%**	**8%**
230909_C2	5,928	Grazing cattle	6,157	30,786	35	0.6%	13%
230909_C2	5,928	Feedlot cattle	-	N/A	-	0.0%	13%
230909_C2	5,928	Farm dams	165	133	5	0.1%	13%
230909_C2	5,928	Termites	N/A	30,786	5	0.1%	13%

Curtain	In-situ curtain emission rate (kg hr^{-1} CH_4)	Upwind non-coal source	Source count	Upwind area (ha)	Upwind CH_4 emission rate (kg hr^{-1} CH_4)	% relative to curtain	Curtain emission rate uncertainty (%)
230909_C2	5,928	CMWG Power Stations	3	N/A	23	0.4%	13%
230909_C2	5,928	Ammonium nitrate plant	0	N/A	-	0.0%	13%
230909_C2	5,928	Road transportation	0	N/A	-	0.0%	13%
230909_C2	5,928	Residential	0	N/A	-	0.0%	13%
230909_C2	5,928	Solid waste disposal	0	N/A	-	0.0%	13%
230909_C2	5,928	Domestic wastewater	0	N/A	-	0.0%	13%
230909_C2	5,928	Gas Development Wells	0	N/A	-	0.0%	13%
230909_C2	5,928	Macropods	5,911	30,786	0	0.0%	13%
230909_C2	5,928	Abandoned wells and boreholes	62	N/A	0	0.0%	13%
230909_C2	5,928	Gas Facilities	-	N/A	-	0.0%	13%
230909_C2	**5,928**	**Total**			**69**	**1.2%**	**13%**
230915_C1	7,372	Grazing cattle	6,285	31,427	36	0.5%	26%
230915_C1	7,372	Feedlot cattle	1	N/A	3	0.0%	26%
230915_C1	7,372	Farm dams	66	43	1	0.0%	26%
230915_C1	7,372	Termites	N/A	31,427	6	0.1%	26%
230915_C1	7,372	CMWG Power Stations	0	N/A	-	0.0%	26%
230915_C1	7,372	Ammonium nitrate plant	0	N/A	-	0.0%	26%
230915_C1	7,372	Road transportation	0	N/A	-	0.0%	26%
230915_C1	7,372	Residential	0	N/A	-	0.0%	26%
230915_C1	7,372	Solid waste disposal	0	N/A	-	0.0%	26%
230915_C1	7,372	Domestic wastewater	0	N/A	-	0.0%	26%
230915_C1	7,372	Gas Development Wells	0	N/A	-	0.0%	26%
230915_C1	7,372	Macropods	6,034	31,427	0	0.0%	26%
230915_C1	7,372	Abandoned wells and boreholes	1	N/A	0	0.0%	26%
230915_C1	7,372	Gas Facilities	-	N/A	-	0.0%	26%
230915_C1	**7,372**	**Total**			**47**	**0.6%**	**26%**
230915_C2	11,078	Grazing cattle	9,779	48,895	56	0.5%	22%
230915_C2	11,078	Feedlot cattle	1	N/A	3	0.0%	22%
230915_C2	11,078	Farm dams	110	69	2	0.0%	22%
230915_C2	11,078	Termites	N/A	48,895	9	0.1%	22%
230915_C2	11,078	CMWG Power Stations	0	N/A	-	0.0%	22%
230915_C2	11,078	Ammonium nitrate plant	0	N/A	-	0.0%	22%
230915_C2	11,078	Road transportation	0	N/A	-	0.0%	22%

Curtain	In-situ curtain emission rate (kg hr^{-1} CH_4)	Upwind non-coal source	Source count	Upwind area (ha)	Upwind CH_4 emission rate (kg hr^{-1} CH_4)	% relative to curtain	Curtain emission rate uncertainty (%)
230915_C2	11,078	Residential	0	N/A	-	0.0%	22%
230915_C2	11,078	Solid waste disposal	0	N/A	-	0.0%	22%
230915_C2	11,078	Domestic wastewater	0	N/A	-	0.0%	22%
230915_C2	11,078	Gas Development Wells	0	N/A	-	0.0%	22%
230915_C2	11,078	Macropods	9,388	48,895	1	0.0%	22%
230915_C2	11,078	Abandoned wells and boreholes	39	N/A	0	0.0%	22%
230915_C2	11,078	Gas Facilities	-	N/A	-	0.0%	22%
230915_C2	**11,078**	**Total**			**71**	**0.6%**	**22%**
230915_C3	9,587	Grazing cattle	10,991	54,954	63	0.7%	85%
230915_C3	9,587	Feedlot cattle	-	N/A	-	0.0%	85%
230915_C3	9,587	Farm dams	113	69	2	0.0%	85%
230915_C3	9,587	Termites	N/A	54,954	10	0.1%	85%
230915_C3	9,587	CMWG Power Stations	0	N/A	-	0.0%	85%
230915_C3	9,587	Ammonium nitrate plant	0	N/A	-	0.0%	85%
230915_C3	9,587	Road transportation	0	N/A	-	0.0%	85%
230915_C3	9,587	Residential	0	N/A	-	0.0%	85%
230915_C3	9,587	Solid waste disposal	0	N/A	-	0.0%	85%
230915_C3	9,587	Domestic wastewater	0	N/A	-	0.0%	85%
230915_C3	9,587	Gas Development Wells	0	N/A	-	0.0%	85%
230915_C3	9,587	Macropods	10,551	54,954	1	0.0%	85%
230915_C3	9,587	Abandoned wells and boreholes	28	N/A	0	0.0%	85%
230915_C3	9,587	Gas Facilities	-	N/A	-	0.0%	85%
230915_C3	**9,587**	**Total**			**76**	**0.8%**	**85%**
230916_C1	3,994	Grazing cattle	8,951	44,753	51	1.3%	32%
230916_C1	3,994	Feedlot cattle	-	N/A	-	0.0%	32%
230916_C1	3,994	Farm dams	149	100	3	0.1%	32%
230916_C1	3,994	Termites	N/A	44,753	8	0.2%	32%
230916_C1	3,994	CMWG Power Stations	0	N/A	-	0.0%	32%
230916_C1	3,994	Ammonium nitrate plant	0	N/A	-	0.0%	32%
230916_C1	3,994	Road transportation	0	N/A	-	0.0%	32%
230916_C1	3,994	Residential	0	N/A	-	0.0%	32%
230916_C1	3,994	Solid waste disposal	0	N/A	-	0.0%	32%
230916_C1	3,994	Domestic wastewater	0	N/A	-	0.0%	32%

Curtain	In-situ curtain emission rate (kg hr^{-1} CH_4)	Upwind non-coal source	Source count	Upwind area (ha)	Upwind CH_4 emission rate (kg hr^{-1} CH_4)	% relative to curtain	Curtain emission rate uncertainty (%)
230916_C1	3,994	Gas Development Wells	0	N/A	-	0.0%	32%
230916_C1	3,994	Macropods	8,593	44,753	1	0.0%	32%
230916_C1	3,994	Abandoned wells and boreholes	126	N/A	0	0.0%	32%
230916_C1	3,994	Gas Facilities	-	-	-	0.0%	32%
230916_C1	**3,994**	**Total**			**63**	**1.6%**	**32%**
230916_C2	4,634	Grazing cattle	20,370	101,849	116	2.5%	15%
230916_C2	4,634	Feedlot cattle	-	N/A	-	0.0%	15%
230916_C2	4,634	Farm dams	318	234	8	0.2%	15%
230916_C2	4,634	Termites	N/A	101,849	18	0.4%	15%
230916_C2	4,634	CMWG Power Stations	0	N/A	-	0.0%	15%
230916_C2	4,634	Ammonium nitrate plant	0	N/A	-	0.0%	15%
230916_C2	4,634	Road transportation	0	N/A	-	0.0%	15%
230916_C2	4,634	Residential	1	N/A	0	0.0%	15%
230916_C2	4,634	Solid waste disposal	0	N/A	-	0.0%	15%
230916_C2	4,634	Domestic wastewater	0	N/A	-	0.0%	15%
230916_C2	4,634	Gas Development Wells	0	N/A	-	0.0%	15%
230916_C2	4,634	Macropods	19,555	101,849	1	0.0%	15%
230916_C2	4,634	Abandoned wells and boreholes	222	N/A	0	0.0%	15%
230916_C2	4,634	Gas Facilities	-	N/A	-	0.0%	15%
230916_C2	**4,634**	**Total**			**144**	**3.1%**	**15%**
230916_C3[a]	13,276	Grazing cattle	15,484	77,421	88	0.7%	39%
230916_C3[a]	13,276	Feedlot cattle	-	N/A	-	0.0%	39%
230916_C3[a]	13,276	Farm dams	374	295	10	0.1%	39%
230916_C3[a]	13,276	Termites	N/A	77,421	14	0.1%	39%
230916_C3[a]	13,276	CMWG Power Stations	2	N/A	14	0.1%	39%
230916_C3[a]	13,276	Ammonium nitrate plant	0	N/A	-	0.0%	39%
230916_C3[a]	13,276	Road transportation	0	N/A	-	0.0%	39%
230916_C3[a]	13,276	Residential	1	N/A	0	0.0%	39%
230916_C3[a]	13,276	Solid waste disposal	1	N/A	32	0.2%	39%
230916_C3[a]	13,276	Domestic wastewater	0	N/A	-	0.0%	39%
230916_C3[a]	13,276	Gas Development Wells	0	N/A	-	0.0%	39%
230916_C3[a]	13,276	Macropods	14,865	77,421	1	0.0%	39%
230916_C3[a]	13,276	Abandoned wells and boreholes	275	N/A	0	0.0%	39%

Curtain	In-situ curtain emission rate (kg hr^{-1} CH_4)	Upwind non-coal source	Source count	Upwind area (ha)	Upwind CH_4 emission rate (kg hr^{-1} CH_4)	% relative to curtain	Curtain emission rate uncertainty (%)
230916_C3[a]	13,276	Gas Facilities	-	N/A	-	0.0%	39%
230916_C3[a]	**13,276**	**Total**			**159**	**1.2%**	**39%**
230916_C4[a]	11,140	Grazing cattle	12,724	63,620	73	0.7%	25%
230916_C4[a]	11,140	Feedlot cattle	-	N/A	-	0.0%	25%
230916_C4[a]	11,140	Farm dams	376	325	11	0.1%	25%
230916_C4[a]	11,140	Termites	N/A	63,620	11	0.1%	25%
230916_C4[a]	11,140	CMWG Power Stations	3	N/A	23	0.2%	25%
230916_C4[a]	11,140	Ammonium nitrate plant	0	N/A	-	0.0%	25%
230916_C4[a]	11,140	Road transportation	0	N/A	-	0.0%	25%
230916_C4[a]	11,140	Residential	1	N/A	0	0.0%	25%
230916_C4[a]	11,140	Solid waste disposal	1	N/A	32	0.3%	25%
230916_C4[a]	11,140	Domestic wastewater	0	N/A	-	0.0%	25%
230916_C4[a]	11,140	Gas Development Wells	0	N/A	-	0.0%	25%
230916_C4[a]	11,140	Macropods	12,215	63,620	1	0.0%	25%
230916_C4[a]	11,140	Abandoned wells and boreholes	261	N/A	0	0.0%	25%
230916_C4[a]	11,140	Gas Facilities	-	N/A	-	0.0%	25%
230916_C4[a]	**11,140**	**Total**			**151**	**1.4%**	**25%**
230917_C1	821	Grazing cattle	9,575	47,875	55	6.6%	42%
230917_C1	821	Feedlot cattle	-	N/A	-	0.0%	42%
230917_C1	821	Farm dams	233	148	5	0.6%	42%
230917_C1	821	Termites	N/A	47,875	9	1.0%	42%
230917_C1	821	CMWG Power Stations	0	N/A	-	0.0%	42%
230917_C1	821	Ammonium nitrate plant	0	N/A	-	0.0%	42%
230917_C1	821	Road transportation	0	N/A	-	0.0%	42%
230917_C1	821	Residential	0	N/A	-	0.0%	42%
230917_C1	821	Solid waste disposal	0	N/A	-	0.0%	42%
230917_C1	821	Domestic wastewater	0	N/A	-	0.0%	42%
230917_C1	821	Gas Development Wells	0	N/A	-	0.0%	42%
230917_C1	821	Macropods	9,192	47,875	1	0.1%	42%
230917_C1	821	Abandoned wells and boreholes	363	N/A	0	0.1%	42%
230917_C1	821	Gas Facilities	-	N/A	-	0.0%	42%
230917_C1	**821**	**Total**			**69**	**8.4%**	**42%**
230917_C2	1,012	Grazing cattle	8,216	41,081	47	4.6%	35%

Curtain	In-situ curtain emission rate (kg hr^{-1} CH_4)	Upwind non-coal source	Source count	Upwind area (ha)	Upwind CH_4 emission rate (kg hr^{-1} CH_4)	% relative to curtain	Curtain emission rate uncertainty (%)
230917_C2	1,012	Feedlot cattle	-	N/A	-	0.0%	35%
230917_C2	1,012	Farm dams	194	118	4	0.4%	35%
230917_C2	1,012	Termites	N/A	41,081	7	0.7%	35%
230917_C2	1,012	CMWG Power Stations	0	N/A	-	0.0%	35%
230917_C2	1,012	Ammonium nitrate plant	0	N/A	-	0.0%	35%
230917_C2	1,012	Road transportation	0	N/A	-	0.0%	35%
230917_C2	1,012	Residential	0	N/A	-	0.0%	35%
230917_C2	1,012	Solid waste disposal	0	N/A	-	0.0%	35%
230917_C2	1,012	Domestic wastewater	0	N/A	-	0.0%	35%
230917_C2	1,012	Gas Development Wells	0	N/A	-	0.0%	35%
230917_C2	1,012	Macropods	7,888	41,081	1	0.1%	35%
230917_C2	1,012	Abandoned wells and boreholes	314	N/A	0	0.0%	35%
230917_C2	1,012	Gas Facilities	-	N/A	-	0.0%	35%
230917_C2	**1,012**	**Total**			**59**	**5.9%**	**35%**
230917_C3	3,765	Grazing cattle	14,500	72,501	83	2.2%	26%
230917_C3	3,765	Feedlot cattle	2	N/A	3	0.1%	26%
230917_C3	3,765	Farm dams	296	132	5	0.1%	26%
230917_C3	3,765	Termites	N/A	72,501	13	0.3%	26%
230917_C3	3,765	CMWG Power Stations	0	N/A	-	0.0%	26%
230917_C3	3,765	Ammonium nitrate plant	0	N/A	-	0.0%	26%
230917_C3	3,765	Road transportation	0	N/A	-	0.0%	26%
230917_C3	3,765	Residential	0	N/A	-	0.0%	26%
230917_C3	3,765	Solid waste disposal	0	N/A	-	0.0%	26%
230917_C3	3,765	Domestic wastewater	0	N/A	-	0.0%	26%
230917_C3	3,765	Gas Development Wells	0	N/A	-	0.0%	26%
230917_C3	3,765	Macropods	13,920	72,501	1	0.0%	26%
230917_C3	3,765	Abandoned wells and boreholes	106	N/A	0	0.0%	26%
230917_C3	3,765	Gas Facilities	-	N/A	-	0.0%	26%
230917_C3	**3,765**	**Total**			**104**	**2.8%**	**26%**
230923_C1	4,582	Grazing cattle	8,791	43,957	50	1.1%	13%
230923_C1	4,582	Feedlot cattle	-	N/A	-	0.0%	13%
230923_C1	4,582	Farm dams	223	106	4	0.1%	13%
230923_C1	4,582	Termites	N/A	43,957	8	0.2%	13%

Curtain	In-situ curtain emission rate (kg hr^{-1} CH_4)	Upwind non-coal source	Source count	Upwind area (ha)	Upwind CH_4 emission rate (kg hr^{-1} CH_4)	% relative to curtain	Curtain emission rate uncertainty (%)
230923_C1	4,582	CMWG Power Stations	0	N/A	-	0.0%	13%
230923_C1	4,582	Ammonium nitrate plant	0	N/A	-	0.0%	13%
230923_C1	4,582	Road transportation	0	N/A	-	0.0%	13%
230923_C1	4,582	Residential	0	N/A	-	0.0%	13%
230923_C1	4,582	Solid waste disposal	1	N/A	32	0.7%	13%
230923_C1	4,582	Domestic wastewater	0	N/A	-	0.0%	13%
230923_C1	4,582	Gas Development Wells	0	N/A	-	0.0%	13%
230923_C1	4,582	Macropods	8,440	43,957	1	0.0%	13%
230923_C1	4,582	Abandoned wells and boreholes	64	N/A	0	0.0%	13%
230923_C1	4,582	Gas Facilities	-	N/A	-	0.0%	13%
230923_C1	**4,582**	**Total**			**94**	**2.0%**	**13%**
230925_C1	8,248	Grazing cattle	8,889	44,445	51	0.6%	14%
230925_C1	8,248	Feedlot cattle	-	N/A	-	0.0%	14%
230925_C1	8,248	Farm dams	133	76	3	0.0%	14%
230925_C1	8,248	Termites	N/A	44,445	8	0.1%	14%
230925_C1	8,248	CMWG Power Stations	0	N/A	-	0.0%	14%
230925_C1	8,248	Ammonium nitrate plant	0	N/A	-	0.0%	14%
230925_C1	8,248	Road transportation	0	N/A	-	0.0%	14%
230925_C1	8,248	Residential	0	N/A	-	0.0%	14%
230925_C1	8,248	Solid waste disposal	0	N/A	-	0.0%	14%
230925_C1	8,248	Domestic wastewater	0	N/A	-	0.0%	14%
230925_C1	8,248	Gas Development Wells	0	N/A	-	0.0%	14%
230925_C1	8,248	Macropods	8,533	44,445	1	0.0%	14%
230925_C1	8,248	Abandoned wells and boreholes	11	N/A	0	0.0%	14%
230925_C1	8,248	Gas Facilities	-	N/A	-	0.0%	14%
230925_C1	**8,248**	**Total**			**62**	**0.7%**	**14%**
230926_C1	222	Grazing cattle	4,096	20,481	40	10.5%	23%
230926_C1	222	Feedlot cattle	-	N/A	-	0.0%	23%
230926_C1	222	Farm dams	31	17	1	0.3%	23%
230926_C1	222	Termites	N/A	20,481	6	1.6%	23%
230926_C1	222	CMWG Power Stations	0	N/A	-	0.0%	23%
230926_C1	222	Ammonium nitrate plant	0	N/A	-	0.0%	23%
230926_C1	222	Road transportation	0	N/A	-	0.0%	23%

Curtain	In-situ curtain emission rate (kg hr^{-1} CH_4)	Upwind non-coal source	Source count	Upwind area (ha)	Upwind CH_4 emission rate (kg hr^{-1} CH_4)	% relative to curtain	Curtain emission rate uncertainty (%)
230926_C1	222	Residential	0	N/A	-	0.0%	23%
230926_C1	222	Solid waste disposal	0	N/A		0.0%	23%
230926_C1	222	Domestic wastewater	0	N/A	-	0.0%	23%
230926_C1	222	Gas Development Wells	0	N/A	-	0.0%	23%
230926_C1	222	Macropods	3,932	20,481	1	0.0%	23%
230926_C1	222	Abandoned wells and boreholes	-	N/A	-	0.0%	23%
230926_C1	222	Gas Facilities	-	N/A	-	0.0%	23%
230926_C1	**222**	**Total**			**47**	**12.6%**	**23%**
230926_C2	5,801	Grazing cattle	14,197	70,986	81	1.4%	16%
230926_C2	5,801	Feedlot cattle	-	N/A	-	0.0%	16%
230926_C2	5,801	Farm dams	376	282	10	0.2%	16%
230926_C2	5,801	Termites	N/A	70,986	13	0.2%	16%
230926_C2	5,801	CMWG Power Stations	3	N/A	22	0.4%	16%
230926_C2	5,801	Ammonium nitrate plant	0	N/A	-	0.0%	16%
230926_C2	5,801	Road transportation	0	N/A	-	0.0%	16%
230926_C2	5,801	Residential	0	N/A	-	0.0%	16%
230926_C2	5,801	Solid waste disposal	0	N/A	-	0.0%	16%
230926_C2	5,801	Domestic wastewater	0	N/A	-	0.0%	16%
230926_C2	5,801	Gas Development Wells	0	N/A	-	0.0%	16%
230926_C2	5,801	Macropods	13,629	70,986	1	0.0%	16%
230926_C2	5,801	Abandoned wells and boreholes	182	N/A	0	0.0%	16%
230926_C2	5,801	Gas Facilities	-	N/A	-	0.0%	16%
230926_C2	**5,801**	**Total**			**126**	**2.2%**	**16%**
230928_C1	9,699	Grazing cattle	5,618	28,092	32	0.3%	12%
230928_C1	9,699	Feedlot cattle	1	N/A	3	0.0%	12%
230928_C1	9,699	Farm dams	63	43	1	0.0%	12%
230928_C1	9,699	Termites	N/A	28,092	5	0.1%	12%
230928_C1	9,699	CMWG Power Stations	0	N/A	-	0.0%	12%
230928_C1	9,699	Ammonium nitrate plant	0	N/A	-	0.0%	12%
230928_C1	9,699	Road transportation	0	N/A	-	0.0%	12%
230928_C1	9,699	Residential	0	N/A	-	0.0%	12%
230928_C1	9,699	Solid waste disposal	0	N/A	-	0.0%	12%
230928_C1	9,699	Domestic wastewater	0	N/A	-	0.0%	12%

Curtain	In-situ curtain emission rate (kg hr^{-1} CH_4)	Upwind non-coal source	Source count	Upwind area (ha)	Upwind CH_4 emission rate (kg hr^{-1} CH_4)	% relative to curtain	Curtain emission rate uncertainty (%)
230928_C1	9,699	Gas Development Wells	0	N/A	-	0.0%	12%
230928_C1	9,699	Macropods	5,394	28,092	0	0.0%	12%
230928_C1	9,699	Abandoned wells and boreholes	1	N/A	0	0.0%	12%
230928_C1	9,699	Gas Facilities	-	N/A	-	0.0%	12%
230928_C1	**9,699**	**Total**			**42**	**0.4%**	**12%**
230928_C2	8,125	Grazing cattle	6,311	31,556	36	0.4%	15%
230928_C2	8,125	Feedlot cattle	1	N/A	3	0.0%	15%
230928_C2	8,125	Farm dams	76	47	2	0.0%	15%
230928_C2	8,125	Termites	N/A	31,556	6	0.1%	15%
230928_C2	8,125	CMWG Power Stations	0	N/A	-	0.0%	15%
230928_C2	8,125	Ammonium nitrate plant	0	N/A	-	0.0%	15%
230928_C2	8,125	Road transportation	0	N/A	-	0.0%	15%
230928_C2	8,125	Residential	0	N/A	-	0.0%	15%
230928_C2	8,125	Solid waste disposal	0	N/A	-	0.0%	15%
230928_C2	8,125	Domestic wastewater	0	N/A	-	0.0%	15%
230928_C2	8,125	Gas Development Wells	0	N/A	-	0.0%	15%
230928_C2	8,125	Macropods	6,059	31,556	0	0.0%	15%
230928_C2	8,125	Abandoned wells and boreholes	1	N/A	0	0.0%	15%
230928_C2	8,125	Gas Facilities	-	N/A	-	0.0%	15%
230928_C2	**8,125**	**Total**			**47**	**0.6%**	**15%**
230929_C1	12,053	Grazing cattle	8,727	43,634	50	0.4%	12%
230929_C1	12,053	Feedlot cattle	-	N/A	-	0.0%	12%
230929_C1	12,053	Farm dams	76	51	2	0.0%	12%
230929_C1	12,053	Termites	N/A	43,634	8	0.1%	12%
230929_C1	12,053	CMWG Power Stations	0	N/A	-	0.0%	12%
230929_C1	12,053	Ammonium nitrate plant	0	N/A	-	0.0%	12%
230929_C1	12,053	Road transportation	0	N/A	-	0.0%	12%
230929_C1	12,053	Residential	0	N/A	-	0.0%	12%
230929_C1	12,053	Solid waste disposal	0	N/A	-	0.0%	12%
230929_C1	12,053	Domestic wastewater	0	N/A	-	0.0%	12%
230929_C1	12,053	Gas Development Wells	0	N/A	-	0.0%	12%
230929_C1	12,053	Macropods	8,378	43,634	1	0.0%	12%
230929_C1	12,053	Abandoned wells and boreholes	5	N/A	0	0.0%	12%

Curtain	In-situ curtain emission rate (kg hr^{-1} CH_4)	Upwind non-coal source	Source count	Upwind area (ha)	Upwind CH_4 emission rate (kg hr^{-1} CH_4)	% relative to curtain	Curtain emission rate uncertainty (%)
230929_C1	12,053	Gas Facilities	-	N/A	-	0.0%	12%
230929_C1	**12,053**	**Total**			**60**	**0.5%**	**12%**
230929_C2	9,389	Grazing cattle	10,233	51,165	58	0.6%	11%
230929_C2	9,389	Feedlot cattle	-	N/A	-	0.0%	11%
230929_C2	9,389	Farm dams	104	62	-	0.0%	11%
230929_C2	9,389	Termites	N/A	51,165	9	0.1%	11%
230929_C2	9,389	CMWG Power Stations	0	N/A	-	0.0%	11%
230929_C2	9,389	Ammonium nitrate plant	0	N/A	-	0.0%	11%
230929_C2	9,389	Road transportation	0	N/A	-	0.0%	11%
230929_C2	9,389	Residential	0	N/A	-	0.0%	11%
230929_C2	9,389	Solid waste disposal	0	N/A	-	0.0%	11%
230929_C2	9,389	Domestic wastewater	0	N/A	-	0.0%	11%
230929_C2	9,389	Gas Development Wells	0	N/A	-	0.0%	11%
230929_C2	9,389	Macropods	9,824	51,165	1	0.0%	11%
230929_C2	9,389	Abandoned wells and boreholes	35	N/A	0	0.0%	11%
230929_C2	9,389	Gas Facilities	-	N/A	-	0.0%	11%
230929_C2	**9,389**	**Total**			**68**	**0.7%**	**11%**
231003_C1	4,607	Grazing cattle	9,038	45,188	52	1.1%	14%
231003_C1	4,607	Feedlot cattle	-	N/A	-	0.0%	14%
231003_C1	4,607	Farm dams	109	80	3	0.1%	14%
231003_C1	4,607	Termites	N/A	45,188	8	0.2%	14%
231003_C1	4,607	CMWG Power Stations	0	N/A	-	0.0%	14%
231003_C1	4,607	Ammonium nitrate plant	0	N/A	-	0.0%	14%
231003_C1	4,607	Road transportation	0	N/A	-	0.0%	14%
231003_C1	4,607	Residential	0	N/A	-	0.0%	14%
231003_C1	4,607	Solid waste disposal	0	N/A	-	0.0%	14%
231003_C1	4,607	Domestic wastewater	0	N/A	-	0.0%	14%
231003_C1	4,607	Gas Development Wells	0	N/A	-	0.0%	14%
231003_C1	4,607	Macropods	8,676	45,188	1	0.0%	14%
231003_C1	4,607	Abandoned wells and boreholes	3	N/A	0	0.0%	14%
231003_C1	4,607	Gas Facilities	-	N/A	-	0.0%	14%
231003_C1	**4,607**	**Total**			**63**	**1.4%**	**14%**
231003_C2	3,928	Grazing cattle	9,888	49,438	56	1.4%	23%

Curtain	In-situ curtain emission rate (kg hr^{-1} CH_4)	Upwind non-coal source	Source count	Upwind area (ha)	Upwind CH_4 emission rate (kg hr^{-1} CH_4)	% relative to curtain	Curtain emission rate uncertainty (%)
231003_C2	3,928	Feedlot cattle	-	N/A	-	0.0%	23%
231003_C2	3,928	Farm dams	172	130	4	0.1%	23%
231003_C2	3,928	Termites	N/A	49,438	9	0.2%	23%
231003_C2	3,928	CMWG Power Stations	0	N/A	-	0.0%	23%
231003_C2	3,928	Ammonium nitrate plant	0	N/A	-	0.0%	23%
231003_C2	3,928	Road transportation	0	N/A	-	0.0%	23%
231003_C2	3,928	Residential	0	N/A	-	0.0%	23%
231003_C2	3,928	Solid waste disposal	0	N/A	-	0.0%	23%
231003_C2	3,928	Domestic wastewater	0	N/A	-	0.0%	23%
231003_C2	3,928	Gas Development Wells	0	N/A	-	0.0%	23%
231003_C2	3,928	Macropods	9,492	49,438	1	0.0%	23%
231003_C2	3,928	Abandoned wells and boreholes	192	N/A	0	0.0%	23%
231003_C2	3,928	Gas Facilities	-	N/A	-	0.0%	23%
231003_C2	**3,928**	**Total**			**71**	**1.8%**	**23%**

800 **[a)]Emissions are not separated into A, B or C since HYSPLIT trajectories were derived according to each curtain. The sum of emissions and uncertainties across the three IS quantifications are reported here.**

Table S11. Summary of estimated upwind CH_4 sources across all curtains included in Table S10. Percentage (%) contributions refer to the contribution of the CH_4 source relative to the total curtain emission rate.

CH_4 source	Mean kg hr^{-1} CH_4	Median kg hr^{-1} CH_4	Min kg hr^{-1} CH_4	Max kg hr^{-1} CH_4	Mean % contribution	Median % contribution	Min % contribution	Max % contribution
Abandoned wells and boreholes	0	0	0	1	0.0%	0.0%	0%	0.1%
Ammonium nitrate plant	0	0	0	0	0.0%	0.0%	0%	0.0%
CMWG Power Stations	4	0	0	23	0.1%	0.0%	0%	0.5%
Domestic wastewater	0	0	0	0	0.0%	0.0%	0%	0.0%
Farm dams	4	3	0	11	0.1%	0.1%	0%	0.6%
Feedlot cattle	1	0	0	3	0.0%	0.0%	0%	0.1%
Gas Development Wells	0	0	0	0	0%	0%	0%	0%
Gas Facilities	0	0	0	0	0.0%	0.0%	0%	0.0%
Grazing cattle	55	52	23	116	2.0%	0.9%	0%	10.5%
Macropods	1	1	0	1	0.0%	0.0%	0%	0.1%
Residential	0	0	0	0	0.0%	0.0%	0%	0.0%
Road transportation	0	0	0	0	0%	0%	0%	0%
Solid waste disposal	4	0	0	32	0.0%	0.0%	0%	0.7%
Termites	9	8	4	18	0.3%	0.1%	0%	1.6%
Total	77	69	28	159	2.6%	1.4%	0.4%	12.6%

SI-12: CH_4 concentration and isotope results for all airborne grab samples collected by the in-situ aircraft

Table S12 shows the CH_4 concentration and isotope results for all airborne grab samples collected by the in-situ aircraft. The data are grouped according to which coal mine(s) were upwind of the sampling location. If four or more isotopic samples were collected upwind of the same coal mine(s), a Keeling plot was used to derive the CH_4 source isotope signature ($\delta^{13}C\text{-}CH_4$ or $\delta^{2}H\text{-}CH_4$; Keeling, 1961).

Figs. S33 and S34 show the Keeling plots used to derive the CH_4 source isotope signatures from each group of samples for $\delta^{13}C\text{-}CH_4$ and $\delta^{2}H\text{-}CH_4$, respectively. Twelve sets were analysed for $\delta^{13}C\text{-}CH_4$, and four sets for $\delta^{2}H\text{-}CH_4$. For three $\delta^{13}C\text{-}CH_4$ sets the concentration range was too narrow to provide sufficient spread in the data, indicating that the plume(s) had not been sampled thoroughly (Figs. I1a, I1c, I1h). These source linear models had low Pearson correlation coefficients ($r<0.5$) and therefore the signature intercepts were omitted from the analyses.

Table S12. Airborne grab samples acquired by the in-situ aircraft and associated CH_4 isotopic signatures.

Sample ID	Upwind coal mine(s)	CH_4 (ppm)	$1/CH_4$ (ppm)	$\delta^{13}C\text{-}CH_4$	$1\sigma\ \delta^{13}C\text{-}CH_4$	$\delta^{2}H\text{-}CH_4$	$1\sigma\ \delta^{2}H\text{-}CH_4$	Analysed using Keeling plot?
230909_Bag01	MC-2	1.959	0.510	-47.898	0.056	-87.6	1.7	Yes - both
230909_Bag02	MC-2	2.28	0.439	-48.754	0.039	-91.9	0.1	Yes - both
230909_Bag03	MC-2	2.347	0.426	-48.822	0.060	-96.2	0.5	Yes - both
230909_Bag04	MC-2	2.623	0.381	-49.500	0.055	-110		Yes - both
230909_Bag05	MC-2	2.426	0.412	-49.056	0.061	-98.8	2.4	Yes - both
230909_Bag06	MC-2	1.991	0.502	-47.978	0.032	-81.2	0.3	Yes - both
230909_Bag07	MC-2	1.955	0.512	-47.853	0.046	-83.4	1.8	Yes - both
230909_Bag08	MC-2	2.025	0.494	-48.137	0.038	-88.9	2.4	Yes - both
230909_Bag10	MC-2	2.022	0.495	-48.035	0.053	-91	0.7	Yes - both
230916_Bag03	MC-2	1.946	0.514	-47.887	0.039	N/A	N/A	Yes - $\delta^{13}C$
230916_Bag06	MC-2	1.967	0.508	-47.933	0.073	N/A	N/A	Yes - $\delta^{13}C$
230916_Bag10	OC-12	1.963	0.509	-47.604	0.043	N/A	N/A	Yes - $\delta^{13}C$
231003_Bag01	OC-12	1.979	0.505	-47.445	0.049	N/A	N/A	Yes - $\delta^{13}C$
231003_Bag02	OC-12	2.044	0.489	-47.193	0.105	N/A	N/A	Yes - $\delta^{13}C$
231003_Bag03	OC-12	2.036	0.491	-47.917	0.025	N/A	N/A	Yes - $\delta^{13}C$
231003_Bag04	OC-12	2.097	0.477	-47.505	0.042	N/A	N/A	Yes - $\delta^{13}C$
231003_Bag05	OC-12	1.991	0.502	-48.182	0.056	N/A	N/A	Yes - $\delta^{13}C$
231003_Bag06	OC-12	2.113	0.473	-47.354	0.009	N/A	N/A	Yes - $\delta^{13}C$
231003_Bag07	OC-12, MC-2	1.981	0.505	-48.244	0.065	N/A	N/A	No - both
231003_Bag10	OC-12, MC-2	1.935	0.517	-48.076	0.037	N/A	N/A	No - both
230916_Bag02	OC-12, OC-13	1.973	0.507	-47.643	0.018	-82.9	1.1	Yes - $\delta^{13}C$

Sample ID	Upwind coal mine(s)	CH_4 (ppm)	$1/CH_4$ (ppm)	$\delta^{13}C\text{-}CH_4$	$1\sigma\ \delta^{13}C\text{-}CH_4$	$\delta^{2}H\text{-}CH_4$	$1\sigma\ \delta^{2}H\text{-}CH_4$	Analysed using Keeling plot?
230916_Bag05	OC-12, OC-13	1.953	0.512	-47.651	0.062	N/A	N/A	Yes - $\delta^{13}C$
230916_Bag07	OC-12, OC-13	1.91	0.524	-47.797	0.034	N/A	N/A	Yes - $\delta^{13}C$
230916_Bag09	OC-12, OC-13	1.922	0.520	-47.742	0.030	-84.1	2.9	Yes - $\delta^{13}C$
231003_Bag08	OC-12, UG-3	2.498	0.400	-50.253	0.018	N/A	N/A	No - both
230906_Bag09	OC-16	1.902	0.526	-47.898	0.036	N/A	N/A	No - both
230906_Bag10	OC-16	1.903	0.525	-47.850	0.032	N/A	N/A	No - both
230906_Bag06	OC-16, OC-17	1.91	0.524	-47.992	0.033	N/A	N/A	No - both
230906_Bag07	OC-16, OC-17	1.901	0.526	-47.775	0.034	N/A	N/A	No - both
230906_Bag08	OC-16, OC-17	1.907	0.524	-47.867	0.003	N/A	N/A	No - both
230906_Bag01	OC-18 to OC-32, UG-4 to UG-8, MC-3	1.946	0.514	-47.824	0.034	N/A	N/A	Yes - $\delta^{13}C$
230906_Bag02	OC-18 to OC-32, UG-4 to UG-8, MC-3	1.943	0.515	-47.919	0.046	N/A	N/A	Yes - $\delta^{13}C$
230906_Bag03	OC-18 to OC-32, UG-4 to UG-8, MC-3	1.948	0.513	-48.000	0.055	N/A	N/A	Yes - $\delta^{13}C$
230906_Bag04	OC-18 to OC-32, UG-4 to UG-8, MC-3	2.056	0.486	-48.283	0.042	N/A	N/A	Yes - $\delta^{13}C$
230927_Bag01	OC-20 to OC-31, UG-4 to UG-8, MC-3	1.955	0.512	-48.050	0.061	N/A	N/A	Yes - $\delta^{13}C$
230927_Bag02	OC-20 to OC-31, UG-4 to UG-8, MC-3	1.912	0.523	-47.932	0.009	N/A	N/A	Yes - $\delta^{13}C$
230927_Bag03	OC-20 to OC-31, UG-4 to UG-8, MC-3	1.958	0.511	-48.016	0.033	N/A	N/A	Yes - $\delta^{13}C$
230927_Bag04	OC-20 to OC-31, UG-4 to UG-8, MC-3	1.919	0.521	-47.905	0.022	N/A	N/A	Yes - $\delta^{13}C$
230927_Bag05	OC-20 to OC-31, UG-4 to UG-8, MC-3	1.964	0.509	-48.103	0.046	-84.7	0.2	Yes - both
230927_Bag06	OC-20 to OC-31, UG-4 to UG-8, MC-3	1.957	0.511	-48.085	0.040	-83.4	0.8	Yes - both
230927_Bag07	OC-20 to OC-31, UG-4 to UG-8, MC-3	1.928	0.519	-47.965	0.041	-82.3	0.3	Yes - both
230927_Bag08	OC-20 to OC-31, UG-4 to UG-8, MC-3	1.94	0.515	-47.837	0.075	-82.4	0.8	Yes - both
230927_Bag09	OC-20 to OC-31, UG-4 to UG-8, MC-3	1.916	0.522	-47.706	0.103	-82.5	2.2	Yes - both
230927_Bag10	OC-20 to OC-31, UG-4 to UG-8, MC-3	2.103	0.476	-48.525	0.031	-91.5	1.3	Yes - both
230915_Bag10	OC-22 to OC-24, UG-5	1.937	0.516	-47.957	0.052	N/A	N/A	Yes - $\delta^{13}C$
230922_Bag01	OC-22 to OC-24, UG-5	2.135	0.468	-48.402	0.034	N/A	N/A	Yes - $\delta^{13}C$
230922_Bag02	OC-22 to OC-24, UG-5	2.001	0.500	-48.131	0.052	N/A	N/A	Yes - $\delta^{13}C$
230922_Bag03	OC-22 to OC-24, UG-5	2.208	0.453	-48.259	0.060	N/A	N/A	Yes - $\delta^{13}C$
230922_Bag04	OC-22 to OC-24, UG-5	2.059	0.486	-48.278	0.063	N/A	N/A	Yes - $\delta^{13}C$
230922_Bag05	OC-22 to OC-24, UG-5	2.17	0.461	-47.976	0.025	N/A	N/A	Yes - $\delta^{13}C$
230922_Bag06	OC-22 to OC-24, UG-5	2.634	0.380	-48.200	0.046	N/A	N/A	Yes - $\delta^{13}C$
230922_Bag07	OC-22 to OC-24, UG-5	1.969	0.508	-48.076	0.014	N/A	N/A	Yes - $\delta^{13}C$
230922_Bag08	OC-22 to OC-24, UG-5	2.034	0.492	-48.028	0.117	N/A	N/A	Yes - $\delta^{13}C$
230922_Bag09	OC-22 to OC-24, UG-5	1.981	0.505	-48.246	0.040	N/A	N/A	Yes - $\delta^{13}C$
230922_Bag10	OC-22 to OC-24, UG-5	2.117	0.472	-48.128	0.055	N/A	N/A	Yes - $\delta^{13}C$
231002_Bag07	OC-22 to OC-24, UG-5	2.011	0.497	-47.714	0.112	N/A	N/A	Yes - $\delta^{13}C$

Sample ID	Upwind coal mine(s)	CH_4 (ppm)	$1/CH_4$ (ppm)	$\delta^{13}C\text{-}CH_4$	$1\sigma\ \delta^{13}C\text{-}CH_4$	$\delta^{2}H\text{-}CH_4$	$1\sigma\ \delta^{2}H\text{-}CH_4$	Analysed using Keeling plot?
231002_Bag01	OC-22 to OC-30, UG-4 to UG-8, MC-3	1.981	0.505	-48.055	0.024	N/A	N/A	Yes - $\delta^{13}C$
231002_Bag02	OC-22 to OC-30, UG-4 to UG-8, MC-3	1.917	0.522	-47.860	0.024	N/A	N/A	Yes - $\delta^{13}C$
231002_Bag03	OC-22 to OC-30, UG-4 to UG-8, MC-3	1.984	0.504	-48.101	0.064	N/A	N/A	Yes - $\delta^{13}C$
231002_Bag04	OC-22 to OC-30, UG-4 to UG-8, MC-3	1.987	0.503	-48.095	0.029	N/A	N/A	Yes - $\delta^{13}C$
231002_Bag05	OC-22 to OC-30, UG-4 to UG-8, MC-3	1.992	0.502	-48.134	0.062	N/A	N/A	Yes - $\delta^{13}C$
231002_Bag06	OC-22 to OC-30, UG-4 to UG-8, MC-3	1.96	0.510	-48.013	0.029	N/A	N/A	Yes - $\delta^{13}C$
230911_Bag01	OC-25 to OC-27, UG-5, UG-6	1.941	0.515	-47.724	0.023	N/A	N/A	Yes - $\delta^{13}C$
230911_Bag02	OC-25 to OC-27, UG-5, UG-6	1.999	0.500	-48.166	0.039	N/A	N/A	Yes - $\delta^{13}C$
230911_Bag03	OC-25 to OC-27, UG-5, UG-6	1.924	0.520	-47.873	0.033	N/A	N/A	Yes - $\delta^{13}C$
230911_Bag04	OC-25 to OC-27, UG-5, UG-6	1.994	0.502	-48.140	0.047	N/A	N/A	Yes - $\delta^{13}C$
230911_Bag05	OC-25 to OC-27, UG-5, UG-6	1.932	0.518	-47.964	0.043	N/A	N/A	Yes - $\delta^{13}C$
230925_Bag01	OC-30	2.174	0.460	-48.400	0.042	N/A	N/A	Yes - $\delta^{13}C$
230925_Bag02	OC-30	2.072	0.483	-48.198	0.032	N/A	N/A	Yes - $\delta^{13}C$
230925_Bag03	OC-30	2.011	0.497	-47.982	0.019	N/A	N/A	Yes - $\delta^{13}C$
230925_Bag04	OC-30	2.089	0.479	-48.280	0.014	-92.2	1.8	Yes - both
230925_Bag05	OC-30	2.249	0.445	-48.638	0.022	-94.5	0.8	Yes - both
230925_Bag07	OC-30	2.078	0.481	-48.399	0.030	-93	0.1	Yes - both
230925_Bag08	OC-30	7.666	0.130	-51.291	0.023	-170.6		Yes - both
230925_Bag09	OC-30	2.026	0.494	-48.203	0.039	N/A	N/A	Yes - $\delta^{13}C$
231004_Bag01	OC-30	2.08	0.481	-48.269	0.048	N/A	N/A	Yes - $\delta^{13}C$
231004_Bag02	OC-30	2.08	0.481	-48.330	0.056	N/A	N/A	Yes - $\delta^{13}C$
231004_Bag03	OC-30	2.096	0.477	-48.215	0.062	N/A	N/A	Yes - $\delta^{13}C$
231004_Bag04	OC-30	2.09	0.478	-48.232	0.038	N/A	N/A	Yes - $\delta^{13}C$
231004_Bag05	OC-30	2.089	0.479	-48.222	0.060	N/A	N/A	Yes - $\delta^{13}C$
231004_Bag06	OC-30	2.097	0.477	-48.328	0.033	N/A	N/A	Yes - $\delta^{13}C$
231004_Bag07	OC-30	2.095	0.477	-48.374	0.054	N/A	N/A	Yes - $\delta^{13}C$
231004_Bag08	OC-30	2.085	0.480	-48.333	0.043	N/A	N/A	Yes - $\delta^{13}C$
231004_Bag10	OC-30	2.075	0.482	-48.478	0.024	N/A	N/A	Yes - $\delta^{13}C$
230915_Bag01	OC-32	1.973	0.507	-47.966	0.067	N/A	N/A	Yes - $\delta^{13}C$
230915_Bag02	OC-32	1.923	0.520	-47.971	0.028	N/A	N/A	Yes - $\delta^{13}C$
230915_Bag03	OC-32	1.959	0.510	-47.987	0.014	-84.3	1.2	Yes - both
230915_Bag04	OC-32	2.024	0.494	-48.069	0.032	-86.6	0.9	Yes - both
230915_Bag05	OC-32	1.929	0.518	-47.877	0.050	N/A	N/A	Yes - $\delta^{13}C$
230915_Bag06	OC-32	1.906	0.525	-48.068	0.006	-89.8	1.3	Yes - both
230915_Bag08	OC-32	1.897	0.527	-47.789	0.058	-83.6	1.7	Yes - both
230915_Bag09	OC-32	2.167	0.461	-48.135	0.048	-91.5	0	Yes - both
230928_Bag01	OC-32	2.583	0.387	-48.439	0.022	N/A	N/A	Yes - $\delta^{13}C$
230928_Bag02	OC-32	2.331	0.429	-48.309	0.041	-97.7	1.7	Yes - both

Sample ID	Upwind coal mine(s)	CH_4 (ppm)	$1/CH_4$ (ppm)	$\delta^{13}C\text{-}CH_4$	$1\sigma\ \delta^{13}C\text{-}CH_4$	$\delta^{2}H\text{-}CH_4$	$1\sigma\ \delta^{2}H\text{-}CH_4$	Analysed using Keeling plot?
230928_Bag03	OC-32	2.185	0.458	-48.171	0.028	-95.8	0.9	Yes - both
230928_Bag04	OC-32	1.979	0.505	-48.119	0.122	-84.3	0.9	Yes - both
230928_Bag05	OC-32	1.912	0.523	-47.706	0.071	-86.2	0.9	Yes - both
230928_Bag06	OC-32	1.933	0.517	-47.883	0.033	-83.9	0.4	Yes - both
230928_Bag07	OC-32	1.985	0.504	-48.067	0.121	N/A	N/A	Yes - $\delta^{13}C$
230928_Bag08	OC-32	1.997	0.501	-48.054	0.078	N/A	N/A	Yes - $\delta^{13}C$
230928_Bag09	OC-32	1.982	0.505	-47.795	0.049	N/A	N/A	Yes - $\delta^{13}C$
230928_Bag10	OC-32			-48.932	0.101	N/A	N/A	Yes - $\delta^{13}C$
230923_Bag01	OC-5, UG-1	1.947	0.514	-47.916	0.063	N/A	N/A	Yes - $\delta^{13}C$
230923_Bag02	OC-5, UG-1	1.916	0.522	-47.796	0.049	N/A	N/A	Yes - $\delta^{13}C$
230923_Bag03	OC-5, UG-1	1.936	0.517	-47.947	0.030	N/A	N/A	Yes - $\delta^{13}C$
230923_Bag04	OC-5, UG-1	1.943	0.515	-48.014	0.037	N/A	N/A	Yes - $\delta^{13}C$
230923_Bag05	OC-5, UG-1	1.941	0.515	-47.888	0.057	N/A	N/A	Yes - $\delta^{13}C$
230923_Bag06	OC-5, UG-1	1.973	0.507	-48.204	0.021	N/A	N/A	Yes - $\delta^{13}C$
230923_Bag07	OC-5, UG-1	1.944	0.514	-48.070	0.040	N/A	N/A	Yes - $\delta^{13}C$
230923_Bag08	OC-5, UG-1	1.969	0.508	-48.256	0.032	N/A	N/A	Yes - $\delta^{13}C$
230923_Bag09	OC-5, UG-1	1.929	0.518	-47.843	0.016	N/A	N/A	Yes - $\delta^{13}C$
230923_Bag10	OC-5, UG-1	1.962	0.510	-48.209	0.030	N/A	N/A	Yes - $\delta^{13}C$
230909_Bag09	UG-3	N/A	N/A	N/A	N/A	N/A	N/A	No - both
230916_Bag01	UG-3	2.316	0.432	-50.632	0.072	-97	0.5	No - both
230916_Bag08	UG-3	1.948	0.513	-48.137	0.028	N/A	N/A	No - both

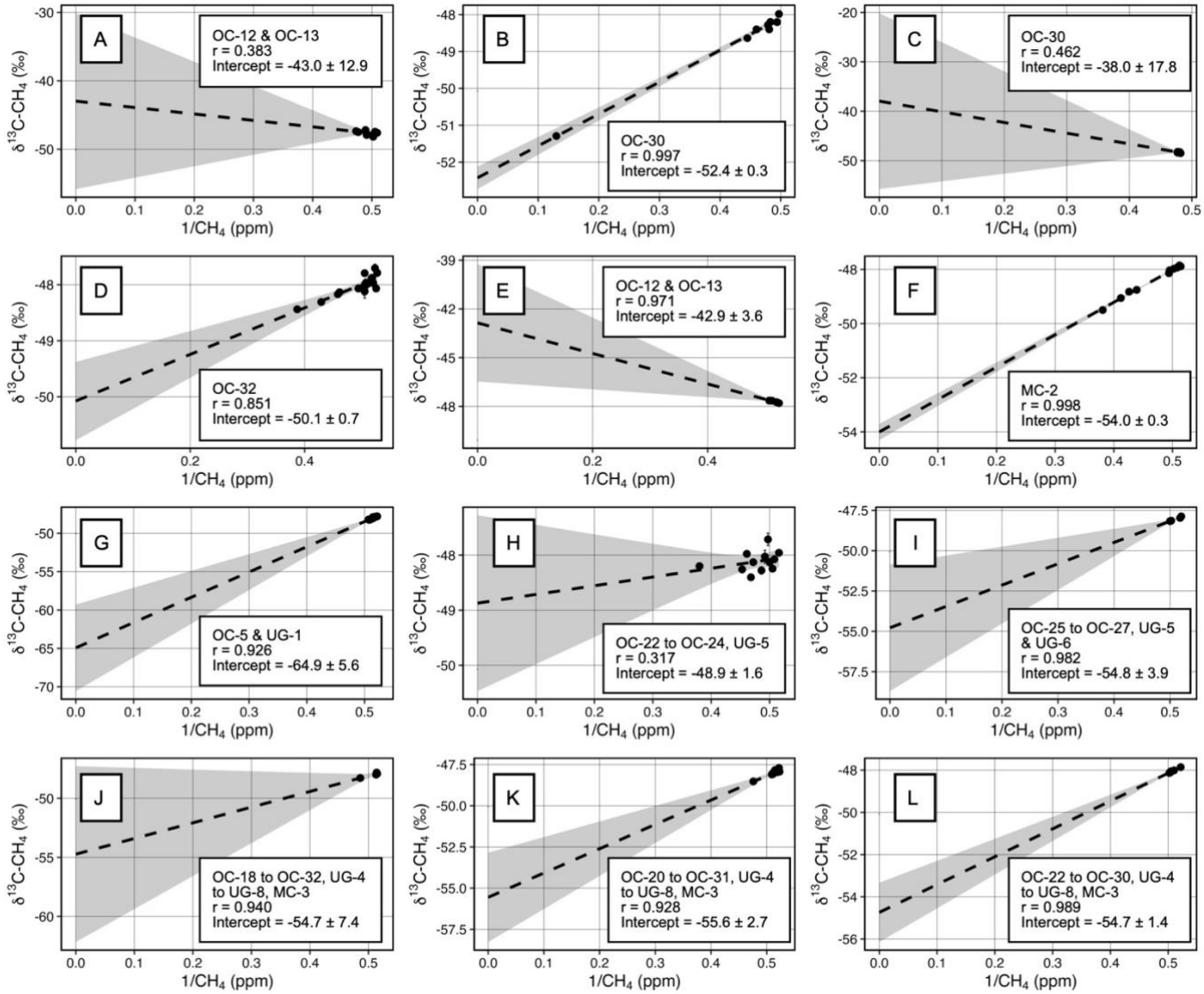

Fig. S33. Keeling plots used to derive the CH_4 source isotope signatures from each group of samples for $\delta^{13}C$-CH_4.

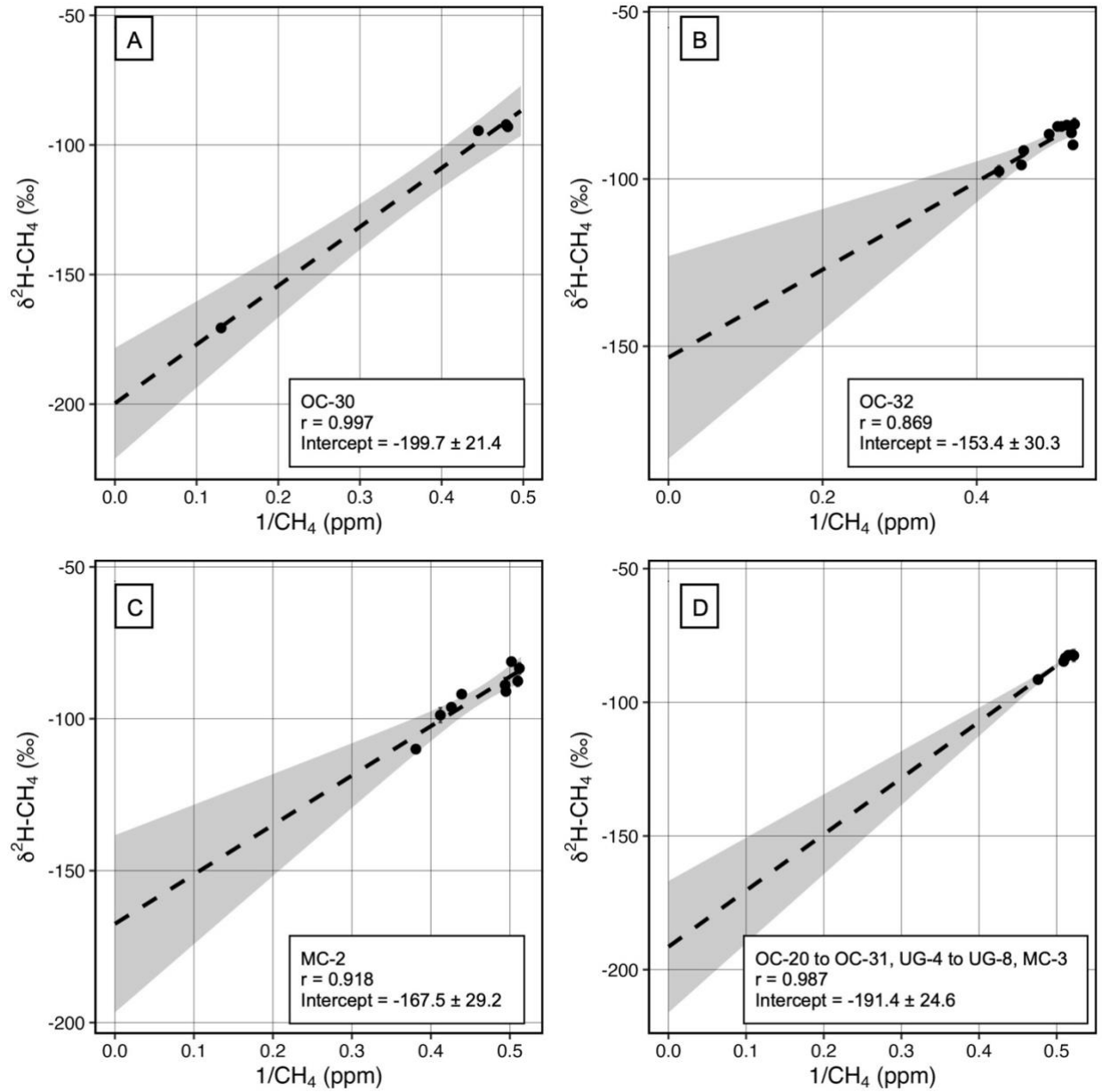

Fig. S34. Keeling plots used to derive the CH_4 source isotope signatures from each group of samples for δ^2H-CH_4.

References

AEMC: QLD: Dawson Valley Pipeline, https://www.aemc.gov.au/energy-system/gas/gas-pipeline-register/qld-north-queensland-gas-pipeline, 2026b.

AEMC: QLD: North Queensland Gas Pipeline, https://www.aemc.gov.au/energy-system/gas/gas-pipeline-register/qld-dawson-valley-pipeline, 2026a.

AEMO: Gas flows and capacity outlooks, https://www.aemo.com.au/energy-systems/gas/gas-bulletin-board-gbb/data-gbb/gas-flows, 2026.

AusDams: Australian Farm Dams, https://ausdams.org/, last access 22/10/2025, 2025.

Australian Government: National Inventory Report 2023, Volume I, Department of Climate Change, Energy, the Environment and Water, https://www.dcceew.gov.au/climate-change/publications/national-inventory-report-2023, 2025a.

Australian Government: National Inventory Report 2023, Volume I, Department of Climate Change, Energy, the Environment and Water, https://www.dcceew.gov.au/climate-change/publications/national-inventory-report-2023, 2025b.

Borchardt, J., Harris, S. J., Hacker, J. M., Lunt, M., Krautwurst, S., Bai, M., Bösch, H., Bovensmann, H., Burrows, J. P., Chakravarty, S., Field, R. A., Gerilowski, K., Huhs, O., Junkermann, W., Kelly, B. F. J., Kumm, M., Lieff, W., McGrath, A., Murphy, A., Schindewolf, J., and Thoböll, J.: Insights into Elevated Methane Emissions from an Australian Open-Cut Coal Mine Using Two Independent Airborne Techniques, Environ. Sci. Technol. Lett., 12, 397–404, https://doi.org/10.1021/acs.estlett.4c01063, 2025.

CER: 2023–24 baselines and emissions data, https://cer.gov.au/markets/reports-and-data/safeguard-data/2023-24-baselines-and-emissions-data, data as at 6/11/2025, last access 19/01/2026, 2025b.

CER: Greenhouse and energy information by designated generation facility 2023–24, https://cer.gov.au/document_page/greenhouse-and-energy-information-designated-generation-facility-2023-24, data as at 28/02/2025, last access 28/02/2025, 2025c.

Commonwealth of Australia: Australian National Greenhouse Accounts Factors For individuals and organisations estimating greenhouse gas emissions August 2023, p. 61, https://www.dcceew.gov.au/sites/default/files/documents/national-greenhouse-account-factors-2023.pdf, 2023.

DCCEEW: Australia's National Greenhouse Accounts, Paris Agreement inventory, https://www.greenhouseaccounts.climatechange.gov.au/, last access 16/01/2026, 2026.

Denison Gas: Denison North, https://denisongas.com.au/operations/denison-north/, 2026.

Erland, B.M., Adams, C., Darlington, A., Smith, M.L., Thorpe, A.K., Wentworth, G.R., Conley, S., Liggio, J., Li, S.M., Miller, C.E. and Gamon, J.A.: Comparing airborne algorithms for greenhouse gas flux measurements over the Alberta oil sands, Atmos. Meas. Tech., 15, 5841-5859, https://doi.org/10.5194/amt-15-5841-2022, 2022.

France, J. L., Bateson, P., Dominutti, P., Allen, G., Andrews, S., Bauguitte, S., Coleman, M., Lachlan-Cope, T., Fisher, R. E., Huang, L., Jones, A. E., Lee, J., Lowry, D., Pitt, J., Purvis, R., Pyle, J., Shaw, J., Warwick, N., Weiss, A., Wilde, S., Witherstone, J., and Young, S.: Facility level measurement of offshore oil and gas installations from a medium-sized airborne aircraft: method development for quantification and source identification of methane emissions, Atmos. Meas. Tech., 14, 71–88, https://doi.org/10.5194/amt-14-71-2021, 2021.

Grigg, A.H., Mullen B., So, H. B., Shelton, H.M., Bisrat, S., Horn, P., and Yatapanage, K.: Sustainable Grazing on Rehabilitated Land in the Bowen Basin Stage 2 - Grazing Trials, ACARP Project C9038, https://www.acarp.com.au/abstracts.aspx?repId=C9038, 2006.

Hacker, J., and Crawford, T.: The BAT-probe: The ultimate tool to measure turbulence from any kind of aircraft (or sailplane), Technical Soaring, 23, 43-46, 1999.

Hacker, J.M., Chen, D., Bai, M., Ewenz, C., Junkermann, W., Lieff, W., McManus, B., Neininger, B., Sun, J., Coates, T., and Denmead, T.: Using airborne technology to quantify and apportion emissions of CH_4 and NH_3 from feedlots, Anim. Prod. Sci., 56, 190-203, https://doi.org/10.1071/AN15513, 2016.

Hersbach, H., Bell, B., Berrisford, P., Hirahara, S., Horányi, A., Muñoz-Sabater, J., Nicolas, J., Peubey, C., Radu, R., Schepers, D., Simmons, A., Soci, C., Abdalla, S., Abellan, X., Balsamo, G., Bechtold, P., Biavati, G., Bidlot, J., Bonavita, M., De Chiara, G., Dahlgren, P., Dee, D., Diamantakis, M., Dragani, R., Flemming, J., Forbes, R., Fuentes, M., Geer, A.,

Haimberger, L., Healy, S., Hogan, R. J., Hólm, E., Janisková, M., Keeley, S., Laloyaux, P., Lopez, P., Lupu, C., Radnoti, G., de Rosnay, P., Rozum, I., Vamborg, F., Villaume, S., and Thépaut, J.: The ERA5 global reanalysis, Q. J. R. Meteorol. Soc., 146, 1999–2049, https://doi.org/10.1002/qj.3803, 2020.

Hoerning, S., and Hayes, P.: Measurement of fugitive methane emissions from an abandoned coal exploration hole in Queensland, Australia using a Quantum Gas LiDAR, Sci. Total Environ., 992, 179925, https://doi.org/10.1016/j.scitotenv.2025.179925, 2025.

Jemena: Queensland Gas Pipeline, https://www.jemena.com.au/gas/pipelines/Queensland-Gas-Pipeline/, 2026.

Keeling, C.D.: The concentration and isotopic abundances of carbon dioxide in rural and marine air, Geochim. Cosmochim. Acta, 24, 277-298, https://doi.org/10.1016/0016-7037(61)90023-0, 1961.

KPMG: Bowen Basin Concept Study, https://www.nrmmrrd.qld.gov.au/__data/assets/pdf_file/0008/1592855/bowen-basin-study-final-report.pdf, 2021.

Krautwurst, S., Fruck, C., Wolff, S., Borchardt, J., Huhs, O., Gerilowski, K., Gałkowski, M., Kiemle, C., Quatrevalet, M., Wirth, M., Mallaun, C., Burrows, J. P., Gerbig, C., Fix, A., Bösch, H., and Bovensmann, H.: Identification and Quantification of CH_4 Emissions from Madrid Landfills using Airborne Imaging Spectrometry and Greenhouse Gas Lidar, Atmos. Chem. Phys., 25, 14669-14702, https://doi.org/10.5194/acp-25-14669-2025, 2025.

Krautwurst, S., Gerilowski, K., Borchardt, J., Wildmann, N., Gałkowski, M., Swolkień, J., Marshall, J., Fiehn, A., Roiger, A., Ruhtz, T., Gerbig, C., Necki, J., Burrows, J. P., Fix, A., and Bovensmann, H.: Quantification of CH4 coal mining emissions in Upper Silesia by passive airborne remote sensing observations with the Methane Airborne MAPper (MAMAP) instrument during the CO_2 and Methane (CoMet) campaign, Atmos. Chem. and Phys., 21, 17345–17371, https://doi.org/10.5194/acp-21-17345-2021, 2021.

Krings, T., Gerilowski, K., Buchwitz, M., Hartmann, J., Sachs, T., Erzinger, J., Burrows, J. P., and Bovensmann, H.: Quantification of methane emission rates from coal mine ventilation shafts using airborne remote sensing data, Atmos. Meas. Tech., 6, 151–166, https://doi.org/10.5194/amt-6-151-2013, 2013.

Krings, T., Gerilowski, K., Buchwitz, M., Reuter, M., Tretner, A., Erzinger, J., Heinze, D., Pflüger, U., Burrows, J. P., and Bovensmann, H.: MAMAP - a new spectrometer system for column-averaged methane and carbon dioxide observations from aircraft: retrieval algorithm and first inversions for point source emission rates, Atmos. Meas. Tech., 4, 1735– 1758, https://doi.org/10.5194/amt-4-1735-2011, 2011.

Lampert, A., Pätzold, F., Asmussen, M. O., Lobitz, L., Krüger, T., Rausch, T., Sachs, T., Wille, C., Sotomayor Zakharov, D., Gaus, D., Bansmer, S., and Damm, E.: Studying boundary layer methane isotopy and vertical mixing processes at a rewetted peatland site using an unmanned aircraft system, Atmos. Meas. Tech., 13, 1937–1952, https://doi.org/10.5194/amt-13-1937-2020, 2020.

Law, S.J., Allison, S.D., Davies, A.B., Flores-Moreno, H., Wijas, B.J., Yatsko, A.R., Zhou, Y., Zanne, A.E., and Eggleton, P.: The challenge of estimating global termite methane emissions, Glob. Chang. Biol., 30, e17390, https://doi.org/10.1111/gcb.17390, 2024.

Lerner, B.M., Gilman, J.B., Aikin, K.C., Atlas, E.L., Goldan, P.D., Graus, M., Hendershot,R., Isaacman-VanWertz, G.A., Koss, A., Kuster, W.C., Lueb, R.A., McLaughlin, R.J., Peischl, J., Sueper, D., Ryerson, T.B., Tokarek, T.W., Warneke, C., Yuan, B., and de Gouw, J.A.: An improved, automated whole air sampler and gas chromatography mass spectrometry analysis system for volatile organic compounds in the atmosphere, Atmos. Meas. Tech., 10, 291–313, 2017, https://doi.org/10.5194/amt-10-291-2017, 2017.

Lunt, M. F., Harris, S. J., Hacker, J., Joynes, I., Robertson, T., Thompson, S., and France, J. L.: An evaluation of airborne mass balance and tracer correlation approaches to estimate site-level CH_4 emissions from LNG facilities using CO_2 as a tracer of opportunity, Atmos. Meas. Tech., 18, 4413-4431, https://doi.org/10.5194/amt-18-4413-2025, 2025.

Malerba, M.E., Wright, N., and Macreadie, P.I.: A continental-scale assessment of density, size, distribution and historical trends of farm dams using deep learning convolutional neural networks, Remote Sens., 13, 319, https://doi.org/10.3390/rs13020319, 2021.

Meat and Livestock Australia: Cattle numbers – as at June 2021 Natural Resource Management Region, https://www.mla.com.au/globalassets/mla-corporate/prices--markets/documents/trends--analysis/fast-facts--maps/mla_cattle-distribution-map-june-2021_v02-final.pdf, 2022.

Mei, L., Rozanov, V., Rozanov, A., and Burrows, J. P.: SCIATRAN software package (V4.6): update and further development of aerosol, clouds, surface reflectance databases and models, Geosci. Model Dev., 16, 1511–1536, https://doi.org/10.5194/gmd-16-1511-2023, 2023.

MiningLink: Dawson valley meridian seam gas, https://www.mininglink.com.au/mine-details/dawson-valley--meridian-seam-gas, 2026.

Mitchell, A.L., Tkacik, D.S., Roscioli, J.R., Herndon, S.C., Yacovitch, T.I., Martinez, D.M., Vaughn, T.L., Williams, L.L., Sullivan, M.R., Floerchinger, C., and Omara, M.: Measurements of methane emissions from natural gas gathering facilities and processing plants: Measurement results, Environ. Sci. Tech., 49, 3219-3227, https://doi.org/10.1021/es5052809, 2015.

Nauer, P.A., Hutley, L.B., and Arndt, S.K.: Termite mounds mitigate half of termite methane emissions, Proc. Natl. Acad. Sci. U.S.A., 115, 13306-13311, https://doi.org/10.1073/pnas.1809790115, 2018.

Neininger, B.G., Kelly, B.F., Hacker, J.M., Lu, X., and Schwietzke, S.: Coal seam gas industry methane emissions in the Surat Basin, Australia: comparing airborne measurements with inventories, Philos. Trans. A Math. Phys. Eng. Sci., 379, 20200458, https://doi.org/10.1098/rsta.2020.0458, 2021.

Pühl, M., Roiger, A., Fiehn, A., Gorchov Negron, A.M., Kort, E.A., Schwietzke, S., Pisso, I., Foulds, A., Lee, J., France, J.L., and Jones, A.E.: Aircraft-based mass balance estimate of methane emissions from offshore gas facilities in the Southern North Sea, Atmos. Chem. Phys., 24, 1005-1024, https://doi.org/10.5194/acp-24-1005-2024, 2023.

QPM Energy: ASX Announcement, https://announcements.asx.com.au/asxpdf/20230405/pdf/45ndl5cz2hqjsb.pdf, 2023.

QPM Energy: Moranbah Project, https://qpmenergy.com.au/moranbah-project/, 2025.

Queensland Government: AG Trends Spatial data portal, https://qldspatial.information.qld.gov.au/AGTrendsSpatial, 2025c.

Queensland Government: Annual coal statistics, https://www.data.qld.gov.au/dataset/annual-coal-statistics, data as at October 2024, last accessed 10/04/2025, 2025a.

Queensland Government: ArcGIS REST Services Directory, https://spatial-gis.information.qld.gov.au/arcgis/rest/services, 2025b.

Queensland Government: Arrow Bowen pipeline project, https://www.qld.gov.au/environment/management/environmental/eis-process/projects/completed/arrow-bowen-pipeline-project, 2025g.

Queensland Government: Petroleum and gas production statistics (December 2024), https://www.data.qld.gov.au/dataset/petroleum-gas-production-and-reserve-statistics, data as at 1 July 2025, last access 20/1/2026, 2025f.

Queensland Government: Queensland Globe, https://qldglobe.information.qld.gov.au/, 2025d.

Queensland Government: State of Queensland (Department of Resources) Geoscientific Information/Boreholes (MapServer), https://spatial-gis.information.qld.gov.au/arcgis/rest/services/GeoscientificInformation/Boreholes/MapServer/generateKml, last access 10/10/2025, 2025e.

Rolph, G., Stein, A., and Stunder, B.: Real-time environmental applications and display system: READY, Environ. Model. Softw., 95, 210-228, https://doi.org/10.1016/j.envsoft.2017.06.025, 2017.

Rozanov, V., Rozanov, A., Kokhanovsky, A., and Burrows, J.: Radiative transfer through terrestrial atmosphere and ocean: Software package SCIATRAN, Journal of Quantitative Spectroscopy and Radiative Transfer, 133, 13–71, https://doi.org/10.1016/j.jqsrt.2013.07.004, 2014.

Santos:

State of Queensland: Queensland Macropod Management Program Annual Report, p.30, https://www.qld.gov.au/__data/assets/pdf_file/0020/584021/mmp-annual-report-2024.pdf, 2024.

Stein, A.F., Draxler, R.R., Rolph, G.D., Stunder, B.J., Cohen, M.D. and Ngan, F.: NOAA's HYSPLIT atmospheric transport and dispersion modeling system, Bull. Amer. Meteor. Soc., 96, 2059-2077, https://doi.org/10.1175/BAMS-D-14-00110.1, 2015.

Thornton, C.M., and Elledge, A.E.: Heavy grazing of buffel grass pasture in the Brigalow Belt bioregion of Queensland, Australia, more than tripled runoff and exports of total suspended solids compared to conservative grazing, Mar. Pollut. Bull., 171, 112704, https://doi.org/10.1016/j.marpolbul.2021.112704, 2021.

Vendl, C., Clauss, M., Stewart, M., Leggett, K., Hummel, J., Kreuzer, M., and Munn, A.: Decreasing methane yield with increasing food intake keeps daily methane emissions constant in two foregut fermenting marsupials, the western grey kangaroo and red kangaroo, J. Exp. Biol., 218, 3425-3434, https://doi.org/10.1242/jeb.128165, 2015.

Zimmerle, D., Vaughn, T., Luck, B., Lauderdale, T., Keen, K., Harrison, M., Marchese, A., Williams, L., and Allen, D.: Methane emissions from gathering compressor stations in the US, Environ. Sci. Tech., 54, 7552-7561, https://doi.org/10.1021/acs.est.0c00516, 2020.